Dendritic crystal growth for weak undercooling. II. Surface energy effects on nonlinear evolution

M. D. Kunka
Department of Applied Mathematics, California Institute of Technology, Pasadena, California 91125

M. R. Foster
Department of Aerospace Engineering, Applied Mechanics and Aviation, The Ohio State University, Columbus, Ohio 43210

S. Tanveer
Department of Mathematics, The Ohio State University, Columbus, Ohio 43210

(Received 18 September 1997; revised manuscript received 20 July 1998)

We extend the previous work of Kunka, Foster, and Tanveer [Phys. Rev. E **56**, 3068 (1997)] by incorporating small but nonzero surface energy effects in the nonlinear dynamics of a conformal mapping function $z(\zeta,t)$ that maps the upper-half ζ plane into the exterior of a dendrite. In this paper, we specifically examine surface energy effects on the singularities of $z(\zeta,t)$ in the lower-half ζ plane, as they move toward the real axis from below. Until the time when any of the singularities of the corresponding zero-surface-energy solution or a surface-energy-generated daughter singularity cluster comes very close to the real axis, the leading-order outer solution is the zero-surface-energy solution in a strip of the lower-half complex that includes the real axis (i.e., the interface). There is an inner region around each singularity of the zero-surface-energy solution where surface energy plays a dominant role. However, the scalings in such an inner region, and hence the equation itself, must be modified when such singularities are very close to the real axis. The relative ordering of anisotropy, surface energy, and singularity strength strongly influences the form of the inner equations and hence their solutions. A singularity with initial strength weaker than some critical value is dissipated over a fast time scale by surface energy effects, leaving no trace of the initial singularity. This cutoff in singularity strength limits the size and growth rate of the interfacial disturbances that singularities generate. Also, the variation of time scale over which surface energy acts, due to differing singularity strengths in an ensemble, is shown to account for a $|y|^{1/2}$ coarsening rate for some intermediate range of distances, $|y|$, from the dendrite tip. As in the case of the isotropic Hele-Shaw problem [S. Tanveer, Philos. Trans. R. Soc. London, Ser. A **343**, 155 (1993)], we find here too that each initial zero of z_ζ gives birth to a ''daughter'' singularity cluster that moves away from the zero and necessarily approaches the real axis, before dispersing. One effect of this ''daughter'' singularity cluster, if it approaches the real axis before any other singularity, is to singularly perturb a smoothly evolving zero-surface-energy solution. In addition, numerical and analytical results for a certain general class of initial conditions indicate that daughter-singularity effects necessarily prevent an interface from ever approaching the cusp implied by the corresponding zero-surface-energy solution. Finally, we find that for a set of localized distortions, the local rescaling of dependent and independent variables (i.e., on an ''inner scale'') leads to the original equations, with an effectively larger surface-energy parameter. [S1063-651X(99)04501-8]

PACS number(s): 81.10.Aj

I. BACKGROUND

Dendritic crystal growth has been a subject of interest to physicists, metallurgists, as well as mathematicians. The most common example of such a growth is the well-known ice crystal. From a physicist's perspective, dendrites constitute a relatively simple but important problem of pattern formation in nonequilibrium growth [3–5]. In metallurgy, dendrites are common to crystal formation in the manufacture of alloys when the growth rate exceeds some critical value. The literature on the subject is vast and reviewed in [3–6], as well as in paper I [1] of our current sequence of papers on this subject. In this paper, we refer only to that work most directly relevant to the issues addressed here.

In the first of a sequence of papers on dendritic crystal growth for weak undercooling [1], we derived asymptotic equations for weak nondimensional undercooling Δ (nondimensionalized appropriately, through a combination of latent and specific heat) for a dendrite that is asymptotically a parabola in the far-field. A Peclet number, P, was introduced in accordance with

$$\Delta = \sqrt{\pi P} e^P \mathrm{erfc}(\sqrt{P}), \tag{1}$$

which is clearly small for small Δ. Based on the length scale a, associated with the far-field parabola, a velocity scale $U = 2DP/a$ was identified, where D is the diffusion coefficient. a and a/U are used to nondimensionalize all lengths and times. We determined that if the initial deviations from an Ivantsov state (parabolic dendrite with a corresponding temperature profile) are limited to an $O(1)$ region near the tip (region I), then the dynamic evolution of the dendrite for the nondimensional time $t \ll P^{-1}$ involves the $O(1)$ tip region only; in that region, the temperature is harmonic to the leading order, with appropriate boundary and far-field matching conditions. It is to be noted that the derivation does not assume that the deviation from the Ivantsov state is small, only that it does not extend all the way to the far-field

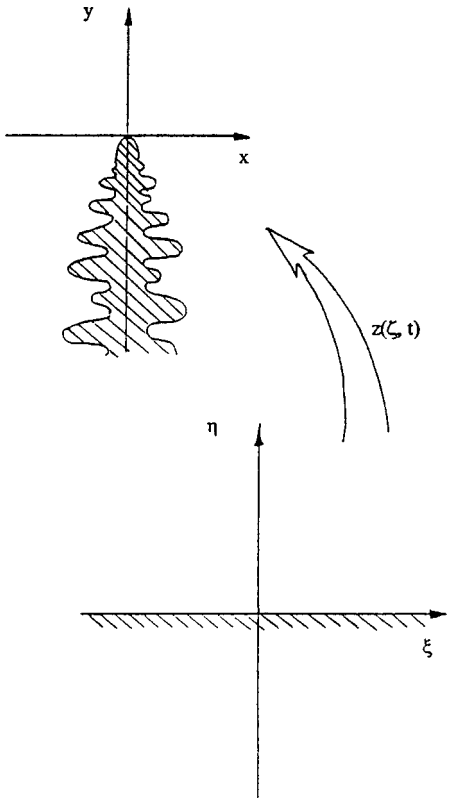

FIG. 1. Conformal mapping from the upper-half ζ plane to the exterior of the dendrite in the z plane.

$O(P^{-1})$ region. This tip-region dynamics was recast in terms of the evolution of the conformal mapping function from an upper-half ζ plane ($\zeta=\xi+i\eta$) to the exterior of the dendrite in the z plane, where $z=x+iy$ (see Fig. 1). This function $z(\zeta,t)$ was shown to satisfy the following nonlinear integro-differential equation for real ζ (i.e., on the ξ axis):

$$z_t=(H+iR)z_\xi, \tag{2}$$

where

$$R(\xi,t)=\frac{1-\mathcal{B}\ \mathrm{Im}\ \omega_\xi}{|z_\xi|^2}, \tag{3}$$

$$-H(\xi,t)=\mathcal{H}\{R\}(\xi,t)\equiv-\frac{1}{\pi}\int_{-\infty}^{+\infty}\frac{d\xi'}{\xi'-\xi}R(\xi',t), \tag{4}$$

$$\omega(\xi,t)=K(\xi,t)+i\mathcal{H}\{K\}(\xi,t), \tag{5}$$

where

$$K(\xi,t)=[1+\alpha f(\xi,t)]\kappa(\xi,t), \tag{6}$$

$$\kappa(\xi,t)=-\frac{1}{|z_\xi|}\ \mathrm{Im}\ \frac{z_{\xi\xi}}{z_\xi}, \tag{7}$$

$$f(\xi,t)=1-\cos 4(\theta-\theta_0)=1-\mathrm{Re}\left(\frac{z_\xi^2}{z_\xi^{*2}}\,e^{-i4\theta_0}\right). \tag{8}$$

The integral in (4) is a principal-value integral. In the above, the nondimensional surface energy parameter $\mathcal{B}$ is given by

$$\mathcal{B}=\frac{c_p\tilde{d}_0T_M}{2aLP} \tag{9}$$

where $\tilde{d}_0$ is the capillary length, c_p is the specific heat, T_M is the melting temperature of a planar interface, and L is the latent heat. Further, in the above, κ is physically the nondimensional curvature and $1+\alpha f$ is a fourfold surface energy anisotropy correction. Here θ the angle between the normal to the interface (pointing towards the melt) and the y axis, while θ_0 is some fixed value denoting a direction along which surface energy is a minimum. We define the set of Eqs. (2)–(8) with $\mathcal{B}=1$ as the ''standard problem.'' We shall see later that this problem arises time and again through a local renormalization in the small $\mathcal{B}$ limit near an approaching complex singularity. The ''standard problem'' can be solved numerically through a boundary integral method, as will be shown in paper III of this paper sequence, without much of the difficulties for small $\mathcal{B}$.

Through a linearization of the equation for $z(\xi,t)$ about some generally time-dependent state, we [1] were able to determine an expression for the growth rate of an initially localized disturbance in terms of the base state, through a Fourier analysis, when the disturbance is far from the tip. In the special case of a base state that is steady and is close to an Ivantsov state, the expressions for the growth rate were in accordance with prior results [7]. Interestingly enough, it was possible to obtain the same results by analytically continuing Eqs. (2)–(8) to the lower-half complex ζ plane and carrying out an asymptotic analysis for the linearized equations near singularities of z_ζ.

It is to be noted that while the lower-half ζ plane does not correspond to any part of the physical domain, singularities of $z(\zeta,t)$ approaching the real axis from below correspond to interfacial distortions. In particular, we found that according to the linearized dynamics, surface energy prevents an initially localized disturbance from remaining localized beyond a certain time. Arbitrarily small initial interfacial distortions (noise), representable by some singularity distribution in Im $\zeta<0$, significantly affect the interface later in time when singularities of the associated zero-surface-energy problem approach or cross Im $\zeta=0$, even though surface energy locally smoothes out all singularities in the linearized dynamics. The extent to which the zero-surface-energy singularity dynamics relates to the growth rate and dispersion of disturbances for small nonzero surface energy was also uncovered. Hence, zero-surface-energy singularity dynamics have both a qualitative and quantitative impact on the physical predictions mentioned above.

The relation between complex singularity dynamics and the evolving physical features of a dendrite transcends the restriction posed by linearized dynamics since a singularity of the conformal map in Im $\zeta<0$ can result in large interfacial distortions when that singularity approaches Im $\zeta=0$. In particular, if we consider an isolated singularity $\zeta_s(t)$ of z_ζ in the lower-half plane so that

$$z_\zeta\sim E_0(t)(\zeta-\zeta_s)^{-\beta} \tag{10}$$

near $\zeta=\zeta_s(t)$, then if $\zeta_s(t)$ is very close to the real axis, we can expect a distortion as sketched in Fig. 2 that is locally rounded off over a length scale determined by singularity

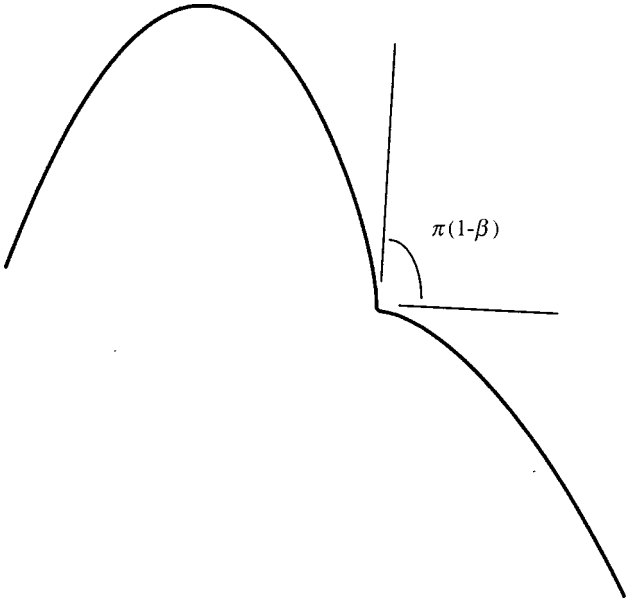

FIG. 2. Dependence of the indentation geometry on the singularity parameter β.

distance $-\mathrm{Im}\,\zeta_s$ from the real axis. Note that if $E_0(t)$ is sufficiently small and/or $|\mathrm{Im}\,\zeta_s|$ is sufficiently large, there will be little effect of a complex singularity ζ_s on the interface shape. The larger $|E_0|$ (singularity ''strength'') is, the larger is the impact region on the interface. arg E_0 determines the orientation of this distortion relative to the y axis. The physical effect of an isolated complex singularity corresponding to $\beta=1$ (pole) is illustrated in Fig. 3, where $n_s = \mathrm{Im}\,\zeta_s$.

It is to be noted that the geometrical features at the interface associated with Eq. (10) discussed above will remain intact for a period of time, even when the actual singularity at $\zeta=\zeta_s(t)$ is smoothed out or replaced by a cluster of other singularities, provided there is some intermediate range: $\mathcal{B}^{\delta} \ll |\zeta-\zeta_s(t)| \ll 1$ for some $\delta>0$ and some set of real ζ for which the behavior (10) persists.

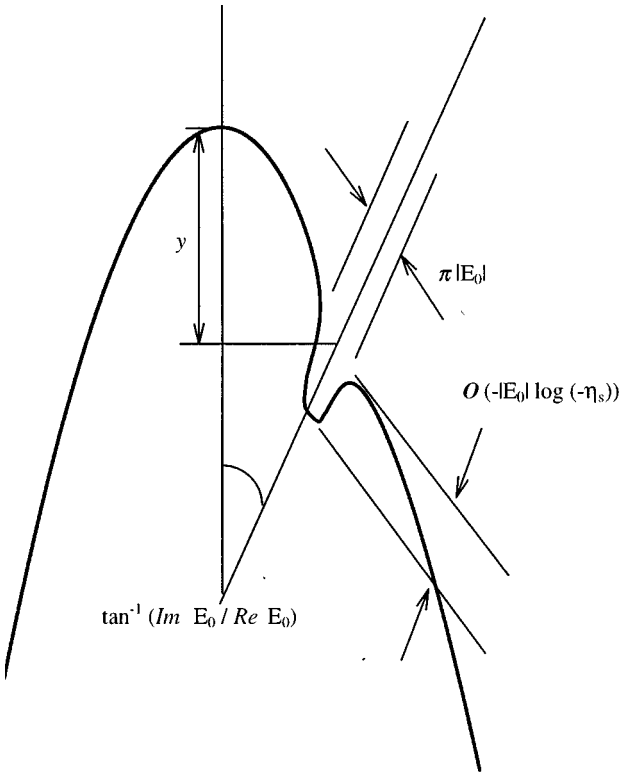

FIG. 3. Geometry of a pole indentation; the logarithm is base e.

Prior work for dendrites [1], as well as for the mathematically analogous Hele-Shaw problem [2,8,9], shows that the zero-surface-energy dynamics preserves the form of the singularity—i.e., β in Eq. (10) remains invariant with time; only its position $\zeta_s(t)$ and its strength $E_0(t)$ evolve (except for a pole where E_0 is invariant). When $\beta<0$, the form (10) is not invariant. Generally for an initial singularity of that kind,

$$z_\zeta \sim A_0(t) + E_0(t)[\zeta-\zeta_s(t)]^{-\beta} \tag{11}$$

for ζ sufficiently close to ζ_s. Such a singularity on the real axis does not introduce discontinuity in slope, except in the nongeneric case for which $A_0=0$ at the same instant as $\mathrm{Im}\,\zeta_s=0$. In this exceptional case, the corner is directed towards the melt, in contrast to the $\beta>0$ case, when it is directed towards the crystal.

All singularities, regardless of their type, were shown to continually approach the real axis with time, though for $\beta > \frac{1}{2}$ they do not impinge the real axis in finite time—indeed they slow down significantly as they come close to the real axis.

A point where $z_\zeta=0$, but z_ζ is otherwise analytic, is referred to as a zero. The geometric distortion shown in Fig. 2 is still valid if we associate $\beta=-1$ with a simple zero, i.e., a zero on the real axis corresponds to a zero-angled cusp on the interface that protrudes into the melt. Prior work reported in [1] has shown that a zero remains invariant with time, when surface energy is neglected, i.e.,

$$z_\zeta \sim z_{\zeta\zeta}(\zeta_0(t),t)[\zeta-\zeta_0(t)] \tag{12}$$

for ζ near $\zeta_0(t)$. The evolution equation for $\zeta_0(t)$, however, is found to be different from that of a singularity $\zeta_s(t)$. In particular, $\zeta_0(t)$ may or may not approach the real axis. For some set of initial conditions, a zero does impact the real axis in finite time. The mathematical solution for the dendrite ceases to be physically meaningful beyond this cusp-formation time.

The connection between the dynamics in the extended domain $\mathrm{Im}\,\zeta \leqslant 0$ and the physical features of an evolving dendrite, as described above, is particularly useful, since there is strong evidence that the zero-surface-energy dynamics in the extended domain is well-posed (see [2,10] for evidence for the mathematically similar Hele-Shaw problem), in contrast to the ill-posed nature of the interfacial evolution itself. In the latter case, the domain is restricted to $\mathrm{Im}\,\zeta=0$. This well-posedness at the zeroth order mathematically justifies a systematic perturbation procedure in the extended complex domain to study how small but nonzero surface energy (with or without anisotropy) alters the zero-surface-energy dynamics. The viewpoint we followed in [1] and here, following the Hele-Shaw analysis with isotropy [2,11], is that the interfacial dynamics is a byproduct of the dynamics in the extended domain.

A necessary drawback to the above-mentioned procedure is that now one must specify initial conditions in the extended complex domain Im $\zeta \leqslant 0$, which obviously cannot be done in an experiment where only the initial interface shape, up to some nonzero error, can be controlled. Connection to the observed statistical features of an experiment can be made only by studying the statistics of an ensemble of complex-plane initial conditions, allowing for every conceivable singularity distribution, and with each member of the ensemble consistent with the given initial shape to within experimental error. Clearly, many different singularity distributions can result in the same approximate interfacial shape. However, an essential precursor to such a statistical study is the thorough description of the dynamics of *all* possible forms for singularities in Im $\zeta<0$. Only when this issue is clarified can one proceed with the statistical study for an ensemble of initial conditions. That such an approach may be relevant to experimental observations is already demonstrated in Sec. III C, where we obtain coarsening results based on an ensemble of particular singularities. However, in general, the analytic continuation of $z(\zeta,0)$ into Im $\zeta<0$, corresponding to a general analytic initial shape, can be expected to contain natural boundaries and perhaps other singularities that are not isolated. Further, even the class of all possible forms of isolated singularities is too broad to study; only a small subset of possible initial conditions contains the specific classes of isolated singularities and zeros, as in Eqs. (10) and (12), that are considered here. Nonetheless, such isolated singularities, when they come close to the real axis, do correspond to a range of interfacial distortions, depending on β. For that reason, we believe that the statistical features of the interfacial dynamics within this limited class of initial conditions are not very different from what is observed in experiment—with the additional proviso that a two-dimensional theory is relevant, at least for scaling predictions.

However, even within the class of possible initial singularities studied here, there are basic mathematical issues concerning the asymptotic matching of inner and outer regions in the complex plane (as the surface-energy parameter goes to zero) that remain unresolved. In carrying it out in the neighborhood of a singularity that is preserved by the zero-surface-energy dynamics, it is observed that the matching is necessarily sectorial—the inner solution does not match the outer solution in every direction in the complex plane; it can be matched in a certain sector only (see Fig. 4). This is not a surprising result, since the steady dendrite problem is known to have the same features. However, unlike the steady problem where there are well-defined global Stokes lines even beyond the immediate vicinity of an inner region that determine local sectors of matching (see [12] for instance), no basic mathematical principle exists for the time-evolving flow. Only local Stokes lines, corresponding to local similarity solutions of the partial differential equations in the inner region, can be identified. We invoke a matching principle based on one used in the Hele-Shaw context [2]. The only direct evidence that such a matching principle is sound is our prior finding, in [1], that there is consistency between results from a Fourier analysis in the real domain and a complex singularity approach involving inner-outer matching for the linearized problem.

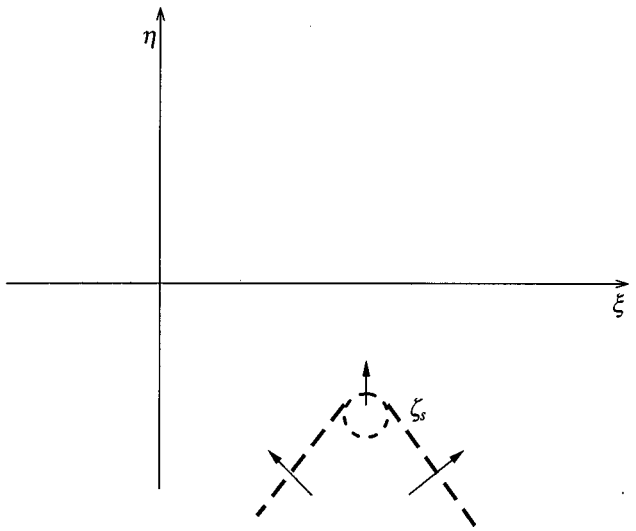

FIG. 4. Schematic of sectorial matching. Arrows indicate direction of matching toward the physical domain.

Further mathematical difficulties arise with initial zeros of z_ζ, since the full investigation of the dynamics at different stages is hampered in many cases by lack of either analytical or numerical solutions to a set of complicated partial differential equations in the complex plane. It is to be noted that the mathematical theory of nonlinear higher-order partial differential equations in the complex plane is quite undeveloped. Progress in this case has been made in this paper, as in [2], with additional ansatz on the dynamics at intermediate stage(s). There is no direct evidence that these ansatz are correct by themselves, though the careful numerical calculations of the interfaces themselves, for a sequence of computations for decreasing surface energy, indirectly confirm the basic features of the analytic theory, both for the associated isotropic Hele-Shaw problem [12] and also for anisotropic Hele-Shaw and dendrite problems. The latter work will be reported as paper III of this sequence of papers.

Despite the qualifiers above and the fact that our method necessarily requires a lengthy investigation of complex dynamics involving many kinds of initial singularities with corresponding inner equations depending on their distance from the real axis as well as the relative ordering of anisotropy and surface energy, this technique is the only one known for the fully nonlinear, time-evolving dendrite in the small-surface-energy limit. This limit is precisely the most difficult to explore computationally, since resolving small capillary lengths necessarily strains the capacities of computers. Further, even for cases where $\mathcal{B}$ is not small, the small-surface-energy limit cannot be avoided at large distances from the dendrite tip, where the curvature of an essentially parabolic interface becomes small.

In this paper, then, we continue our study of complex singularities initiated in [1] by including small but nonzero surface energy ($0<\mathcal{B}\ll 1$) in the nonlinear dynamics in the extended complex domain, generally taking anisotropy into account. The purpose of this paper is to address, partly or wholly, the following important issues.

(i) How does a nonzero $\mathcal{B}$ alter singularities described in Eq. (10)? Do the alterations and modifications to the singularity stay confined to a small cluster around $\zeta_s(t)$? Is there

an intermediate spatial scale over which the behavior (10) is relevant as $\mathcal{B}\to 0$? If so, is there a limitation on the order of $|E_0(0)|$ and the time for which this behavior persists? How does anisotropy in surface energy come into play? The main results relevant to these issues appear in Sec. II C.

(ii) What are the temporal and spatial scales over which surface-energy effects become important to the real axis dynamics for a singularity corresponding to $\beta>\frac{1}{2}$? Recall that according to zero-surface-energy dynamics, such singularities do not impinge the real axis in finite time, though they continually approach it. This question is discussed at the end of Sec. III A.

(iii) For singularities corresponding to $0<\beta<\frac{1}{4}$, which are known, in the absence of surface energy, to impact the real axis in finite time (leading to corners at the interface), what are the smallest length and time scales associated with a small nonzero $\mathcal{B}$, when Im $\zeta_s(t)\to 0$? The scales are discussed at the end of Sec. III B.

(iv) What can be said about the growth rate of interfacial distortions associated with approaching complex singularities discussed above in Eqs. (1)–(3)? How does surface energy, by dissipating weak singularities, determine a cutoff in the growth rate? How does anisotropy affect the result? The answers to these questions are explained in Sec. III C 2. It is often stated in the literature that interfacial distortions that point towards the crystal appear to remain stationary in the laboratory frame. Possible limitations on the time scale over which stationarity is valid are discussed in Sec. III C 1.

(v) What is the effect of anisotropic surface energy on an initial zero? Is there a ''daughter singularity'' $\zeta_d(t)$ that emerges from an initial zero $\zeta_0(0)$, as for the isotropic Hele-Shaw problem [2,11]? If so, how does anisotropy alter the structure of the cluster of actual singularities of z_ζ that are centered at $\zeta_d(t)$? These issues are discussed in Sec. IV.

(vi) How does a daughter singularity impacting the real axis affect the interfacial features? As with the isotropic Hele-Shaw problem, can one expect the daughter singularity impact time to indicate when an actual interface will veer off from the corresponding zero-surface-energy solution? Sections V B and V C deal with these issues.

(vii) How are interfacial cusps, associated with the impact of a zero $\zeta_0(t)$ on the real axis in finite time, prevented by small surface-energy effects? Are small nonzero surface-energy effects only important when the interface becomes close to a cusp, i.e., when curvature of the zero-surface-energy solution becomes large? Or, is it that the interface never comes close to cusp formation because it necessarily veers off from the corresponding zero-surface-energy solution significantly before any $\zeta_0(t)$ can impact the real axis. In the context of complex singularity dynamics, the two scenarios are distinguished by the following question: does a daughter singularity at $\zeta=\zeta_d(t)$ necessarily impact the real axis before the corresponding zero at $\zeta=\zeta_0(t)$?

(viii) What is the evolution in time of a given disturbance that may be associated with many different complex singularity distributions but causes an $O(1)$ localized deviation in interfacial slope from a smooth background state? Is there a rescaling under which the equations remain invariant in the small-surface-energy limit? What does such an invariance tell us about the dynamics?

(ix) How do surface energy and anisotropy modify or confirm the coarsening scenario that we proposed in [1]? The selection effect of surface energy on an ensemble of assumed singularities of different strengths is examined in Sec. III C 3, resulting in a prediction for the coarsening rate over a range of distances from the dendrite tip [see Eq. (124) and comments following it]. The daughter singularity effect and the concomitant selection of local tip characteristics are also found to qualitatively influence coarsening, as discussed in Sec. VII.

Note that while some of the issues listed appear theoretical in nature, apparently related more to complex singularity dynamics than the interface itself, the nature of our investigation precludes meaningful separation of the two. For instance, whether or not a singularity initially far from the real axis is dissipated by surface energy before hitting the real axis determines if corresponding physical distortions at the interface would eventually be observed.

II. PERTURBATION EXPANSION NEAR A SINGULARITY NOT CLOSE TO THE REAL AXIS

In the analysis presented here, we restrict our attention to singularities for which $\beta>0$, since it turns out that a form (11) for $\beta<0$, with $A_0(t)$ strictly $O(1)$, implies that surface-energy effects near the singularity location at $\zeta=\zeta_s(t)$ do not perturb z_ζ to the leading order. This fact means that the linearized analysis in [1] in a neighborhood of $\zeta_s(t)$ remains valid. However, there are special cases for $\beta<0$, with $A_0(t)=o(1)$, for which the linearized results discussed in [1] cannot be justified. Such exceptional cases are not analyzed in the current paper.

The analytic continuation of Eqs. (2)–(8) to the lower half-plane was determined [1] to be

$$z_t=c_1 z_\zeta+q_2-\mathcal{B}\,\frac{\omega_\zeta-\tilde{\omega}_\zeta}{\tilde{z}_\zeta}, \tag{13}$$

where

$$q_1(\zeta,t)=\frac{1}{\pi}\int_{-\infty}^{\infty}\frac{d\xi'}{\xi'-\zeta}\,R(\xi',t), \tag{14}$$

$$q_2(\zeta,t)=\frac{2i}{\tilde{z}_\zeta(\zeta,t)}, \tag{15}$$

$$\omega(\zeta,t)=2K(\zeta,t)+\frac{1}{\pi i}\int_{-\infty}^{+\infty}\frac{d\xi'}{\xi'-\zeta}\,K(\xi',t), \tag{16}$$

$$K(\zeta,t)=[1+\alpha f(\zeta,t)]\kappa(\zeta,t), \tag{17}$$

$$f(\zeta,t)=1-\frac{1}{2}\left(\frac{z_\zeta^2}{\tilde{z}_\zeta^2}\,e^{-i4\theta_0}+\frac{\tilde{z}_\zeta^2}{z_\zeta^2}\,e^{i4\theta_0}\right), \tag{18}$$

$$\kappa(\zeta,t)=-\frac{1}{2iz_\zeta^{1/2}\tilde{z}_\zeta^{1/2}}\left(\frac{z_{\zeta\zeta}}{z_\zeta}-\frac{\tilde{z}_{\zeta\zeta}}{\tilde{z}_\zeta}\right), \tag{19}$$

where

$$\tilde{F}(\zeta,t)=(F(\zeta^*,t))^* \tag{20}$$

is an analytic function which is equal to F^* on the real axis, where $*$ denotes complex conjugation. It is to be noted that $\tilde{z}(\zeta,t)$ is analytic in the lower-half ζ-plane (except at ∞). If expression (16) for ω is used in Eq. (13), one obtains

$$z_t = q_1 z_\zeta + q_2 + \frac{\mathcal{B}}{i\tilde{z}_\zeta^{3/2}}(-2z_\zeta^{-1/2})_{\zeta\zeta} - \frac{\mathcal{B}\alpha e^{-i4\theta_0}}{2i\tilde{z}_\zeta^{7/2}}(\tfrac{2}{3}z_\zeta^{3/2})_{\zeta\zeta} - \frac{\mathcal{B}\alpha e^{i4\theta_0}\tilde{z}_\zeta^{1/2}}{2i}(-\tfrac{2}{5}z_\zeta^{-5/2})_{\zeta\zeta} + \mathcal{B}r(\zeta,t), \quad (21)$$

where $r(\zeta,t)$ lumps together all other surface energy terms that contain derivatives of z with respect to z of orders smaller than the ones explicitly shown in Eq. (21).

Beginning with the lower-half-plane Eq. (21), we assume a regular perturbation expansion in powers of $\mathcal{B}$ in the asymptotic limit $\mathcal{B}\to 0$. The regular perturbation is denoted by

$$z \sim z_0 + \mathcal{B}z_1 + \cdots, \quad (22)$$

$$\zeta_s \sim \zeta_{s_0} + \mathcal{B}\zeta_{s_1} + \cdots, \quad (23)$$

$$q_1 \sim q_{1_0} + \mathcal{B}q_{1_1} + \cdots, \quad (24)$$

$$q_2 \sim q_{2_0} + \mathcal{B}q_{2_1} + \cdots, \quad (25)$$

$$\omega \sim \omega_0 + \cdots, \quad (26)$$

where subscript 0 has been used to denote the corresponding zero-surface-energy quantities that have been analyzed in the previous paper [1]. (Note: They appear without subscript 0 in [1].)

A. Review of zeroth-order results

Substitution of the above perturbation expansion into Eq. (22) and extraction of $O(1)$ terms obviously leads to the zero-surface-energy problem studied in Sec. IV onwards in the previous paper. From prior work [1], we know that there exists a solution to the zero-surface-energy equations for which

$$z_0(\zeta,t) = g(\zeta,t) + \sum_{j=1}^{N} \frac{E_j(\zeta,t)}{1-\beta_j}[\zeta-\zeta_j(t)]^{1-\beta_j}, \quad (27)$$

where $g(\zeta,t)$ and $E_j(\zeta,t)$ are analytic for Im $\zeta \leqslant 0$ and satisfy certain integro-differential equations, β_j is a constant (possibly different for each j), N is an arbitrary positive integer, and $\zeta_j(t)$ evolves in time according to an equation [1]. In the special case $\beta_j = 1$, the term $(\zeta-\zeta_j)^{1-\beta_j}/(1-\beta_j)$ in Eq. (27) is to be understood as $\ln(\zeta-\zeta_j)$. Exact solutions with β_j all equal to 1 have appeared in the context of the Hele-Shaw literature [13–17] earlier and we [1] also discussed such solutions in the dendrite context.

The form of the solution (27) means that singularities are preserved by the zero-surface-energy dynamics, a result known in the Hele-Shaw context from prior work [2,8,9]. Specifically, it is known that sufficiently close to any singularity type (27), denoted in general by ζ_s, we obtain

$$z_\zeta \sim E_0(t)[\zeta-\zeta_s(t)]^{-\beta}, \quad (28)$$

with $\beta > 0$. For $\beta < 0$, β not an integer, the local behavior is generally given by

$$z_\zeta \sim A_0(t) + E_0(t)[\zeta-\zeta_s(t)]^{-\beta}, \quad (29)$$

since $A_0(t)$ is generally nonzero. From the known evolution equation [1], it can be deduced that the ''strength'' of the singularity $E_0(t)$ in Eqs. (28) and (29) and its location $\zeta_s(t)$ evolve in accordance with

$$E_0(t) = E_0(0)\exp\left((1-\beta)\int_0^t dt' q_{1\zeta}(\zeta_s(t'),t')\right), \quad (30)$$

$$\dot{\zeta}_s = -q_1(\zeta_s(t),t). \quad (31)$$

The relations (28)–(31) characterizing the local behavior of a singularity hold more generally, even when global solutions are not necessarily in the form (27). In [1], it was also determined that for any ζ in the lower half-plane, Im $q_1(\zeta,t) < 0$, which, from Eq. (31), implies that singularities of the type (28) approach the real axis. [Actually, all singularities, regardless of their form, satisfy the relation (31).]

Zero-surface-energy singularity behavior depends on the value of β. Within the class of singularities (28), we found that those singularities with $\beta < \frac{1}{4}$ reach the real axis in finite time, whereas those corresponding to $\beta > \frac{1}{2}$ asymptote the real axis for $t\to\infty$. The case $\frac{1}{4} \leqslant \beta \leqslant \frac{1}{2}$ remains unresolved. We also found that among all singularities corresponding to $\beta > \frac{1}{2}$, simple poles ($\beta = 1$) approach the real axis exponentially in time, but branch points ($\beta \neq$ integer) approach algebraically in time. Therefore, for a more general initial condition that contains singularities of the type (28) with many different β, the indentations on the physical interface, over the short run, will be dominated by poles approaching the real axis.

B. First-order perturbation and nonuniformity near ζ_s

The extraction of the $O(\mathcal{B})$ term in Eqs. (22)–(26) expansion, on the other hand, produces the following equation:

$$z_{1t} - q_{1_0}z_{1\zeta} = q_{1_1}z_{0\zeta} + q_{2_1} + r_0 + \frac{1}{i\tilde{z}_{0\zeta}^{3/2}}(-2z_{0\zeta}^{-1/2})_{\zeta\zeta} - \frac{\alpha e^{-i4\theta_0}}{2i\tilde{z}_{0\zeta}^{7/2}}(\tfrac{2}{3}z_{0\zeta}^{3/2})_{\zeta\zeta} - \frac{\alpha e^{i4\theta_0}\tilde{z}_{0\zeta}^{1/2}}{2i} \times \left(-\frac{2}{5}z_{0\zeta}^{-5/2}\right)_{\zeta\zeta}. \quad (32)$$

The nonuniformity caused by the presence of $q_{1_1}z_{0\zeta}$ in Eq. (32) can be overcome if the zeroth-order approximation to the advective speed of a singularity ζ_s is corrected as

$$\dot{\zeta}_s = -q_{1_0}(\zeta_s(t),t) - \mathcal{B}q_{1_1}(\zeta_s(t),t), \quad (33)$$

meaning that we use the two-term perturbation expansion in Eq. (23), with

$$\dot{\zeta}_{s0} = -q_{1_0}(\zeta_{s0}(t),t), \quad \zeta_{s0}(0)=\zeta_s(0), \tag{34}$$

$$\dot{\zeta}_{s1} = -\zeta_{s1} q_{1_{0\zeta}}(\zeta_{s0}(t),t) - q_{1_1}(\zeta_{s0}(t),t), \quad \zeta_{s1}(0)=0. \tag{35}$$

The last three terms on the right of Eq. (32) can clearly become singular where z_{0_ζ} is singular, resulting in the possibility of $\mathcal{B}z_1$ in Eq. (22) being larger or of the same order as z_0, i.e., the assumed asymptotic expansion (22) then becomes inconsistent (disordered). To determine if and when this happens, we have to study the local behavior near $\zeta = \zeta_s$ of the outer-perturbation series.

Since the local behavior of the zero-surface-energy solution $z_{0\zeta} \sim E_0(t)(\zeta-\zeta_{s_0})^{-\beta}$, $\beta>0$ also induces a singular behavior of z_1, when the correction to the singularity speed is not accounted for, we seek a slight modification of the outer asymptotic expansion in the immediate neighborhood of a singularity in the form

$$z_\zeta \sim E_0(t)[\zeta-\zeta_s(t)]^{-\beta} + \mathcal{B}E_1(t)[\zeta-\zeta_s(t)]^{\delta_1} + \mathcal{B}\alpha E_2(t)[\zeta-\zeta_s(t)]^{\delta_2} + \mathcal{B}\alpha E_3(t)[\zeta-\zeta_s(t)]^{\delta_3}, \tag{36}$$

where ζ_s is determined in accordance with Eq. (33). In the usual cases, the two-term local expansion above should include only one of the terms involving E_1, E_2, or E_3. However, by including all three terms in Eq. (36), we make allowance for different possibilities depending on $O(|E_0|)$, β, and $|\zeta-\zeta_s|$. From Eq. (36), it follows that the leading-order perturbation to z_0 has the following local behavior near $\zeta = \zeta_{s0}$:

$$z_{1\zeta} \sim \beta\zeta_{s_1}(t)E_0(t)[\zeta-\zeta_{s_0}(t)]^{-\beta-1} + E_1(t)[\zeta-\zeta_{s_0}(t)]^{\delta_s} + \alpha E_2(t)[\zeta-\zeta_{s_0}(t)]^{\delta_2} + \alpha E_3(t)[\zeta-\zeta_{s_0}(t)]^{\delta_3}. \tag{37}$$

Substituting Eq. (37) into Eq. (32), we obtain

$$\delta_1 = \tfrac{1}{2}\beta - 3, \quad \delta_2 = -\tfrac{3}{2}\beta - 3, \quad \delta_3 = \tfrac{5}{2}\beta - 3 \tag{38}$$

and the evolution equation for the singularity strength,

$$\dot{E}_1(t) - (\tfrac{1}{2}\beta-2)q_{1_{0\zeta}}(\zeta_{s_0}(t),t)E_1(t) = -\frac{\beta(\beta-2)(\beta-4)}{4i\tilde{z}_{0\zeta}^{3/2}(\zeta_{s_0}(t),t)E_0^{1/2}(t)}, \tag{39}$$

$$\dot{E}_2(t) + (\tfrac{3}{2}\beta+2)q_{1_{0\zeta}}(\zeta_{s_0}(t),t)E_2(t) = \frac{e^{-i4\theta_0}\beta(3\beta+2)(3\beta+4)E_0^{3/2}(t)}{8i\tilde{z}_{0\zeta}^{7/2}(\zeta_{s_0}(t),t)}, \tag{40}$$

$$\dot{E}_3(t) - (\tfrac{5}{2}\beta-2)q_{1_{0\zeta}}(\zeta_{s_0}(t),t)E_3(t) = \frac{e^{i4\theta_0}\beta(5\beta-2)(5\beta-4)\tilde{z}_{0\zeta}^{1/2}(\zeta_{s_0}(t),t)}{8iE_0^{5/2}(t)}, \tag{41}$$

with initial conditions

$$E_1(0)=E_2(0)=E_3(0)=0. \tag{42}$$

This set of linear first-order ordinary differential equations can be readily integrated, if desired. It is to be noted that the addition of a possible term in Eq. (36) of the form $E_{1,1}(t)[\zeta-\zeta_s(t)]^{\delta_1+1}$ does not effect the equations (39)–(42) because of Eq. (33). Similarly, an additional higher-order term in the form $[\zeta-\zeta_s(t)]^{1+\delta_2}$ or $[\zeta-\zeta_s(t)]^{1+\delta_3}$ in Eq. (36) does not effect Eqs. (39)–(42).

An explanatory note is in order about local behavior (37) when $|E_0(t)| \ll 1$. From exact expressions for z_0 that contain singularities of the type considered here, one can expect that even for $\beta>0$, there is an $O(1)$ correction $A_0(t)$ as in Eq. (29). Therefore, in order for the leading-order behavior $z_\zeta \sim E_0[\zeta-\zeta_s(t)]^{-\beta}$ to be valid, one must require

$$|\zeta-\zeta_s| \ll |E_0|^{1/\beta}. \tag{43}$$

The same restriction (43) must also hold for Eqs. (36) and (37).

Further, in deriving Eq. (36), it was implicitly assumed that it is acceptable to replace $\tilde{z}_{0\zeta}$ and global terms q_{10}, etc. by the first few terms of the Taylor expansion at $\zeta=\zeta_s(t)$. However, these terms have singularities at $\zeta=\zeta_s^*(t)$ in the upper-half plane. We must therefore require that $|\zeta-\zeta_s| \ll |\zeta_s-\zeta_s^*|$, i.e., $|\zeta-\zeta_s| \ll |\eta_s|$. Hence, when ζ_s approaches the real axis, the domain of validity of Eq. (36) shrinks so that Eq. (36) cannot hold on the real axis itself.

We now examine the behavior of the two-term outer-asymptotic expansion (36) in a neighborhood defined by Eq. (43) to determine if and when this asymptotic expansion becomes disordered for $t \ll 1$. On integrating Eqs. (37)–(39), it follows that the expansion indeed fails if any or all of the following conditions hold.

(i) $E_0^{3/2}(0)/[\mathcal{B}t(\zeta-\zeta_s)^{3\beta/2-3}] = O(1)$: This condition can be satisfied if the following conditions (ia) or (ib) are satisfied:

(ia) $0<\beta<2$ and $|\zeta-\zeta_s| = O(\mathcal{B}t/E_0^{3/2})^{2/[3(2-\beta)]}$

for any $t>0$;

(ib) $\beta \geqslant 2$, $t_i = E_0^{3/\beta}/\mathcal{B} \ll 1$, $t \gg t_i$

in a subregion of $|\zeta-\zeta_s| \ll E_0^{1/\beta}$ where condition (i) holds.

(ii) $E_0^{7/2}(0)/[\mathcal{B}\alpha t(\zeta-\zeta_s)^{7\beta/2-3}] = O(1)$: The condition (ii) can hold if either (iia) or (iib) holds:

(iia) $0<\beta<\frac{6}{7}$, $|\zeta-\zeta_s| = O[\mathcal{B}\alpha t/E_0^{7/2}(0)]^{2/(6-7\beta)}$

for any $t>0$;

(iib) $\beta \geqslant \frac{6}{7}$, $t_{ii} = E_0^{3/\beta}/(\mathcal{B}\alpha) \ll 1$, $t \gg t_{ii}$

in a subregion of $|\zeta-\zeta_s| \ll E_0^{1/\beta}$, where condition (ii) holds.

(iii) $(\zeta-\zeta_s)^{\beta/2+3}/[E_0^{1/2}(0)\mathcal{B}\alpha t] = O(1)$: This condition holds for any $\beta>0$ when $(\zeta-\zeta_s) = O[E_0^{1/2}(0)\mathcal{B}\alpha t]^{2/(\beta+6)} \ll E_0^{1/\beta}$.

Note that $t_{ii} \gg t_i$. Further, it is to be noted that the conditions $t_i \ll 1$ and $t_{ii} \ll 1$ for $\beta>2$ and $\beta>\frac{6}{7}$, respectively, necessarily require that $E_0(0)$ be sufficiently small. When $E_0(0)$ is not that small, the regular perturbation expansion

(36) does not break down for $\beta>2$ when anisotropy $\alpha=0$. On the other hand, the presence of anisotropy ($\alpha\neq 0$) guarantees that there is a local region where the outer perturbation expansion does not hold because condition (iii) necessarily holds sufficiently close to $\zeta=\zeta_s$.

C. Results from inner equations centered at $\zeta_s(t)$

As is well known in perturbation theory, the disordering of an assumed asymptotic perturbation expansion in powers of $\mathcal{B}$, as seen in the preceding section, suggests that one should seek appropriate rescaling of the dependent and independent variables before determining the asymptotic limit $\mathcal{B}\to 0$. This procedure results in an ''inner'' equation near $\zeta_s(t)$.

The arguments leading to the choice of these rescalings, as well as the examination of solutions to the leading-order inner equation, are quite elaborate and are relegated to Appendix A. The results depend very much on the relative orderings of $E_0(0)$, $\mathcal{B}$, and α. In this connection, it is appropriate to note that if $E_0(0)$ is not independent of $\mathcal{B}$ but scales as some positive power of $\mathcal{B}$ smaller than 1, then while $z_{0\zeta}$ would not contain such a singularity, there would be an intermediate term in the outer-perturbation expansion (22) (between 0 and 1) that would contain this particular singularity. Furthermore, if the anisotropy α scales with some positive power of $\mathcal{B}$, instead of being independent of it, one would have to similarly insert another, possibly fractional power of $\mathcal{B}$, into the outerperturbation expansion (22). Nonetheless, these changes do not affect the validity of Eq. (36) as the two-term outer expansion in the neighborhood of a singularity. We do not discuss a case where $E_0(0)$ scales with a power of $\mathcal{B}$ larger than 1 since such weak singularities are seen to dissipate over a fast time scale, just as for those discussed below for $E_0=o(\mathcal{B}^{\beta/3})$.

The main result from Appendix A is that an initial singularity of the type (10), which is initially not ''too close'' (in the sense defined precisely in the next section) to the real axis, transforms into many singularities clustered over the small inner region (actually, it contains multiple inner regions) around $\zeta=\zeta_s(t)$. Yet, except for the case of weak singularities, there exists an intermediate regime defined by $B^{\delta}\ll|\zeta-\zeta_s(t)|\ll 1$ with $\zeta-\zeta_s(t)$ in some complex sector, where Eq. (10) holds for at least $O(1)$ times, or until $\zeta_s(t)$ comes ''too close'' to the real axis. Figure 5 illustrates the inner regions around $\zeta_s(t)$ for strongly anisotropic surface energy. Pictorially similar results hold, though with different scalings (see Appendix A) for weakly anisotropic surface energy. The only exception to the behavior in Eq. (10) over some range of distances occurs for an initially weak singularity, defined by the condition $E_0(0)=o(\mathcal{B}^{\beta/3})$. Here scaling arguments reveal that on a fast time scale the singularity will have dissipated so that there will be no trace of its initial nature. Effects of singularities, therefore, will not be visible on the interface. This result, along with those presented in the next section about weak singularities near the real axis, limits the smallest observable length scales and the largest possible growth rates of distortions at the interface that can be associated with complex singularities of the type (10).

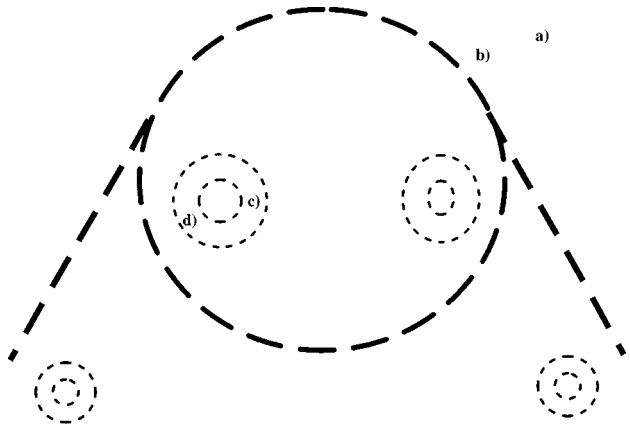

FIG. 5. Schematic of singularity structure in the presence of strongly anisotropic surface energy. (a) Outer singularity $z_\zeta \sim E_0(t)[\zeta-\zeta_s(t)]^{-\beta}$, (b) size of inner region $O(\mathcal{B}^{2(1+\lambda)+\mu/\beta+6})$, (c) inner singularity (there are actually a countably infinite number of inner singularities) $z_\zeta\sim C(t)[\zeta-\zeta_{\rm in}(t)]^{2/3}$, (d) size of inner-inner region $O(\mathcal{B}^{3/4\{2[(\beta+2/3)\delta-\mu]-\lambda\}})$.

III. INNER SCALES FOR SINGULARITIES NEAR THE REAL AXIS

In this section, we investigate the behavior of singularities that are ''too close'' to the real axis for the results in the preceding section to hold. Here, one cannot simplify the global integral terms like q_1, q_2, as well as terms like $\tilde{z}_\zeta$, etc. in Eq. (21). Previously, we merely replaced such a term by its Taylor expansion near $\zeta=\zeta_s$. Now, the proximity of ζ_s to the real axis introduces too strong variations in these quantities. The condition ''too-close'' is more precisely defined by requiring that Im $\zeta_s=O(\mathcal{B}^{\delta})$, where $\mathcal{B}^{\delta}$ defines the inner scale appropriate for the case under consideration (it differs for different $\mathcal{B}$ and E_0, as will be shortly seen). Such a situation can arise in two different ways: (i) $\zeta_s(0)$ is ''too close'' to the real axis or (ii) $\zeta_s(t)$, initially further out, is now ''too close'' to the real axis, something that must eventually happen for all $\zeta_s(t)$.

Recall from [1] that for zero surface energy, isolated singularities with $\beta>\frac{1}{2}$ do not reach the real axis in finite time, whereas those corresponding to $0<\beta<\frac{1}{4}$ impinge the real axis in finite time. (Recall that the case $\frac{1}{4}\leqslant\beta\leqslant\frac{1}{2}$ remains uncertain and will not be discussed here.) In this section, we restrict the discussion of surface-energy effects to two subcases: $0<\beta<\frac{1}{4}$ and $\frac{1}{2}<\beta\leqslant 1$. The case $\beta>1$ is not considered here because we expect the influence of such singularities to be minimal over the time scale of tip advance. Prior numerical calculations [10] suggest that for β significantly larger than 1, the singularity approach towards the real axis is slow compared to poles, with $\beta=1$.

We will be chiefly concerned with the derivation of consistent inner equations, but with less discussion of the resulting solutions. The main purpose is to derive scaling results, which shed some light on the spatial and temporal scales for interfacial distortions. Since the singularity location is close to the real axis, there is no advantage in using the analytically continued lower-half equation (21). In this case, all the complicated terms, lumped together in the $\mathcal{B}r(\zeta,t)$, become the same order as the other surface energy terms. It is more

convenient to directly analyze the integro-differential equation (2) on $\zeta=\xi+i0$.

A. The case $\frac{1}{2}<\beta\leqslant 1$

As noted previously, for $\mathcal{B}=0$, singularities with $\beta>\frac{1}{2}$ asymptote the real ξ axis as $t\to\infty$. We know, from the analysis in [1], that as a $\frac{1}{2}<\beta\leqslant 1$ singularity nears the real axis, it tends to $\xi=\pm\infty$, unless $\mathrm{Re}\,E_0=0$ (a special nongeneric case). For a singularity with $\frac{1}{2}<\beta<1$, for which $\xi_s\to+\infty$ as it nears the real axis,

$$E_0(t)\sim C_1 t^{1/2},\quad \xi_s(t)\sim(2I_2 t)^{1/2},$$
$$\eta_s\sim -C_3 t^{-1/[2(1-\beta)]},\quad t\to\infty, \tag{44}$$

where C_1 and C_3 are positive constants related to the initial location of the singularity, and I is given by

$$I=\frac{1}{\pi}\int_{-\infty}^{\infty} R(\xi',t)\,d\xi', \tag{45}$$

which is assumed to be a constant, as will be the case for a constant tip velocity (even if the far field is time dependent).

For the case $\beta\equiv 1$, however, the behavior is different, and is given by

$$E_0(t)=E_0(0),\quad \xi_s\sim(2It)^{1/2}, \tag{46}$$

and for $\mathrm{Re}\,E_0>0$, which necessarily corresponds to singularities for which $\xi_s(t)\to+\infty$ as $t\to\infty$ (see [1]),

$$\eta_s\sim -C_3\exp\left[-\frac{2}{\mathrm{Re}(E_0)}\left(\frac{t}{2I}\right)^{1/2}\right],\quad t\to\infty. \tag{47}$$

Similar results hold for $\mathrm{Re}\,E_0<0$, in which case $\xi_s(t)\to-\infty$ as $t\to\infty$. There is an important difference, then, between the special case $\beta=1$ and other singularities in this range: The initial singularity strength, E_0, is preserved in the $\beta=1$ case, whereas for $\frac{1}{2}<\beta<1$, at sufficiently long times, the order of E_0 is always large. Note that this latter point is complicated by the fact that the exact relation between C_1 and $E_0(0)$ is not known. In what follows, we take

$$E_0(t)=\mathcal{B}^{\mu}\hat{E}_0(t), \tag{48}$$

where $\mu\geqslant 0$.

We take $-\eta_s(t)=O(\mathcal{B}^{\delta})$, where δ is to be determined as below, and move toward a derivation of the inner equation. For singularities that were initially at an $O(1)$ distance from the real axis, the results (44) and (47) imply that, at this stage,

$$t=O(\mathcal{B}^{-2\delta(1-\beta)})\quad \text{for } \tfrac{1}{2}<\beta<1,$$
$$t^{1/2}=O(-\mathcal{B}^{\mu}\ln(\mathcal{B}))\quad \text{for } \beta\equiv 1. \tag{49}$$

We decompose the mapping locally as

$$z\sim z_0(t)+\mathcal{B}^{\mu+\delta(1-\beta)}G(\chi,t), \tag{50}$$

$$\xi=\xi_s(t)+\mathcal{B}^{\delta}\chi, \tag{51}$$

where $\xi_s(t)$ is the real part of the singularity location $\zeta_s(t)$. With a view to finding an asymptotic expression for $H(\xi(\chi,t),t)$ for small $\mathcal{B}$, with $\chi=O(1)$, we notice that

$$\begin{aligned}H(\xi,t)-H(\xi_s(t),t)&=\frac{\xi-\xi_s(t)}{\pi}\oint_{-\infty}^{\infty}\frac{d\xi' R(\xi',t)}{(\xi'-\xi)(\xi'-\xi_s)}\\
&=\int_{-\infty}^{\xi_s-\epsilon_1}+\int_{\xi_s+\epsilon_1}^{\infty}+\oint_{\xi_s-\epsilon_1}^{\xi_s+\epsilon_1}d\xi'\,\frac{\xi-\xi_s(t)}{(\xi'-\xi)[\xi'-\xi_s(t)]}R_0(\xi',t)\\
&\quad+\int_{-\infty}^{\xi_s-\epsilon_1}+\int_{\xi_s+\epsilon_1}^{\infty}d\xi'\,\frac{\xi-\xi_s(t)}{(\xi'-\xi)[\xi'-\xi_s(t)]}[R(\xi',t)-R_0(\xi',t)]+\\
&\quad\oint_{-\xi_s-\epsilon_1}^{\xi_s+\epsilon_1}d\xi'\,\frac{\xi-\xi_s(t)}{(\xi'-\xi)[\xi'-\xi_s(t)]}[R(\xi',t)-R_0(\xi',t)],\end{aligned} \tag{52}$$

where $\mathcal{B}^{\delta/3}\ll\epsilon_1\ll\mathcal{B}^{\mu/\beta}$ and R_0 is an outer approximation of R valid to within an error $o(\mathcal{B}^{(2\beta-1)\delta-2\mu})$ for $|\xi-\xi_s|>\epsilon_1$, with the property that locally near $\xi_s(t)$,

$$R_0\sim|E_0|^{-2}[\xi-\xi_s(t)]^{2\beta}. \tag{53}$$

Expanding $(\xi'-\xi)^{-1}$ in powers of $(\xi-\xi_s)$, it is clear that the first two integrals on the right of Eq. (52) have the asymptotic behavior, near $\xi=\xi_s$,

$$\int_{-\infty}^{\xi_s-\epsilon_1}+\int_{\xi_s+\epsilon_1}^{\infty}d\xi'\left[\frac{\xi-\xi_s(t)}{(\xi'-\xi_s)^2}+\frac{[\xi-\xi_s(t)]^2}{(\xi'-\xi_s)^3}+\cdots\right]\times R_0(\xi',t). \tag{54}$$

The third integral on the right of Eq. (52) can be rewritten as

$$\oint_{\xi_s-\epsilon_1}^{\xi_s+\epsilon_1}d\xi'\left[\frac{\xi-\xi_s(t)}{(\xi'-\xi_s)^2}+\frac{[\xi-\xi_s(t)]^2}{(\xi'-\xi_s)(\xi'-\xi_s)^2}\right]R_0(\xi',t), \tag{55}$$

which, when added to contributions from the first two integrals on the right of Eq. (52), written as in Eq. (54), gives an asymptotic contribution for $\beta<1$,

$$\sim \hat{H}_1(t)\mathcal{B}^{\delta}\chi + o(\mathcal{B}^{2\beta\delta-\mu}), \tag{56}$$

where

$$\hat{H}_1 \equiv \frac{\chi}{\pi}\int_{-\infty}^{\infty}\frac{d\xi'}{(\xi'-\xi_s)^2}R_0(\xi',t). \tag{57}$$

In the case of $\beta=1$, $\mu=0$, Eq. (52) has to be modified by an additional contribution, so we have

$$H(\xi,t)-H(\xi_s(t),t)\sim \hat{H}_1(t)\mathcal{B}^{\delta}\chi+\hat{H}_2(t)\mathcal{B}^{2\delta}\chi^2+o(\mathcal{B}^{2\delta}), \tag{58}$$

where

$$\hat{H}_2 \equiv \frac{\chi}{\pi}\int_{-\infty}^{\infty}\frac{d\xi'}{(\xi'-\xi_s)^3}R_0(\xi',t). \tag{59}$$

In general, the last integral in Eq. (52) gives a contribution $\mathcal{B}^{2\beta\delta-2\mu}\tilde{H}$, where

$$\tilde{H}(\chi,t)=\frac{\chi}{\pi}\int_{-\infty}^{\infty}\frac{d\chi'}{\chi'(\chi'-\chi)}[\tilde{R}(\chi',t)-|\hat{E}_0|^{-2}|\chi'|^{2\beta}] \tag{60}$$

and

$$\tilde{R}(\chi,t)=\frac{1-\mathcal{B}^{1-\mu-(2-\beta)\delta}\mathrm{Im}\,\Omega_{\chi}}{|G_{\chi}(\chi,t)|^2}, \tag{61}$$

$$\mathrm{Im}\,\Omega_{\chi}=\int_{-\infty}^{\infty}\frac{d\chi'}{\chi'-\chi}K_{\chi}(\chi,t), \tag{62}$$

$$K(\chi,t)=-\left(1+\alpha\left[1-\frac{1}{|G_{\chi}|^4}\,\mathrm{Re}(G_{\chi}^4 e^{-4i\theta_0})\right]\right)\times\frac{1}{|G_{\chi}(\chi,t)|}\,\mathrm{Im}\left(\frac{G_{\chi\chi}}{G_{\chi}}\right). \tag{63}$$

Combining contributions (56)–(60), we have finally that

$$H(\chi,t)\sim H(\chi_s(t),t)+\mathcal{B}^{\delta}\chi\hat{H}_1(t)+\mathcal{B}^{2\delta}\chi^2\hat{H}_2(t)+\mathcal{B}^{2\beta\delta-2\mu}\tilde{H}(\chi,t) \tag{64}$$

and $\hat{H}_2(t)\equiv 0$ for $\beta\neq 1$.

With this approximation of H for $\chi=O(1)$ and the result

$$R(\xi(\chi,t),t)\sim \mathcal{B}^{2\beta\delta-2\mu}\tilde{R}(\chi,t), \tag{65}$$

it follows from substituting Eqs. (50) and (51) into Eq. (2) that in the limit $\mathcal{B}\to 0$, $\chi=O(1)$, we have

$$G_t=\{\hat{H}_1(t)\chi+\mathcal{B}^{\delta}\hat{H}_2(t)\chi^2+\mathcal{B}^{\beta\delta-\mu}[\tilde{H}(\chi,t)+i\tilde{R}(\chi,t)]\}G_{\chi} \tag{66}$$

provided we choose

$$\dot{\xi}_s(t)=-H(\xi_s(t),t). \tag{67}$$

There are two distinct subcases examined below.

1. A not-too-weak singularity: $\mu<\beta/2$

In this subcase, an appropriate choice for δ is

$$\delta=\frac{(1-\mu)}{2-\beta}, \tag{68}$$

which makes the surface-energy term $O(1)$ in the expression for $\tilde{R}$ in Eq. (61). Since the inner region scales like $\mathcal{B}^{\delta}\ll\mathcal{B}^{\mu/\beta}$, the outer asymptotic behavior $z_{\zeta}\sim E_0(\zeta-\xi_s)^{-\beta}$ determines the matching condition $G_{\chi}\sim\chi^{-\beta}$ as $\chi\to\pm\infty$. We also note that the term $\mathcal{B}^{\delta}\hat{H}_2(t)\chi^2=O(\mathcal{B}^{\beta\delta-\mu})$ only when $\mu\equiv 0$ and $\beta\equiv 1$, but is otherwise small and hence neglected. That surface-energy effects cannot occur to the leading order in $O(1)$ time follows by noticing that if we were to write an equation for the next order regular perturbation term z_1, then the equation has a forcing $\mathcal{B}\,\mathrm{Im}\omega_{0\xi}/(z_{0\xi}^*)$ that is not large near $\xi=\xi_s(t)$.

It is convenient to introduce the parameter

$$\Delta\equiv\mathcal{B}^{\beta\delta-\mu}, \tag{69}$$

which is small in this regime. It is clear from Eq. (66) that the surface-energy effects enter on a long time scale. If

$$\tilde{t}\equiv\Delta t, \tag{70}$$

we expect that

$$G\sim G_0(\chi,t,\tilde{t})+\Delta G_1(\chi,t,\tilde{t})+\cdots, \tag{71}$$

which leads to

$$G_{0t}=(\hat{H}_1)_0 G_{0\chi}. \tag{72}$$

Since the integral occurring in $\hat{H}_1$ is in fact $-\dot{\eta}_s/\eta_s$, the solution to Eq. (72) is given by

$$G_0=G_0(\chi/\eta_s(\overline{t}),\tilde{t})\equiv G_0(\tilde{\chi},\tilde{t}), \tag{73}$$

where

$$\tilde{\chi}=\chi/(-\eta_s). \tag{74}$$

For $\tilde{t}\ll 1$, one gets essentially the zero-surface-energy solution, rewritten in the inner variables,

$$G_0(\tilde{\chi},\tilde{t})\sim\frac{c}{1-\beta}(\tilde{\chi}+i)^{1-\beta}, \tag{75}$$

where $C_1C_3=\mathcal{B}^{\mu}(c/1-\mathcal{B})$ for $\beta<1$ and $E_0(0)=c\mathcal{B}^{\mu}$ for $\beta=1$.

It is convenient also to decompose both $\tilde{R}$ and $\tilde{H}$ obtained by substituting $G_{\chi}=G_{0\tilde{\chi}}(-\eta_s)$ into those expressions and writing

$$\tilde{H}+i\tilde{R}=\eta_s^2[\tilde{H}_0(\tilde{\chi},\tilde{t})+i\tilde{R}_0(\tilde{\chi},\tilde{t})]-\eta_s[\acute{H}_0(\tilde{\chi},\tilde{t})+i\acute{R}_0(\tilde{\chi},\tilde{t})], \tag{76}$$

where

$$\tilde{R}_0(\tilde{\chi},\tilde{t})=\frac{1}{|G_{0\tilde{\chi}}(\tilde{\chi},\tilde{t})|^2}, \tag{77}$$

$$\tilde{H}_0(\tilde{\chi},\tilde{t})=\frac{\tilde{\chi}}{\pi}\int \frac{d\tilde{\chi}'}{\tilde{\chi}'(\tilde{\chi}'-\tilde{\chi})}[\tilde{R}_0(\tilde{\chi},\tilde{t})-c^{-2}\tilde{\chi}^{2\beta}], \tag{78}$$

$$\acute{R}_0\equiv-\frac{\mathrm{Im}(\Omega_{0\tilde{\chi}})}{|G_{0\tilde{\chi}}|^2}, \tag{79}$$

$$\acute{H}_0=\frac{\tilde{\chi}}{\pi}\int_{-\infty}^{\infty}\acute{R}_0(\chi')\frac{d\chi'}{(\chi'-\tilde{\chi})\chi'}. \tag{80}$$

Then, G_1 obeys

$$G_{1t}(\tilde{\chi},t,\tilde{t})=-\eta_s(t)[\tilde{H}_0+i\tilde{R}_0+\hat{H}_2(t)\tilde{\chi}^2]G_{0\tilde{\chi}} +(-G_{0\bar{t}}+[\acute{H}_0+i\acute{R}_0]G_{0\tilde{\chi}}). \tag{81}$$

We note $\eta_s(t)$ is integrable up to $t=\infty$. Also, it can safely be assumed that $\hat{H}_2(t)$ (which is an average feature of the interface) is bounded in time, so that the integral of $\eta_s(t)\hat{H}_2(t)$ exists all the way to $t=\infty$. Thus, the only term that can give rise to a secular growth in G (in this case a linear function of t) is the last term. We can avoid this secular growth by requiring that G_0 evolve in slow time $\tilde{t}$ in such a way that that the last term vanishes,

$$G_{0\tilde{t}}=(\acute{H}_0+i\acute{R}_0)G_{0\tilde{\chi}}. \tag{82}$$

It is to be noted from Eqs. (44) and (68)–(70) that for fixed $\beta<1$, by the time surface-energy effects begin to have an impact [i.e., $t=O(1/\Delta)$], the disturbance causes a local indentation on the physical interface over an arc-length distance

$$O(\mathcal{B}^{\delta}\eta_s(t))^{1-\beta}=O(\mathcal{B}^{1/2}\tilde{t}^{-1/2}). \tag{83}$$

This result is not unexpected, since a linear stability analysis of a planar interface suggests that surface energy effects become significant when the local wavelength is $O(\mathcal{B}^{1/2})$.

For $\beta=1$, it follows from Eqs. (47) and (68)–(70) that by the time surface energy becomes important, this pole will have caused a relatively deep indentation on the interface (see Fig. 6), for

$$\tilde{t}=O(-\mathcal{B}^{\mu}\ln[-\eta_s(t)])=O(\mathcal{B}^{\mu-1/2}\sqrt{\tilde{t}})\gg 1, \tag{84}$$

with indentation width $\pi E_0(0)=O(\mathcal{B}^{\mu})\gg\mathcal{B}^{1/2}$, since the condition $\mu<\beta/2$ translates to $\mu<\frac{1}{2}$ when $\beta=1$.

We do not discuss here the details of the borderline case $\mu=\beta/2$, for which it is clear that $\Delta=1$, so that there is no separation of slow and fast time scales. In the next subsection, we discuss the case of weak singularities for $1\geqslant\beta>\frac{1}{2}$.

We note that while we have not discussed the solution to Eq. (82), there is prior work in the context of the Hele-Shaw cell [18,19] that is immediately relevant since Eq. (82) is precisely the equation of interfacial motion in the case when there is no fluid suction or injection, i.e., when the interface relaxes due to surface energy effects only. It has been rigorously shown [18] that if the interface is initially close to circular in a radial geometry, it relaxes to a circle. However, numerical evidence [19] suggests that for a sufficiently deformed interface (as in the shape of a dumbbell), the interface can pinch-off due to surface-energy effects. Extrapolating that result here for this geometry, we expect that for $\bar{t}\gg 1$, the interfacial deformation will relax to a planar interface unless the deformation is very large, in which case the interface may pinch-off.

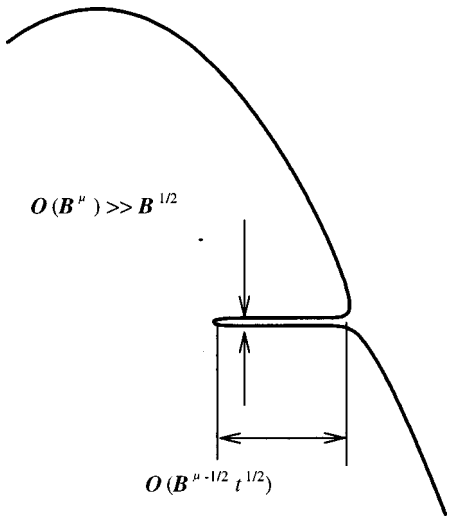

FIG. 6. Stage when surface energy becomes important at the interface for a $\beta=1$ singularity.

2. Weak singularity: $\mu>\beta/2$

This case can arise only if the initial singularity location is so close to the axis that $-\eta_s(0)=O(\mathcal{B}^{\mu/\beta})$. Otherwise, from analysis of the preceding section, we know that, for $\mu\geqslant\beta/3$, the singularity is dissipated over a fast time scale, before it can impact the real axis. So, we consider here only singularities in this class that are initially very close to the real axis.

In this case, it is appropriate to choose

$$\delta=\mu/\beta \tag{85}$$

and a fast time scale

$$\bar{t}=\mathcal{B}^{1-2\mu/\beta}t. \tag{86}$$

Then, from Eq. (66), it follows that the leading-order evolution equation is now given by

$$G_{\bar{t}}=(\acute{H}_0+i\acute{R}_0)G_{\chi}, \tag{87}$$

where

$$\acute{R}_0\equiv-\frac{\mathrm{Im}(\Omega_{0\chi})}{|G_{0\chi}|^2}, \tag{88}$$

$$\acute{H}_0=\frac{\chi}{\pi}\int_{-\infty}^{\infty}\acute{R}_0(\chi')\frac{d\chi'}{(\chi'-\chi)\chi'}. \tag{89}$$

The far-field matching condition in this case must reflect the local outer behavior

$$z_{0\xi} \sim A_0(t) + E_0(t)[\xi - \xi_s(t) - i\eta_s(t)]^{-\beta}. \tag{90}$$

We do not solve Eqs. (87)–(89) here, but note that such singularities for $\beta < 1$ correspond to distortions of the physical interface that are localized over an arc length of

$$O(\mathcal{B}^{\mu+\delta(1-\beta)}) = O(\mathcal{B}^{\mu/\beta}).$$

For $\beta = 1$, the total length of indentation associated with the approach of the $\beta = 1$ singularity is $O(\mathcal{B}^{\mu-1/2}) \ll 1$, whereas the width of the indentation is

$$\mathcal{B}^{\mu} \ll \mathcal{B}^{1/2}.$$

In either case, the smallest length scale associated with the disturbance is much smaller than the capillary length, and from physical considerations it is expected to dissipate very quickly [i.e., over a $\bar{t} = O(1)$ scale].

We therefore conclude that the weak singularities, initially close to the real axis, will be wiped out by surface-energy effects over a fast time scale, just like similarly weak singularities further out.

How do the results in Sec. III A relate to queries in item (ii) in Sec. I? If singularities of the type $\frac{1}{2} < \beta \leqslant 1$ are too weak, i.e., $\mu > \beta/2$, then they are dissipated by surface-energy effects over a fast scale so that the effect of such singularities of the corresponding zero-surface-energy problem are not relevant to interfacial deformations. Earlier in Sec. II C, we stated that weak initial singularities satisfying the criteria $\mu > \beta/3$ that are at $O(1)$ distance from the real axis are wiped out by surface-energy effects on a fast time scale before they can make their effects felt on the real axis. Thus, only those singularities satisfying the restriction $\frac{1}{2} > \beta \geqslant \frac{1}{3}$ that are initially close to the real axis can possibly influence interfacial deformation only for a short time.

For stronger singularities, i.e., $\mu < \beta/2$, surface energy and anisotropy effects act on a much longer time scale than the time scale of the dendrite tip advance, as implicit in Eq. (70). The approach of such zero-surface-energy singularities affects the visible features of the interface, though they do not cause actual interfacial singularities, having failed to reach the real axis in finite time. Since the poles ($\beta = 1$) approach most rapidly, the interfacial features will be dominated by parallel-sided indentations that become deeper in time, until surface-energy effects dissipate them over a long time scale $\mathcal{B}^{\mu-1/2}$, over which there is no trace left of the singular nature $(\zeta - \zeta_s)^{-\beta}$ of z_ζ. The anisotropy, while important in the inner-equation dynamics, plays no role in this scaling.

B. The case $0 < \beta < \frac{1}{4}$

In the absence of surface energy, this class of singularities hits the real axis in finite time and the inner region around ζ_s is now defined when surface-energy effects appear in the leading-order approximation of R. Here, for the sake of simplicity of exposition, we will limit our discussion to $E_0(0) = O(1)$, i.e., $\mu = 0$. Weaker singularities dissipate even faster and have an even weaker impact on the interface.

We introduce inner space and time variables χ, τ in accordance with

$$\xi = \xi_s(t) + \mathcal{B}^{\delta}\chi, \tag{91}$$

$$t = t_c + \mathcal{B}^{2-3\delta}\tau, \tag{92}$$

where t_c is the singularity impact time for $\mathcal{B} \equiv 0$. We also introduce an inner dependent variable,

$$z(\xi, t) = z_0(t) + \mathcal{B}^{1-\delta}G(\chi, \tau), \tag{93}$$

where

$$\delta = \frac{1}{2(1-\beta)}. \tag{94}$$

We notice that with this use of rescaled variables,

$$\mathrm{Im}(\omega_\xi)(\xi, t) = \mathcal{B}^{-1}\ \mathrm{Im}(\Omega_\chi)(\chi, \tau), \tag{95}$$

where $\mathrm{Im}\,\Omega_\chi$ is defined below in Eq. (102). Thus, with the choice of δ in Eq. (94), the surface-energy term $\mathcal{B}\ \mathrm{Im}\ \omega_\xi$ in Eq. (3) is $O(1)$. The choice of scale factors $\mathcal{B}^{2-3\delta}$ and $\mathcal{B}^{1-\delta}$ in Eqs. (91) and (93) reflects the need to include surface-energy modifications in the leading-order inner equation and to match G_χ to the outer solution, whose local behavior in the matching region is given by

$$z_{0\xi} \sim E_0(t)(\xi - \xi_s - i\eta_s)^{-\beta} \ \text{ for } \ \mathcal{B}^{\delta} \ll |\xi - \xi_s(t)| \ll E_0^{1/\beta}. \tag{96}$$

In order to obtain the leading-order inner equation, it is convenient to rewrite $H(\xi, t)$ in the form (52). Substituting Eqs. (91), (92), and (93) into Eqs. (2), (3), (5)–(8), and (52), one finds in the limit $\mathcal{B} \to 0$ the evolution equations

$$\dot{z}_0(t) = 0, \tag{97}$$

$$\dot{\xi}_s(t) = -H(\xi_s(t), t), \tag{98}$$

$$G_\tau = (H_1 + iR)G_\chi, \tag{99}$$

where

$$H_1(\chi, \tau) = \frac{\chi}{\pi} \int_{-\infty}^{\infty} \frac{d\chi' R(\chi', \tau)}{\chi'(\chi' - \chi)}, \tag{100}$$

$$R(\chi, \tau) = \frac{1 - \mathrm{Im}(\Omega_\chi)}{|G_\chi|^2}, \tag{101}$$

$$\mathrm{Im}(\Omega_\chi) = -\frac{1}{\pi} \int_{-\infty}^{\infty} \frac{d\chi'}{\chi' - \chi} \left\{ \frac{\partial K}{\partial \chi}(\chi, \tau) \right\}, \tag{102}$$

$$K(\chi, \tau) = [1 + \alpha f(\chi, \tau)]\kappa(\chi, \tau), \tag{103}$$

$$f(\chi, \tau) = 1 - \frac{1}{|G_\chi|^4}\ \mathrm{Re}(G_\chi^4 e^{-i4\theta_0}), \tag{104}$$

$$\kappa(\chi, \tau) = -\frac{1}{|G_\chi|}\ \mathrm{Im}\left(\frac{G_{\chi\chi}}{G_\chi} \right). \tag{105}$$

Except for the differences between H_1 and H, the integro-differential equation (99) is of the form (2) with scaled variables χ and τ replacing ξ and t, $\mathcal{B}$ being renormalized to 1. The anisotropy α remains a parameter in the equations. Indeed, the inner equations are the same for any $O(1)$ anisotropy, since on the real axis, $f=1-\alpha\cos 4(\theta-\theta_0)$ is always $O(1)$.

We also need the matching conditions to earlier time ($\tau\to-\infty$) and to the outer solution ($\chi\to\infty$). The outer and earlier-time solutions on the real axis are given by Eq. (96). Since

$$\eta_s\sim -c_2\mathcal{B}^{\delta}(-\tau)^{1/1-4\beta}, \tag{106}$$

$$E_0(t)\sim\alpha_1\mathcal{B}^{1-(2-\beta)\delta}(-\tau)^{-\beta/1-4\beta}\quad\text{as}\quad\tau\to-\infty, \tag{107}$$

where the expressions for η_s and E_0 are obtained from [1], the matching conditions become

$$G_\chi\sim c_1(-\tau)^{-\beta/1-4\beta}[\chi+ic_2(-\tau)^{1/1-4\beta}]^{-\beta}$$

$$\text{as}\quad\chi\to\infty\quad\text{or}\quad\tau\to-\infty. \tag{108}$$

We do not know much about the solution to Eq. (99). However, a few things can be deduced simply from the scaling in Eq. (93) and the earlier-time matching condition (108). It is clear that the disturbance associated with this singularity is localized in the physical domain to an arc-length distance of $O(E_0(0)\mathcal{B}^{(1-2\beta)/[2(1-\beta)]}(-\tau)^{-\beta/(1-4\beta)})\ll\mathcal{B}^{1/2}$ for $\tau=O(1)$. It is known from a local linearized stability analysis that disturbances associated with local wave numbers much larger than $\mathcal{B}^{-1/2}$ quickly dissipate. Thus, it is to be expected that the solutions G to Eq. (99) will tend to zero over a fast time scale τ; perhaps even before $-\tau=0$, beyond which the matching condition (108) cannot hold. Thus, beyond $O(\mathcal{B}^{1/[2(1-\beta)]})$, after impact time t_c, one can expect such singularity effects to be absent in the interfacial indentations.

A sketch (Fig. 7) illustrates the localization and indentation caused by such a singularity before it dissipates, addressing issue (iii) in Sec. I.

C. Implications of scaling results for indentation dimensions

Having discussed how surface energy affects singularities close to the real axis, we highlight here a few implications for spatial and temporal scales of indentations on the physical interface. As before, we define μ in accordance to the relation $E_0=O(\mathcal{B}^{\mu})$. The subsections III C 1 and III C 2 address issue (iv) in Sec. I.

1. Stationarity of indentation in the lab frame

First, we show that an indentation corresponding to the approach of a $\beta>0$ complex singularity is stationary in the laboratory frame on the $O(1)$ time scale over which the tip advances. Stationary indentations are well known in experiment [20]. However, we are unaware of any analytical derivation of this property for the fully nonlinear problem, though it is a remarkably simple consequence of our formulation (2).

Our results in the preceding subsection suggest that a disturbance associated with a complex singularity at $\zeta_s=\xi_s(t)+i\eta_s(t)$ with $|\eta_s(t)|$ sufficiently small corresponds to a disturbance centered at a physical point $z=z(\xi_s(t),t)$, where $\xi_s(t)=-H(\xi_s(t),t)$. However, from Eq. (2), it is clear that

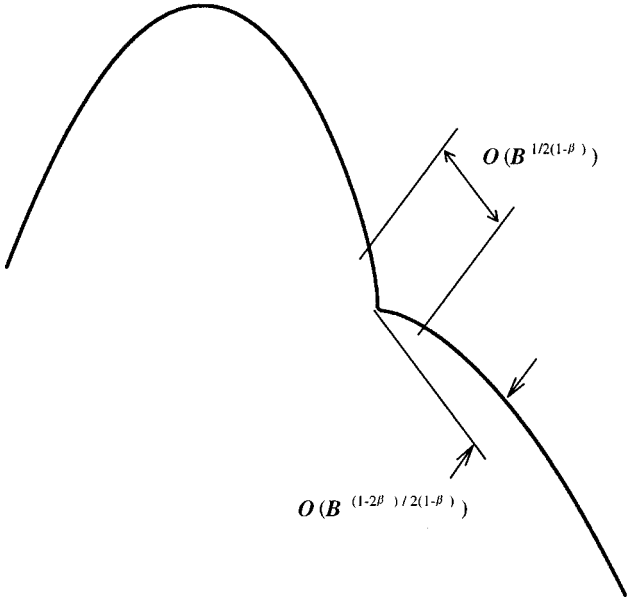

FIG. 7. Stage when surface energy becomes important at the interface for a singularity with $0<\beta<1/4$.

$$\frac{d}{dt}z(\xi_s(t),t)=\frac{i[1-\mathcal{B}\ \mathrm{Im}\ \omega_\xi(\xi_s(t),t)]}{|z_\xi(\xi_s(t),t)|}. \tag{109}$$

For each of the cases dealt with in the preceding subsection, it is clear that for singularities that do not dissipate quickly, the right-hand side of Eq. (109) is $O(\mathcal{B}^{\beta\delta-\mu})\ll 1$. Thus as $\mathcal{B}\to 0$, we obtain the asymptotic result that the corresponding $z(\xi_s(t),t)$ is stationary, but only on an $O(1)$ time scale—the time scale of tip motion.

There is a longer time scale, identified here as $O(\mathcal{B}^{(\mu-\beta\delta)})$, over which the geometric nature of the indentation also changes. We also note that without the i factor, the right-hand side of Eq. (109) is simply the normal velocity of the interface at a point corresponding to $\xi_s(t)$. Over the longer time scale this indentation can advance along y, i.e., along the tip-advance direction.

2. Growth of disturbances

It is possible to comment on the nonlinear growth of the disturbances as a function of $|y|$, $|y|$ being the axial distance from the dendrite tip, provided we assume that the dendrite tip is moving at a constant speed. There is no assumption that the background state is globally steady, as assumed in previous calculations [7,21]. It is clear that a t dependence on the growth of a disturbance translates into a similar $|y|$ dependence, since $|y|=It$ for a dendrite tip moving uniformly. In [1], we quoted the result that the localized disturbance associated with the approach of a conformal-mapping singularity grows in a most pronounced way for $\beta=1$ (simple pole), causing z_ζ, associated with this singularity, to grow exponentially like

$$\exp\left[\frac{1}{\mathrm{Re}\,E_0}\left(\frac{2|y|}{I^2}\right)^{1/2}\right] \quad \text{for } \beta=1 \tag{110}$$

if $\mathrm{Re}\,E_0\neq 0$ and for

$$P^{-1}\gg|y/I|\gg\max\{1,(\mathrm{Im}\,E_0/\mathrm{Re}\,E_0)^2\},$$

where it is assumed $P^{-1}\gg(\mathrm{Im}\,E_0/\mathrm{Re}\,E_0)^2$. Relation (110) implies that the depth of the indentation grows as $O(E_0/\mathrm{Re}\,E_0\sqrt{2y/I^2})$, while its width remains constant at $\pi|E_0|$. When $\mathrm{Re}\,E_0$ is small relative to $\mathrm{Im}\,E_0$ and

$$\left(\frac{\mathrm{Im}\,E_0}{\mathrm{Re}\,E_0}\right)^2\gg\frac{y}{I}\gg\left|\frac{\mathrm{Im}\,E_0}{\mathrm{Re}\,E_0}\right|,$$

then z_ξ associated with the pole grows as

$$\exp\left(\frac{|y|}{I\ \mathrm{Im}\,E_0}\right). \tag{111}$$

Ultimately, for large enough $|y|$, Eq. (110) becomes valid unless $\mathrm{Re}\,E_0=0$ (a nongeneric case). However, the zero-surface-energy dynamics places no restriction on how small $\mathrm{Re}\,E_0$ can be. We now explore how surface energy does pose a restriction. There are two subcases, depending on whether or not the pole that causes the indentation is initially close to the real axis.

a. Poles initially close to the real axis. We learned in Sec. III A that if poles initially located close to the real axis are sufficiently weak, in the sense that $\mu>\frac{1}{2}$, then their effects on the interface far from the tip will not be observed since they will be quickly dissipated by surface-energy effects. This leaves us with the restriction $\mu<\frac{1}{2}$. Now, there are two possible cases to examine: (a) $\mathrm{Re}\,E_0=O(|E_0|)=O(\mathcal{B}^\mu)$ and (b) $\mathrm{Re}\,E_0/\mathrm{Im}\,E_0=O(\mathcal{B}^{\hat\alpha})$ for $\hat\alpha>0$.

(i) Growth rate for Re $E_0=O(E_0)=O(\mathcal{B}^\mu)$. In this case, it is clear that requiring $\mu<\frac{1}{2}$ places an effective restriction: $\mathrm{Re}\,E_0\gg\mathcal{B}^{1/2}$, implying from Eq. (110) that the complex singularity causes the associated localized deviation of z_ξ (from the background state) to grow no faster than

$$\exp(k_1\mathcal{B}^{-1/2}\sqrt{|y|/I^2}) \tag{112}$$

for $1\ll|y/I|\ll P^{-1}$ and $|y/I|\ll\mathcal{B}^{-1+2\mu}$ (so that surface-energy effects have not wiped out any remnant of this singularity). In Eq. (112), the constant k_1 is independent of $\mathcal{B}$. The corresponding indentation depth (see Fig. 8) grows algebraically as

$$\sqrt{|y|/I^2} \tag{113}$$

while the indentation width has a lower limit $O(\mathcal{B}^{1/2})$. It is to be noted that as μ becomes progressively closer to the lower limit $\frac{1}{2}$, the upper bound (112) is closer to being attained; however, the range of $|y|$ for which the growth result (112) holds is restricted since $\mathcal{B}^{-1+2\mu}\to 1$ in that limit.

(ii) Growth rate for Re E_0/Im $E_0=O(\mathcal{B}^{\hat\alpha})\ll 1$, with $E_0=O(\mathcal{B}^\mu)$. In this case, $|y|\gg\mathcal{B}^{-2\hat\alpha}$ before the result (110) can apply. However, surface-energy effects become significant for $t=|y|/U=O(\mathcal{B}^{-1+2\mu})$, with $\mu<\frac{1}{2}$, and will dissipate the pole indentation only over this long time scale. So,

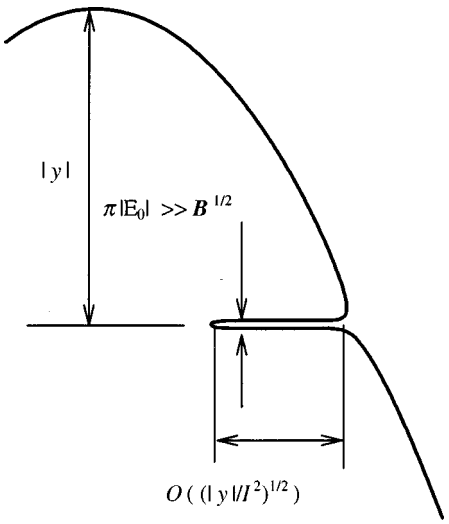

FIG. 8. Interfacial growth for a pole singularity with $\mathrm{Re}\,E_0=O(E_0)=O(\mathcal{B}^\mu)$.

for the results on growth rate to be relevant, it is necessary that $\mathcal{B}^{-2\hat\alpha}\ll|y|\ll\mathcal{B}^{-1+2\mu}$. Thus, we need

$$\hat\alpha<-\mu+\tfrac{1}{2}. \tag{114}$$

Equation (110) implies that z_ξ associated with the pole locally grows as

$$\exp(k_1\mathcal{B}^{-\mu-\hat\alpha\delta}\sqrt{|y|/I^2}). \tag{115}$$

Given the restriction (114), it follows that the above is again limited by Eq. (112), with corresponding indentation depth

$$\mathcal{B}^{-\hat\alpha}\sqrt{y/I^2} \tag{116}$$

and width $O(\mathcal{B}^\mu)\gg\mathcal{B}^{1/2}$. In the intermediate case, when $\mathcal{B}^{-\hat\alpha}\ll|y/I|\ll\mathcal{B}^{-2\hat\alpha}$, it follows that z_ξ associated with the complex singularity grows like

$$\exp(k_1\mathcal{B}^{-\mu}|y/I|) \tag{117}$$

and this is sharply bounded by an expression of the type

$$\exp(k_1\mathcal{B}^{-1/2}|y/I|). \tag{118}$$

The corresponding indentation depth in this regime scales as

$$|y/I|. \tag{119}$$

Notice, however, that for the largest growth rate $\mu\to\frac{1}{2}^-$ and hence $\hat\alpha\to 0$—in that case, there is a shrinkage in the intermediate range of $|y|$ for which the above growth applies. Thus, in all cases, Eqs. (112) and (113) accurately describe the largest possible growth.

b. Poles initially far from the real axis. We discussed in Sec. II C that singularities that are not too close to the real axis, but so weak that $\mu>\beta/3$, dissipate on a fast time scale. Therefore, the effect of such singularities will not be observed in interfacial indentation. Therefore, we have a cutoff $\mu<\beta/3$, which for poles means that

$$\mu<\tfrac{1}{3}. \tag{120}$$

With this cutoff, it follows that if $\mathrm{Re}\, E_0 = O(|E_0|)$, then the growth rates of the associated localized deviation of z_ζ from the background state will be bounded by

$$\exp(k_1 \mathcal{B}^{-1/3} \sqrt{y/I^2}). \tag{121}$$

The indentation width, however, still scales with

$$\sqrt{y/I^2} \tag{122}$$

and its width scales as $O(\mathcal{B}^{1/3}) \gg \mathcal{B}^{1/2}$. On the other hand, if $\mathrm{Re}\, E_0 = O(\mathcal{B}^{\hat{\alpha}} E_0)$, then the previous analysis still holds, yielding results (112) and (113). Note that anisotropy, while important in the inner-equation dynamics, does not play any role in the scaling above.

We conclude by observing that surface-energy effects put effective restrictions on the growth rates of disturbances associated with the complex singularities considered here. We have thus addressed the issues raised in point (iv) of Sec. I.

3. Coarsening due to an ensemble of poles

In [1], we described a scenario for coarsening in terms of the approach of poles of differing strengths. However, in that $\mathcal{B} \equiv 0$ analysis, there was no mechanism for scale selection. We extend that scenario here by considering surface-energy effects.

From the above results for a specific singularity, we could alternately pose the following situation: Suppose there is an initial distribution of many poles, with varying strengths, satisfying $\mathrm{Re}\, E_0 = O(E_0)$. (Note, if $\mathrm{Re}\, E_0$ is relatively too small compared to $\mathrm{Im}\, E_0$, the resulting interface distortion is more in the form of tip-splitting than side-branching.) Suppose we examine large distances $|y|$ from the tip, but with $|y/I| \ll P^{-1}$, so that we are in region I, and $|y/I| \ll \mathcal{B}^{-1}$, so that surface energy has not dissipated poles for which E_0 is strictly order 1. We can ask the following question: What is the value of E_0 that contributes most to the indentation seen at that location? Since surface energy acts over a time scale $\mathcal{B}^{-1+2\mu}$, it follows that the value of μ that contributes maximally is determined by the relation

$$\mathcal{B}^{1-2\mu_m} |y/I| = O(1). \tag{123}$$

Values for $\mu < \mu_m$ correspond to larger $\mathrm{Re}\, E_0$ in the relation (110) and therefore have smaller growth rates. Poles corresponding to values of $\mu > \mu_m$, but within the range $\mu < \frac{1}{2}$, will have dissipated before reaching y (corresponding to $t = |y|/I$). Solving for μ_m in Eq. (123) and using $E_m = O(\mathcal{B}^{\mu_m})$, we obtain

$$E_m = k \mathcal{B}^{1/2} \sqrt{y/I} \tag{124}$$

for some constant k. Therefore, the indentation width $\pi |E_m|$ associated with such poles is $O(\mathcal{B}^{1/2} \sqrt{y/I})$. This can be viewed as a coarsening characteristic. The $\sqrt{|y|}$ dependence of coarsening, found here, differs from the theoretical $|y|^{1/3}$ rate found by Voorhees and Glicksman [22] from very general considerations of a mean-field theory. However, there need not be any contradiction since the results quoted here are valid for the intermediate range $1 \ll |y/I| \ll \mathcal{B}^{-1}$, before surface energy has had a chance to fully affect indentations of $O(1)$ widths. It is interesting to note that, in the experiments cited in the same reference, the kinetic coarsening exponents vary between $\frac{1}{4}$ and $\frac{1}{2}$, though the authors express doubt about whether ''asymptotic'' coarsening conditions were met in these experiments.

IV. PERTURBATION NEAR A ZERO NOT CLOSE TO THE REAL AXIS

First, we note that general initial conditions, including those containing poles only, contain zeros of z_ζ, where z is otherwise analytic. In this section, we restrict discussion to an initial simple zero, whose initial distance from the real axis is much greater than $\mathcal{B}^{2/7}$. For zeros that are closer, see Sec. V C.

A. Regular perturbation expansion and nonuniformities

We now examine how an assumed regular perturbation for z_ζ in the form (22) becomes disordered near a zero at $\zeta = \zeta_0(t)$. The procedure followed here is similar to that described in Sec. II, except that we replace powers of $[\zeta - \zeta_s(t)]$ by $[\zeta - \zeta_0(t)]$. In the neighborhood of a zero,

$$z_{0\zeta} \sim z_{0\zeta\zeta}(\zeta_0(t),t)[\zeta - \zeta_0(t)], \tag{125}$$

where the speed of a zero is given by

$$\dot{\zeta}_0 = -q_1(\zeta_0(t),t) - \frac{q_{2_\zeta}(\zeta_0(t),t)}{z_{0\zeta\zeta}(\zeta_0(t),t)}. \tag{126}$$

It is found in a sufficiently close neighborhood of $\zeta_0(t)$ that a particular solution to z_1 satisfying Eq. (32) has the local asymptotic behavior

$$z_{1_\zeta} \sim A_0(t)[\zeta - \zeta_0(t)]^{-5/2} + \alpha F_0(t)[\zeta - \zeta_0(t)]^{-9/2} \tag{127}$$

for $t > 0$, where

$$A_0(t) = -\frac{3}{2i} \frac{z_{0\zeta\zeta}^{1/2}(\zeta_0(t),t)}{\tilde{z}_{0\zeta}^{3/2}(\zeta_0(t),t) q_{2_\zeta}(\zeta_0(t),t)}, \tag{128}$$

$$F_0(t) = \frac{7}{4i} e^{i4\theta_0} \frac{\tilde{z}_{0\zeta}^{1/2}(\zeta_0(t),t)}{z_{0\zeta\zeta}^{3/2}(\zeta_0(t),t) q_{2_\zeta}(\zeta_0(t),t)}. \tag{129}$$

However, the behavior (127) is not uniformly valid as $t \to 0^+$ since for initial conditions independent of $\mathcal{B}$, $z_1(\zeta,0) = 0$ is required. In order to correct Eq. (127) so that it is uniformly valid for small t as well, we notice that the associated homogeneous equation for z_1 from Eq. (32) has a solution z_H with local singular behavior

$$z_{H_\zeta} \sim A_1(t)[\zeta - \zeta_d(t)]^{-5/2} + \alpha F_1(t)[\zeta - \zeta_d(t)]^{-9/2} \tag{130}$$

near $\zeta = \zeta_d(t)$, where

$$\dot{\zeta}_d(t) = -q_1(\zeta_d(t),t), \tag{131}$$

$$A_1(t) = A_1(0) \exp\left(-\tfrac{3}{2} \int_0^t dt' q_{1_\zeta}(\zeta_d(t'),t') \right), \tag{132}$$

$$F_1(t)=F_1(0)\exp\left(-\tfrac{7}{2}\int_0^t dt' q_{1_\zeta}(\zeta_d(t'),t')\right). \quad (133)$$

By choosing

$$\zeta_d(0)=\zeta_0(0), \quad A_1(0)=-A_0(0), \quad F_1(0)=-F_0(0), \quad (134)$$

the sum of the local expressions (127) and (130) tends to zero as $t\to 0$ for fixed $\zeta-\zeta_0\neq 0$, as required. Thus, a uniformly valid expression in t for the local singular behavior near $\zeta=\zeta_0(t)$ is

$$z_{1_\zeta}\sim A_0(t)[\zeta-\zeta_0(t)]^{-5/2}+\alpha F_0(t)[\zeta-\zeta_0(t)]^{-9/2} + A_1(t)[\zeta-\zeta_d(t)]^{-5/2}+\alpha F_1(t)[\zeta-\zeta_d(t)]^{-9/2}. \quad (135)$$

For t not too small, it is clear that Eq. (127) still describes the local asymptotic behavior. However, the introduction of a new singular point at $\zeta=\zeta_d(t)$ in Eq. (135), which moves with speed (131), different from the speed of the zero located at $\zeta=\zeta_0(t)$ [see Eq. (126)], ensures that these two points separate from each other with time.

This appearance of a new singularity means that the regular perturbation expansion $z_{0_\zeta}+\mathcal{B}z_{1_\zeta}+\cdots$ breaks down at a point $\zeta_d(t)$, where its local behavior for t not too small is described by

$$z_\zeta\sim z_{0_\zeta}(\zeta_d(t),t)+\mathcal{B}A_1(t)[\zeta-\zeta_d(t)]^{-5/2} + \mathcal{B}\alpha F_1(t)[\zeta-\zeta_d(t)]^{-9/2}. \quad (136)$$

Note that the zero-surface-energy solution z_{0_ζ} is neither singular nor zero at $\zeta=\zeta_d(t)$ for $t>0$. This new singularity we name, as elsewhere (cf. [2,11]), a ''daughter singularity,'' since it is ''born'' out of the initial zero $\zeta_0(0)$ at $t=0^+$ through surface-energy effects. Note that this daughter singularity, at $\zeta=\zeta_d$, moves like any other singularity of the $\mathcal{B}=0$ problem, and therefore necessarily approaches the real axis, unlike its parent, $\zeta_0(t)$, which may or may not. We emphasize that a daughter singularity corresponding to each initial zero is not a singularity of z_ζ or even $z_{0\zeta}$, but only of $z_1,z_2,\ldots$ of the outer asymptotic expansion (22), which is itself invalid at $\zeta=\zeta_d$.

At very early times, there is no distinction between the inner region of the daughter and that of the zero $\zeta_0(t)$ of z_{0_ζ}. As we will see in what follows, similar to the isotropic Hele-Shaw flow, the solution to the inner equation contains many actual singularities of z_ζ. Thus, $\zeta_d(t)$ defines the center of a (daughter) singularity cluster, until the time when $\zeta_d(t)$ impacts the real axis. Beyond that time, all the actual singularities within such a cluster disperse. The concept of a daughter singularity cluster ceases to be meaningful beyond the impact time.

An examination of the equation for z_2 (and $z_3,\ldots$) indicates that there are no further points aside from ζ_s, $\zeta_0(t)$, and $\zeta_d(t)$, where the regular perturbation expansion in powers of $\mathcal{B}$ becomes disordered, a situation similar to what has been found in the isotropic Hele-Shaw setting [2]. We conclude this section by noting that in the perturbation expansion leading to the local expression (136), we assumed α to be independent of $\mathcal{B}$. However, that is clearly not necessary for the validity of Eq. (136). Even if α scales as some positive power of $\mathcal{B}$, the local behavior of the outer perturbation expansion is still determined by Eq. (136), even though the ansatz (22) needs to be modified to account for a possibly fractional power of $\mathcal{B}$.

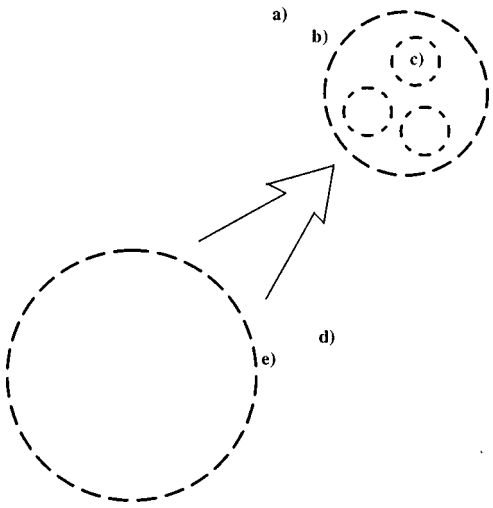

FIG. 9. Weakly anisotropic zero with emerging daughter singularity. (a) Outer daughter singularity $z_\zeta\sim z_{0\zeta}+\mathcal{B}A_1(t)[\zeta-\zeta_d(t)]^{-5/2}$, (b) size of daughter singularity's inner region $O(\mathcal{B}^{1/3})$, (c) inner singularity (countably infinite in number) $z_\zeta\sim C(t)[\zeta-\zeta_{\rm in}(t)]^{-4/3}$, (d) outer zero $z_\zeta\sim z_{0\zeta\zeta}[\zeta-\zeta_0(t)]$, (e) size of zero singularity's inner region $O(\mathcal{B}^{2/7})$.

B. Inner equations around $\zeta_0(t)$ and $\zeta_d(t)$

Near each $\zeta_0(t)$ and $\zeta_d(t)$, we noted already that the assumed asymptotic expansion in powers of $\mathcal{B}$ becomes invalid, suggesting the need for inner expansions centered at $\zeta_0(t)$ and $\zeta_d(t)$. The arguments for finding the necessary rescalings in the inner equations are very involved and depend not only on the anisotropy, but also generally on time. Since the dynamics of the inner scale does not directly affect the interface shape when daughter singularities and zeros are not close to the real axis, we have relegated this set of arguments to Appendix B. What emerges from these scaling arguments is summarized in Fig. 9 for a weakly anisotropic case [a similar picture holds for a strongly anisotropic case (see Appendix B), though with different scalings]—a zero spawns a ''daughter singularity,'' with both the zero $\zeta_0(t)$ and the daughter $\zeta_d(t)$ defining generally separate inner regions that contain clusters of actual singularities of z_ζ. For t sufficiently small, these two inner regions are initially part of one inner region around $\zeta_0(t)$ when $\zeta_d(t)$ is sufficiently close to $\zeta_0(0)$. Since the daughter singularity at $\zeta=\zeta_d(t)$ necessarily moves towards the real domain, its effect must eventually be felt at the interface, though other singularities can significantly shield its impact over $O(1)$ time (see [11]). The zero $\zeta_0(t)$ is not actually a zero of z_ζ, when surface tension is included; however, it remains a zero in the sense that there is an intermediate scale—$1\gg|\zeta-\zeta_0(t)|\gg\mathcal{B}^{2/7}$ in some complex sector, where Eq. (12) is still valid—i.e., it remains a zero in the outer-asymptotic sense as $\mathcal{B}\to 0$. It is in this sense that we continue to refer to $\zeta_0(t)$ as a zero.

The inner region around $\zeta_0(t)$, on the other hand, plays no role in the interfacial dynamics unless $\zeta_0(t)$ comes close to the real axis, which, unlike $\zeta_d(t)$, may happen for certain classes of initial conditions. However, it is possible that the zero-surface-energy motion of a $\zeta_0(t)$ towards the real axis is thwarted by a daughter singularity impact on the real axis which modifies the shape of the interface [and hence q_1 and q_{2_ζ} in Eq. (126)]. This indeed happens for certain initial conditions, as exemplified in [11] and Appendix C.

In the following section, we discuss scalings for the inner equations, when a daughter singularity $\zeta_d(t)$ or a zero $\zeta_0(t)$ is so close to the real axis that the results of this section are no longer valid.

V. INNER EQUATIONS FOR DAUGHTER SINGULARITIES OR ZERO CLOSE TO REAL AXIS

As in Appendix B, it is convenient to define λ so that

$$\alpha = \mathcal{B}^{\lambda}, \tag{137}$$

where $\lambda \geqslant 0$. The localized equations of the form (B4) (in Appendix B) do not remain valid for strong anisotropy ($\lambda < \frac{1}{2}$) when a daughter singularity comes within $O(\mathcal{B}^{2(1+\lambda)/9})$ of the real axis, and $O(\mathcal{B}^{1/3})$ for weak anisotropy ($\lambda > \frac{1}{2}$) because it is no longer possible to replace global quantities such as q_1, q_2 and $\tilde{z}_\zeta$ by their leading-order Taylor expansions at $\zeta = \zeta_d$.

As for singularities, surface-energy effects enter into the global integral terms at the leading order and thus define new inner scales. However, the appropriate scales depend on what is inherited from the earlier stage and are therefore different for the cases of weak and strong anisotropy.

However, in each case, we will see that at first the surface-energy effects within the inner region are not important to the leading order over the fast time scale induced by the nearness of a daughter singularity cluster close to the real axis. During this zero-surface-energy phase of evolution, the inner singularities within the daughter singularity's inner region advect toward the real axis, causing the daughter singularity's inner region to get closer to the real axis, at the same time continually spreading along the real axis. This effect leads to a break-up of the daughter singularity cluster into subclusters. Finally, surface energy becomes important at the leading order when these subclusters come within an $O(\mathcal{B}^{1/2})$ distance of the real axis. The resulting scaled inner equation is found to be the same as the original equation for $\mathcal{B}=1$, a problem that has been studied numerically and will be reported in paper III of this paper sequence. Such a renormalization in the dynamics allows us to understand the effects of the daughter singularity cluster in selecting locally steady dendritic characteristics.

A. Weakly anisotropic case: $\lambda > \frac{1}{2}$

We try to find inner variables around a point ξ_d that initially coincides with Re ζ_d. While the concept of daughter singularity ζ_d does not makes sense beyond $t = t_d$, when Im $\zeta_d(t_d)=0$, $\xi_d(t)$ will be defined beyond this time by evolving it in accordance with

$$\dot{\xi}_d(t) = -H(\xi_d(t),t). \tag{138}$$

From the results in Appendix B 1 A, it is clear that a suitable choice of inner spatial variable when $-\text{Im}\,\zeta_d = -\eta_d = O(\mathcal{B}^{1/3})$ is

$$\chi = \mathcal{B}^{-1/3}[\xi - \xi_d(t_d)]. \tag{139}$$

Since, the outer matching condition is $z_{0\xi}(\xi_d(t),t)$, which is $O(1)$, it follows that the dependent variable should be defined through

$$z(\xi,t) = z_0(t_d) + \mathcal{B}^{1/3} G(\chi,\tau). \tag{140}$$

Going back to Eq. (2), it is easily seen that this evolution must occur over a fast time scale, given by

$$\tau = \mathcal{B}^{-1/3}(t - t_d). \tag{141}$$

Substituting these inner scales into Eq. (2), we find that the leading-order inner equation at this stage is

$$G_\tau = Q_1 G_\chi + Q_2, \tag{142}$$

with matching condition

$$G_\chi(\chi,\tau) \sim z_{0\zeta}(\zeta_d(t_d),t_d) \quad \text{as} \quad \chi \to \pm\infty, \tag{143}$$

where

$$Q_1(\chi,\tau) = \frac{1}{\pi} \int_{-\infty}^{\infty} \frac{d\chi'}{\chi' - \chi} \frac{1}{|G_\chi(\chi',\tau)|^2}, \tag{144}$$

$$Q_2(\chi,\tau) = \frac{i}{G_\chi^*(\chi,\tau)}. \tag{145}$$

These inner equations are the local equivalent of the zero-surface-energy equation that was studied in [1], when examined on the real axis, so surface-energy effects have disappeared from the leading order. We know that Eq. (142), when studied in the real χ domain, is ill-posed, but is well-posed in the extended domain that includes the lower-half χ plane. Therefore, prediction on the dynamics of Eq. (142) must necessarily involve information on the initial condition in the lower-half complex χ plane; i.e., we need to know the details of the inner solution around a daughter singularity before it strikes the real axis. This information is not readily available to us, since the inner equations in Appendix B have yet to be solved.

Nonetheless, a few conclusions can easily be drawn. We know for instance that a daughter singularity cluster contains many weak singularities, each of which appears to be a $-\frac{4}{3}$ singularity of z_ζ (see [2,11] for related Hele-Shaw results), except on an inner-inner scale. A $-\frac{4}{3}$ singularity of the zero-surface-energy problem is known to asymptote the real axis. Further, it approaches $\chi = \pm\infty$ like $\pm\tau^{1/2}$, as it approaches the real axis like $\tau^{-1/2}$.

Thus, the daughter singularity cluster spreads out along ξ axis with time as

$$|\xi_{\text{in}} - \xi_d| \sim \mathcal{B}^{1/6}(t - t_d)^{1/2} \quad \text{for} \quad 1 \gg t - t_d \gg \mathcal{B}^{1/3}. \tag{146}$$

The corresponding η width of this cluster, defined by the maximum distance to the real axis of individual singularities within this cluster, shrinks like

$$|\eta_{\rm in}| \sim \mathcal{B}^{1/2}(t-t_d)^{-1/2} \quad \text{for } 1 \gg t-t_d \gg \mathcal{B}^{1/3}. \tag{147}$$

The daughter singularity cluster flattens against the real axis, and when $t-t_d=O(1)$, the flattened inner region has width $\mathcal{B}^{1/6}$ and thickness $\mathcal{B}^{1/2}$; at this stage surface energy becomes important.

We now consider the evolution of a cluster of singularities at $\zeta=\zeta_{\rm in}$, moving along the real ζ axis after the daughter singularity's inner region has flattened. We examine an inner region about $\xi_{\rm in}$ (since ξ_d no longer makes sense). We also require surface energy effects to be important at the leading order. The appropriate inner variables are

$$\chi=\mathcal{B}^{-1/2}[\xi-\xi_{\rm in}(t)], \tag{148}$$

$$\tau=\mathcal{B}^{-1/2}(t-t_{\rm in}), \tag{149}$$

$$z(\xi,t)\sim z_0(t)+\mathcal{B}^{1/2}G(\chi,\tau), \tag{150}$$

where

$$\dot{\xi}_{\rm in}=-H(\xi_{\rm in}(t),t) \tag{151}$$

and $t_{\rm in}$ defines a time when $\eta_{\rm in}=O(\mathcal{B}^{1/2})$. The inner equations are

$$G_\tau=(H+iR)G_\chi \tag{152}$$

with

$$H(\chi,\tau)=-\mathcal{H}\{R\}(\chi,\tau), \tag{153}$$

$$R(\chi,\tau)=\frac{1-\mathrm{Im}(\Omega_\chi)}{|G_\chi|^2}, \tag{154}$$

$$\mathrm{Im}(\Omega_\chi)=\mathcal{H}\left\{\frac{\partial K}{\partial \chi}\right\}(\chi,\tau), \tag{155}$$

$$K(\chi,\tau)=[1+\alpha f(\chi,\tau)]\kappa(\chi,\tau), \tag{156}$$

$$f(\chi,\tau)=1-\frac{1}{|G_\chi|^4}\,\mathrm{Re}(G_\chi^4 e^{-i4\theta_0}), \tag{157}$$

$$\kappa(\chi,\tau)=-\frac{1}{|G_\chi|}\,\mathrm{Im}\left(\frac{G_{\chi\chi}}{G_\chi}\right). \tag{158}$$

The far-field matching condition becomes

$$G_\chi(\chi,\tau)\sim z_{0\zeta}(\zeta_{\rm in}(t_{\rm in}),t_{\rm in}) \quad \text{as } \chi\to\infty. \tag{159}$$

Thus, the evolution of a neighborhood of the interface, where complex singularities associated with a daughter singularity cluster approach, is governed by the ''standard problem,'' as defined in Sec. I.

Since each cluster is governed by the standard problem, the entire $O(\mathcal{B}^{1/6})$ region adjacent to the daughter impact point is governed by the standard problem with $\mathcal{B}=1$. Especially important is the impact with the origin of the daughter singularity related to the Ivantsov zero, insuring that the crystal tip is governed by the standard problem, even though the zero-surface-energy solution by itself does not indicate (through the $\mathcal{B}=0$ interfacial curvature) that surface-energy effects become important at the tip.

B. Strongly anisotropic case: $\lambda<\frac{1}{2}$

Since in this case the outermost scale around a daughter singularity is known to be proportional to $O(\mathcal{B}^{(2/9)(1+\lambda)})$ just before the daughter singularity impacts the real axis, we expect that the appropriate scale here is

$$\chi=\mathcal{B}^{-(2/9)(1+\lambda)}[\xi-\xi_d(t_d)], \tag{160}$$

$$z(\xi,t)\sim z_0(t_d)+\mathcal{B}^{(2/9)(1+\lambda)}G(\chi,\tau). \tag{161}$$

Substituting into Eq. (2), it is clear that the evolution at this stage proceeds on a fast time scale

$$\tau=\mathcal{B}^{-(2/9)(1+\lambda)}(t-t_d), \tag{162}$$

$$z(\xi,t)\sim z_0(t_d)+\mathcal{B}^{(2/9)(1+\lambda)}G(\chi,\tau). \tag{163}$$

We find that the inner equations are the same as the zero-surface-energy equations (142) and (144), though with somewhat different definitions of G, χ, and τ.

Since the leading-order equation is just the equation for zero-surface-energy dynamics, it follows from results in [1] that individual singularities within the daughter singularity cluster approach the real axis over the time scale $O(\mathcal{B}^{(2/9)(1+\lambda)})$. Once individual singularities are within a smaller $[O(\mathcal{B}^{1/2})]$ distance of the real ζ axis, by which time the daughter singularity cluster will have dispersed significantly, the inner equation is once again given by the standard problem, as defined by Eqs. (152)–(158) above. Computations to be reported in paper III of this paper sequence suggest that the asymptotic long-time state for the standard problem is independent of the far-field and/or initial condition. This result is significant because it suggests that the ''standard problem,'' as it arises in differing contexts, with a dissimilar initial and far-field matching condition, has a ''standard'' long-time behavior for all cases.

C. Inner equations for zeros near the real axis

In this section, we investigate the behavior of a zero that is too close to the real axis for the analysis of Sec. IV to be valid. This can happen either because (i) $\zeta_0(0)$ was initially very close to the real axis or (ii) $\zeta_0(t)$ came close to the real axis later in time. The arguments below do not distinguish between the two cases. It is to be noted that evidence discussed in the next subsection indicates that the scenario (ii) is not possible.

We begin with the equations written on the real axis [(2)–(8)] and use the inner variables

$$\chi=\mathcal{B}^{-1/3}[\xi-\xi_0(t_c)], \tag{164}$$

$$\tau=\mathcal{B}^{-1}(t-t_c), \tag{165}$$

$$z(\xi,t)\sim z_0(t)+\mathcal{B}^{2/3}G(\chi,\tau), \tag{166}$$

$$\mathrm{Im}(\omega_\zeta)(\xi,t)=\mathcal{B}^{-1}\,\mathrm{Im}(\Omega_\chi)(\chi,\tau), \tag{167}$$

where $t_c=0$ for case (i) and equals the time when Im $\zeta_0(t)=0$ in case (ii). Then to the leading order as $\mathcal{B}\to 0$, with $\chi=O(1)$, we obtain

$$\dot{z}_0(t)=0. \tag{168}$$

The evolution of $G(\chi,\tau)$ is seen to be governed by Eqs. (152)–(158), i.e., the standard problem. Note, however, that the definitions of χ and τ differ from those previously defined. We also note that the inner equations are independent of the relative ordering of anisotropy α and surface energy $\mathcal{B}$, since f cannot be large.

The initial-/far-field matching condition in our case is

$$G_\chi \sim c_1(\chi+c_2). \tag{169}$$

Therefore, the evolution in the inner region around the tip of an initial near-cusp with small surface energy is exactly the same as the evolution of an initial parabola with $\mathcal{B}=1$. In paper III of this paper sequence, we solve the dendrite problem numerically using a boundary-integral approach, based on Eq. (2), for $\mathcal{B}=O(1)$. By doing so, we will also find the fate of an interface that is initially a near-cusp. The scaling introduced here then determines an evolution time scale for $\mathcal{B}\to 0$.

D. Which one reaches the real axis first—the daughter singularity or the zero?

Given the dramatic effect of daughter singularities on the real-axis dynamics (i.e., interface shape), a relevant question is whether a daughter singularity $\zeta_d(t)$ necessarily strikes the real axis before its corresponding precursor zero $\zeta_0(t)$, with which it initially coincided. This is an important question for the following reason: Recall from the zero-surface-energy dynamics that a zero $\zeta_0(t)$, if and when it approaches the real axis, causes an initially smooth interface to form a cusp. Surface energy is expected to prevent cusp formation; however, if indeed a $\zeta_0(t)$ approaches the real axis, one would expect that as $\mathcal{B}\to 0$, a near-cusp forms. On the other hand, if $\zeta_d(t)$ always approaches the real axis before the corresponding $\zeta_0(t)$, then the interface can never come close to cusped shape. This issue appeared in the mathematically analogous isotropic Hele-Shaw problem before and will also be demonstrated for the anisotropic case in paper III—the impact of a daughter singularity causes the interface to veer off from the corresponding zero-surface-energy solution even when the interface is smooth and far from forming a cusp. As the shape changes, so does the motion of $\zeta_0(t)$ and numerical evidence shows that this change is enough to prevent $\zeta_0(t)$ from ever coming close to the real axis. Thus, if the answer to the question posed above is in the affirmative, then the cusp-forming solution found in [1] has no physical significance; the actual physical interface will have veered off from the idealized solution much before the solution comes close to forming a narrow structure. In Appendix C, we present some evidence (both analytical and numerical) based on certain classes of initial conditions (poles), to support our contention that daughter singularities always arrive at the real axis prior to their corresponding zeros. It is to be noted that in this respect, there appears to be a difference between a Hele-Shaw interface driven by suction at a finite point [26] and one for which the sink is at infinity [11]. Analogy with the dendrite as far as daughter singularity impact preceding the zero appears to hold only in the latter case.

VI. NONLINEAR LOCALIZED INTERFACIAL DISTURBANCES

Given our observations that daughter singularity impact is to be expected for a generic initial condition, and that this impact causes active features of a dendrite to be formed with appropriate orientation of minimal surface energy directions, we inquire into the evolution of a disturbance that is initially localized, but causes a strictly $O(1)$ change in z_ζ. While the importance of studying this particular kind of disturbance can be understood better in terms of the expected daughter singularity impacts, there is no necessity of relating such localized disturbances to any necessary singularity in the complex plane. The fate of such disturbances follows merely from the assumed scalings of the disturbance on the real axis and the findings of paper III on the limiting dynamics on the inner scale.

We introduce, as before, the local scaled variable

$$\chi=(\zeta-\xi_s)/\epsilon, \tag{170}$$

where ϵ is a measure of the localization of the disturbance. When $\chi=O(1)$, it is appropriate to introduce the local variable $G(\chi,t)$ through

$$z(\zeta(\chi,t),t)=z_0(\xi_s(t),t)+\epsilon G(\chi,t). \tag{171}$$

This scaling ensures that for $\chi=O(1)$, the deviation of z_ζ from $z_{0\zeta}$ is $O(1)$. We also note that localized disturbances where $|z_\zeta|\gg 1$ can also be accommodated in the inner equation obtained for G since none of the assumptions made in deriving the equation for G is violated when $|G_\chi|\gg 1$ in some localized neighborhood in the χ domain. We note that any localized disturbance in the ζ plane for which $|z_\zeta|\gg 1$ must have an outer-inner region for which the scaling (171) is appropriate, as otherwise it is not possible to match with an $O(1)z_{0\zeta}$. We note that the requirement that the wave packet be spatially concentrated around $\zeta=\xi_s(t)$ implies that an appropriate boundary condition on G as $|\chi|\to\infty$ is given by

$$G_\chi \to z_{0\zeta}(\zeta_s(t),t), \tag{172}$$

which is a constant. A comment is in order about the initial hypothesis that there is no ϵ-scale variation of $z_0(\zeta,t)$. As shall be seen in the derivation of the equations, this can be relaxed by just assuming that there is no small-scale variation of $z_{0\zeta}$ within an ϵ neighborhood of $\zeta_s(t)$. This allows us to include in this formalism multiple wave packets that are localized on different parts of the interface. With G as given by Eq. (171), it is easily seen that

$$\mathcal{B}\ \mathrm{Im}(\omega_\zeta)(\xi_s+\epsilon\chi,t)\sim\frac{\mathcal{B}}{\epsilon^2}\,\mathrm{Im}(\Omega_\chi)=\frac{\mathcal{B}\epsilon^{-2}}{\pi}\,\fint_{-\infty}^{\infty}\frac{d\chi'}{\chi'-\chi}\,\frac{\partial}{\partial\chi'}\left[\frac{1}{|G_{\chi'}|}\,\mathrm{Im}\,\frac{G_{\chi'\chi'}}{G_{\chi'}}\right]. \tag{173}$$

It is also clear that

$$R(\xi_s+\epsilon\chi,t)=\mathcal{R}(\chi,t)=\frac{1-\mathcal{B}\epsilon^{-2}\mathrm{Im}(\Omega_{\chi'})}{|G_{\chi'}|^2}. \tag{174}$$

Now consider the asymptotics of $H(\zeta,t)$ for $\chi=O(1)$ in the limit $\epsilon\to0$. The integral for H can be broken up into

$$H(\zeta(\chi,t),t)=H^{\mathrm{out}}(\chi,t)+H^{\mathrm{in}}(\chi,t), \tag{175}$$

where

$$H^{\mathrm{out}}(\chi,t)=\left[\int_{-\infty}^{\xi_s(t)-\delta}+\int_{\xi_s(t)+\delta}^{\infty}\right]\frac{d\xi}{\xi-\xi_s-\epsilon\chi}\,R(\xi,t), \tag{176}$$

$$H^{\mathrm{in}}(\chi,t)=\fint_{-\delta/\epsilon}^{\delta/\epsilon}\frac{d\chi'}{\chi'-\chi}\,\mathcal{R}(\chi',t). \tag{177}$$

In the above, δ is a constant conveniently chosen with the restriction $\epsilon\ll\delta\ll1$. The end result of the asymptotic analysis will yield answers completely independent of δ. Since, $R(\xi,t)\sim R^0(\xi,t)$ outside an ϵ neighborhood of ξ_s, it follows that

$$H^{\mathrm{out}}(\chi,t)\sim\frac{1}{\pi}\left[\int_{-\infty}^{\xi_s-\delta}+\int_{\xi_s+\delta}^{\infty}\left\{\frac{1}{\xi-\xi_s(t)}+\frac{\epsilon\chi}{[\xi-\xi_s(t)]^2}\right\}R^0(\xi,t)d\xi\right]+O\left(\frac{\epsilon^2}{\delta^2}\right), \tag{178}$$

which can be written as

$$\begin{aligned}H^{\mathrm{out}}(\chi,t)\sim{}&H_0(t)+\epsilon H_1(t)\chi+\frac{\epsilon\chi}{\pi\delta}\left[R^0(\xi_s-\delta,t)+R^0(\xi_s+\delta,t)\right]\\&-\frac{1}{\pi}\fint_{-\delta/\epsilon}^{\delta/\epsilon}\frac{d\chi'}{\chi'}\left[R^0(\xi_s+\epsilon\chi',t)+\epsilon\chi R^0_\xi(\xi_s+\epsilon\chi',t)\right]+O(\epsilon^2\delta^{-2}),\end{aligned} \tag{179}$$

where

$$H_0(t)=\frac{1}{\pi}\fint_{-\infty}^{\infty}\frac{d\xi}{\xi-\xi_s}\,R^0(\xi,t), \tag{180}$$

$$H_1(t)=\frac{1}{\pi}\fint_{-\infty}^{\infty}\frac{d\xi}{\xi-\xi_s}\,R^0_\xi(\xi,t). \tag{181}$$

Further simplification of the asymptotic series (179) is possible, giving

$$H^{\mathrm{out}}(\chi,t)\sim H_0(t)+\epsilon H_1(t)\chi+\frac{2\epsilon\chi R^0(\xi_s,t)}{\pi\delta}-\frac{2}{\pi}\,\delta R^0_\xi(\xi_s,t)+O(\epsilon^2\delta^{-2},\epsilon\delta). \tag{182}$$

Now, we examine the asymptotic behavior of $H^{\mathrm{in}}(\chi,t)$. Using the fact that $\mathcal{R}(\chi,t)\to R^0(\xi_s+\epsilon\chi,t)$ rapidly as $|\chi|\to\infty$, it follows that

$$\begin{aligned}H^{\mathrm{in}}(\chi,t)\sim{}&\frac{1}{\pi}\fint_{-1}^{1}d\chi'\,\frac{\mathcal{R}(\chi',t)}{\chi'-\chi}+\frac{1}{\pi}\left[\fint_{-\infty}^{-1}+\fint_{1}^{\infty}\right]d\chi'\left\{\frac{\mathcal{R}(\chi',t)}{\chi'-\chi}-\frac{R^0(\xi_s+\epsilon\chi',t)}{\chi'}-\frac{\chi}{\chi'^2}\,R^0(\xi_s+\epsilon\chi',t)\right\}\\&+\frac{1}{\pi}\left[\fint_{-\delta/\epsilon}^{-1}+\fint_{1}^{\delta/\epsilon}\right]d\chi'\left[\frac{R^0(\xi_s+\epsilon\chi',t)}{\chi'}+\frac{\chi}{\chi'^2}\,R^0(\xi_s+\epsilon\chi',t)\right]+O(\epsilon^2\delta^{-2}),\end{aligned} \tag{183}$$

$$H^{\rm in}(\chi,t)\sim\frac{1}{\pi}\int_{-1}^{1}\frac{d\chi'}{\chi'-\chi}\,\mathcal{R}(\chi',t)+\frac{1}{\pi}\left[\int_{-\infty}^{-1}+\int_{1}^{\infty}\right]d\chi'\left\{\frac{\mathcal{R}(\chi',t)}{\chi'-\chi}-\frac{R^0(\xi_s+\epsilon\chi',t)}{\chi'}-\frac{\chi}{\chi'^2}\,R^0(\xi_s+\epsilon\chi',t)\right\}$$
$$+\frac{2}{\pi}\,(\delta-\epsilon)R^0_\xi(\xi_s,t)-\frac{2\chi}{\pi}\,R^0(\xi_s,t)\left[\frac{\epsilon}{\delta}-1\right]+O(\epsilon^2\delta^{-2}). \tag{184}$$

On combining $H^{\rm out}$ and $H^{\rm in}$, we find

$$H(\xi_s+\epsilon\chi,t)\sim H_0(t)+\epsilon H_1(t)\chi+\frac{1}{\pi}\int_{-1}^{1}d\chi'\,\frac{\mathcal{R}(\chi',t)}{\chi'-\chi}$$
$$+\frac{1}{\pi}\left[\int_{-\infty}^{-1}+\int_{1}^{\infty}\right]d\chi'\left\{\frac{\mathcal{R}(\chi',t)}{\chi'-\chi}-\frac{R^0(\xi_s+\epsilon\chi',t)}{\chi'}-\frac{\chi}{\chi'^2}\,R^0(\xi_s+\epsilon\chi',t)\right\}$$
$$-\frac{2\epsilon}{\pi}\,R^0_\xi(\xi_s,t)+\frac{2\chi}{\pi}\,R^0(\xi_s,t)+O(\epsilon^2\delta^{-2},\epsilon\delta). \tag{185}$$

Note that the above is true for any δ satisfying $\epsilon\ll\delta\ll1$. We now take the somewhat more restrictive ordering $1\gg\delta\gg\epsilon^{1/2}$, for which case the expression (185) determines H to $o(\epsilon)$. On integrating by parts the last term in the second integral in Eq. (185), and using

$$\int_{1}^{1}\frac{d\chi'}{\chi'}\,R^0(\xi_s+\epsilon\chi',t)=\frac{2\epsilon}{\pi}\,R_\xi(\xi_s,t)+O(\epsilon^2), \tag{186}$$

it follows that up to and including $O(\epsilon)$ terms,

$$H(\xi_s+\epsilon\chi,t)\sim H_0(t)+\epsilon H_1(t)\chi+\mathcal{H}^{(\epsilon)}(\chi,t), \tag{187}$$

where

$$\mathcal{H}^{(\epsilon)}(\chi,t)=\frac{1}{\pi}\int_{-\infty}^{\infty}d\chi'\left\{\frac{\mathcal{R}(\chi',t)}{\chi'-\chi}-\frac{R^0(\xi_s+\epsilon\chi',t)}{\chi'}\right\}. \tag{188}$$

It is clear that

$$\mathcal{H}^{(\epsilon)}(\chi,t)\to\mathcal{H}(\chi,t)\quad\text{for }\epsilon\to0, \tag{189}$$

where

$$\mathcal{H}(\chi,t)=\frac{1}{\pi}\int_{-\infty}^{\infty}\frac{d\chi'}{\chi'-\chi}\,\mathcal{R}(\chi',t). \tag{190}$$

The evolution equation then becomes

$$G_\tau=[\mathcal{H}+i\mathcal{R}]G_\chi, \tag{191}$$

where

$$\tau=t/\epsilon. \tag{192}$$

This equation describes the disturbance evolution for $\xi=O(1)$ over the fast $O(\epsilon)$ time scale; however, it is inaccurate over the $O(1)$ time scale. To get the correct equation over this longer time scale, it is necessary to retain $H_1(t)$ and $\mathcal{H}^{(\epsilon)}$ in Eq. (187) to obtain instead of Eq. (191)

$$G_t=\frac{1}{\epsilon}\,[\epsilon H_1(t)\chi+\mathcal{H}^{(\epsilon)}(\chi,t)+i\mathcal{R}(\chi,t)]G_\chi. \tag{193}$$

Notice that if we introduce a change of variable,

$$\chi=F(t)\nu,\quad F(t)\equiv e^{-\int_0^t dt\,H_1(t)}, \tag{194}$$

then we obtain

$$G_{\tau_1}(\nu,\tau_1)=\frac{1}{\epsilon}\,[\mathcal{H}^{(\epsilon)}(\nu,t)+i\mathcal{R}(\nu,t)]G_\nu, \tag{195}$$

where

$$\tau_1=\int_0^t F(t)dt, \tag{196}$$

with

$$\mathcal{R}(\nu,t)=\frac{1}{|G_\nu(\nu,t)|^2}\left[1-\frac{\mathcal{B}}{F(t)\epsilon^2}\,\mathrm{Im}\;\Omega_\nu(\nu,t)\right] \tag{197}$$

and

$$\mathrm{Im}\;\Omega_\nu(\nu,t)=\frac{1}{\pi}\int_{-\infty}^{\infty}\frac{d\nu'}{\nu'-\nu}\,\frac{\partial}{\partial\nu'}\left[\frac{1}{|G_{\nu'}|}\,\mathrm{Im}\left(\frac{G_{\nu'\nu'}}{G_{\nu'}}\right)\right]. \tag{198}$$

In the above, it is clear that $F(t)$ is an increasing function of time; thus effective spatial localization of the disturbance is actually $\epsilon F(t)$, which increases with time, corresponding to ''Zeldovich stretching.'' It is clear from the above that the evolution on a shorter ϵ spatial scale also occurs on a faster $O(\epsilon)$ time scale. Now assume $\mathcal{B}\ll1$. We notice that the fastest time scale that appears is $O(\mathcal{B}^{1/2})$ as in the case of linearized disturbances and this is for disturbances with $\epsilon=O(\mathcal{B}^{1/2})$. For such localized disturbances, terms arising from the product of surface energy and curvature play an $O(1)$ role, as in the linearized analysis. However, the nonlinear equations do give more accurate information on the renormalization aspect of the dynamics that are not present in the linearized equations.

Note that Eq. (191) on the shorter scale evolution is once again the same form as the original Eqs. (2)–(8), except that the effective surface energy is increased from $\mathcal{B}$ to $\mathcal{B}\epsilon^{-2}$. For $\mathcal{B}\ll 1$ and $\epsilon\ll\mathcal{B}^{1/2}$, the surface-energy term is formally small and therefore the limiting dynamics as $\mathcal{B}\to 0$ is relevant at both $O(1)$ and $O(\epsilon)$ scales. The boundary conditions at ∞ are different in the ζ and χ variable, however; in one case, we match to a parabola at infinity and in the other case, the far-field state is a straight line. However, as suggested by the computation in paper III, the initial-/far-field matching conditions have no effect on the long-time asymptotic state—a steady tip emerging in a direction of minimal surface energy (in the presence of anisotropy) and a continually ballooning tip without surface-energy anisotropy.

With this property, taken as an assumption for the purposes of the present paper, it follows from the renormalization property shown in this section that at smaller and smaller scales—all the way up to a cutoff scale of $O(\mathcal{B}^{1/2})$, the dynamics is expected to be self-affine in the presence of surface-energy anisotropy, at least within the class of disturbances considered in this section.

VII. DISCUSSION

In this second part of a three part sequence of papers, we have incorporated small but nonzero surface-energy effects, with generally nonzero anisotropy, into the dynamics of $z(\zeta,t)$ in Im $\zeta\leqslant 0$, in the small Peclet number (P) limit. The analysis throughout required allowed times to be long in terms of some inverse power of $\mathcal{B}$, but limited in the (small) Peclet number by $t\ll P^{-1}$. This investigation has so far been possible for initial conditions that contain only singularities in the lower-half ζ plane of the type given in Eq. (28).

We are hampered here by a lack of rigorous mathematical support. There are no theorems known to us that guarantee existence of solutions for all time for nonzero surface energy. Further, there is no guarantee that if the initial interface is analytic, it will remain so even for a short time. Indeed, in Sec. III A 1, we report that, with the approach of a not-too-weak singularity with $\beta>\frac{1}{2}$, the interface evolves over a long time. Over this long time scale, the inner equation for a disturbance on the interface is precisely what one would obtain for a Hele-Shaw interfacial disturbance with no forcing. In this latter case, there is numerical evidence [19] suggesting pinch-off, provided the initial interface is sufficiently distorted. Thus, we do not expect global existence of solutions for a general initial condition. Nonetheless, since the time scale of the process described is long compared to that for tip advance, one can examine the interface before such an eventuality is realized. Here, we proceed with the assumption that $z(\zeta,t)$ indeed remains analytic and univalent in Im $\zeta\geqslant 0$, at least on the time scale of interest. Further, given that zero-surface-energy dynamics is expected to be well-posed in Im $\zeta\leqslant 0$, given similar results for Hele-Shaw flows [2,10], we have proceeded with a formal procedure of inner and outer expansions near each point where an assumed ''outer'' asymptotic expansion fails. This procedure resembles what has been done for isotropic Hele-Shaw flows [2]. Anisotropic surface energy, when sufficiently strong, significantly alters the inner equations of the singularities, generally requiring multiple inner regions. In carrying out a matched asymptotic expansion procedure, we tread again in areas of uncertain mathematical validity: We are unaware of any rigorous theory for global inner/outer matching for nonlinear time evolving partial differential equations in a complex domain. (This issue is currently under rigorous mathematical investigation; see [23].)

Therefore, the matching principle we invoke, discussed in detail in Appendix A, rests on other grounds. It is similar to that utilized in the Hele-Shaw context [2], where it proved satisfactory. What is more, it has been confirmed analytically for the linearized problem [1]. Further, interfacial evolution predictions based on the analytic theory for the Hele-Shaw flow [2] have thus far been consistent with numerical calculations [11], lending additional support to the basic premises of this principle.

In the case of the analysis of an initial zero, there are further uncertainties about the nature of the inner-equation dynamics, since there are time scales when that dynamics is described by a complex nonlinear partial differential equation whose solutions are unknown. In those cases, we have proceeded with further assumptions, as seen in Sec. V and Appendix B, about the nature of these solutions. We believe the basic premises to be correct since the scalings they imply about interfacial deformations are consistent with earlier numerical calculations [11] for the isotropic case and those presented in paper III of this paper sequence for strong isotropy.

Despite the qualifiers, the limitations on the nature of initial singularities, and the drawback of having to carry out an elaborate investigation in the lower-half complex plane, we have reported here what we believe to be the first analytical investigation of the fully nonlinear dendrite dynamics in the limit of vanishingly small surface energy. As a by-product, we have obtained qualitative and quantitative information on the interfacial evolution, which we list below, answering, at least, some of the queries of Sec. I.

(i) Starting with some analytic interfacial shape, within the class for which the analytic continuation of $z(\xi+i0,0)$ into the lower-half complex plane contains singularities only of the type given by Eq. (28), then all singularities continually approach the real axis [1], even as small surface energy alters and modifies their structures. This latter result follows from our findings in Sec. II (and Appendix A) that the zero-surface-energy singularities are in fact centers of inner regions where surface energy is important. Though surface energy is expected to prevent singularities from actually impinging on the real axis on the time scale of the dendrite tip advance, the continual approach towards the real axis of many singularities causes interfacial distortion over small scales. The nature of an indentation depends on several parameters: the values of β and $E(0)$, the initial distance from the real axis, and values of the surface-energy parameter $\mathcal{B}$ and anisotropy index α. The dependencies are detailed in Sec. III.

(ii) It is well known from complex variable theory that small changes in the initial shape, $z(\xi+i0,0)$, can have radical effects on the corresponding singularity distribution in $z(\zeta,0)$ in Im$(\zeta)<0$. Thus, sensitive dependence of the interfacial dynamics (indeed, noise effects, as popularly described in the literature) can all be traced to the effect described in [1]. For one initial condition, singularities initially far from the axis come close to the real axis and cause interfacial

indentations that are not seen for a slightly different initial shape without corresponding complex singularities. Thus, the mechanism amplifies the differences in initial conditions. This sensitivity to initial conditions is not unexpected, since the zero-surface-energy interfacial evolution problem is known to be ill-posed. Therefore, the evolution for small nonzero surface energy is expected to be characterized by large, though bounded, Lyapunov exponents.

(iii) Prior investigation [1] suggest that among the singularities considered here, poles approach the real axis the fastest. For poles, whose strengths are not too weak, the investigation in Sec. III shows that surface-energy effects act on a slow time scale only. Until the time when surface energy does become important, interfacial features are therefore dominated by approaching poles, i.e., parallel-sided indentations. To the extent that any two-dimensional, one-sided model can be relevant to actual three-dimensional dendrites, this picture is in qualitative congruence with experimental observations (see [20], for instance). Experiments also suggest a predominance of indentations initially aligned at 60° with the tip-advance direction. We are unable to explain this feature so far, but expect that it has to do with properties of the solutions of the strongly anisotropic inner equations, which are yet to be fully understood.

(iv) For a particular pole whose residue (strength) has real and imaginary parts of the same order, as is necessary for side-branching rather than tip-splitting, we find that there is a range of distance $|y|$ from the tip, over which the indentation depth scales as $\sqrt{|y|}$ and the width is constant, as discussed in Sec. III. The level of anisotropy does not affect this result.

(v) For an ensemble of poles that would account for side-branching (see [1]), it is shown in Sec. III C that the selective effects of surface energy on poles of differing strengths ($|E_0|$) cause dendritic indentation widths to coarsen as $\sqrt{|y|}$, over an intermediate range of distances from the tip. Our coarsening scaling differs from the theoretical equilibrium results of Voorhees and Glicksman [22], who obtained a $|y|^{1/3}$ scaling using a mean-field approach. Since our results hold solely in an intermediate range over which surface energy has not completely dissipated the pole features, there is not necessarily a contradiction. Interestingly, the experimental results referred to in [22] give support to any exponent between $\frac{1}{4}$ and $\frac{1}{2}$.

(vi) While the zero-surface-energy dynamics predicts interfacial cusp formation for dendrites for some class of initial conditions, our investigation reported in Sec. V D (and in detail in Appendix C) suggests that any nonzero surface energy creates new singular structures centered around a ''daughter singularity'' that prevent the interfacial cusp formation. Instead, the daughter singularity impact marks the time beyond which the interface shape veers dramatically away from the corresponding zero-surface-energy solution. This importance of the daughter singularity is consistent with results for the isotropic Hele-Shaw problem [11].

(vii) In many cases, for a daughter singularity cluster or an initial zero (see Sec. V) in the vicinity of the real axis, the inner equation is identical to the original equations (13)–(20) except that $\mathcal{B}$ is now effectively 1—what we have called the ''standard problem.'' This renormalization feature is also developed in Sec. VI in a more general context for any localized distortion that causes an $O(1)$ deviation of the slope from a slowly varying background state. The importance to the overall dynamics comes in combination with the tip-characteristic-selection results to be reported in Sec. III: The solution to the standard problem results in a steady dendrite tip, in the presence of anisotropy only, with the resulting emergent tip aligned in a direction of minimal surface energy. The resulting emergent tip satisfies conditions of steady-state microscopic solvability theory, even as the far field is unsteady. Given that a general initial condition will have many zeros of z_ζ in the lower-half plane, daughter singularity effects are likely to be quite common. Each time a daughter singularity impacts the real axis, local tip structures result along directions of minimal surface energy. Thus, for a fourfold anisotropic dendrite developing side-branching, each side branch results in a secondary tip aligned at right angles to the original tip. Renormalization characteristics then suggest that this process continues, with side branches of side branches forming tertiary tips, etc., in preferred directions. Given a distribution of poles close to the real axis, causing deep interfacial indentations, one might expect that the impacts of daughter singularities associated with zeros will result in secondary dendrites. What remains to be resolved is the frequency with which these daughter singularities impacts cause tip selection. If these impacts occur intermittently, one can expect emergent tips between some neighboring indentations and not others. This dynamical feature can manifest itself as an additional mechanism for coarsening, since the selected near-parabolic tips advance in a direction of minimal surface energy more rapidly than those not selected.

Our investigation of the small undercooling, small-surface-energy effects on a dendrite began by taking the limit of $P \to 0$ and then studying surface-energy effects for $\mathcal{B} \ll 1$. Such a procedure requires some relative ordering, with P much smaller than some positive power of $\mathcal{B}$. The precise restriction is harder to determine for complex plane dynamics because one must study the dynamics in an analytically continued domain. We have yet to make a precise determination of such a parametric restriction.

Further, we have not considered the case of singularities that are initially far from the real axis but have large strengths (large residues for the case of poles). These issues, along with the dynamics for other forms of singularities not considered here, will be studied in the future in order to clarify if the overall interfacial dynamics are indeed dominated by the class of initial conditions, considered here, as we suspect them to be.

ACKNOWLEDGMENTS

We have benefited from discussions with Professor Greg Baker and Professor Seppo Korpela. This research was supported by the National Aeronautics and Space Administration (Grant Nos. NAG3-1415 and NAG3-1947). M.K. received additional support from the NASA Graduate Student Researchers Program (Grant No. NGT-51072). S.T. also acknowledges additional partial support from the Department of Energy (Grant No. DE-FG02-92ER25119) and the University of Chicago MRSEC.

APPENDIX A: INNER EQUATIONS FOR SINGULARITIES NOT CLOSE TO THE REAL AXIS

We investigate here the inner equations that appropriately account for surface energy effects in a local neighborhood of a singularity of the outer-asymptotic expansion located at $\zeta = \zeta_s$. We do so by scaling both dependent and independent variables in a local neighborhood of $\zeta_s(t)$ with suitable powers of $\mathcal{B}$ and then taking the limit $\mathcal{B} \to 0$. In this section, we restrict attention to the case where $|\mathrm{Im}\, \zeta_s| \gg \mathcal{B}^\delta$, where $\delta > 0$ depends on α and $E_0(0)$ and will be determined in each case as below. We allow for the possibility that $\alpha \ll 1$ and $|E_0(t)| \ll 1$. Thus, one has to consider different possible relative orderings of α, $|E_0(t)|$, and $\mathcal{B}$. We will assume, for simplicity of algebraic manipulations, that

$$\alpha = \hat{\alpha} \mathcal{B}^\lambda, \tag{A1}$$

$$E_0(0) = \hat{E}_0(0) \mathcal{B}^\mu, \tag{A2}$$

so that assumptions on ordering are reflected through the exponents $\lambda, \mu \geqslant 0$. Note that each of $\hat{\alpha}$ and $\hat{E}_0(0)$ in the above are strictly $O(1)$ [in the sense that it is not $o(1)$], as $\mathcal{B} \to 0$. It is not necessary to assume a power-law dependence as in Eqs. (A1) and (A2); all the results quoted here hold if $O(\mathcal{B}^\lambda)$ and $O(\mathcal{B}^\mu)$ are understood as $O(\alpha)$ and $O(E_0(0))$, respectively.

Consider a neighborhood of $\zeta_s(t) = \zeta_{s0} + \mathcal{B}\zeta_{s1}$, where the outer-asymptotic behavior is given by Eq. (36) for $\beta > 0$. We define inner variables χ, τ, and G as

$$\zeta - \zeta_s(t) = \mathcal{B}^\delta \frac{1}{C_0(t)} \chi(\zeta, t), \tag{A3}$$

$$C_1(t) = \mathcal{B}^\psi \tau(t), \tag{A4}$$

$$z(\zeta, t) \sim \int_0^t dt' q_2(\zeta_s(t'), t') + \mathcal{B}^{\mu + (1-\beta)\delta} \hat{E}_0(0) G(\chi(\zeta, t), \tau(t)). \tag{A5}$$

The appropriate choice of constants δ, ψ and the functions $C_0(t)$ and $C_1(t)$ will be determined shortly. The choice of δ and ψ in each of the subsections is to be understood in the context of that subcase only. When Eqs. (A3)–(A5) are substituted into Eq. (21), then after collecting all possible dominant order contributions, we obtain the following inner equation, provided there are no zero-surface-energy singularities within $\mathcal{B}^\delta$ of the real axis:

$$\begin{aligned}
&\mathcal{B}^{-\psi} \dot{C}_1(t) G_\tau + \left(\frac{\dot{C}_0(t)}{C_0(t)} - q_{1_\zeta}(\zeta_s(t), t) \right) \chi G_\chi - \frac{q_{2\zeta}(\zeta_s(t), t) \chi \mathcal{B}^{\beta\delta - \mu}}{C_0(t) E_0(0)} \\
&\quad = \mathcal{B}^{1 - (3/2)\mu - [3(2-\beta)/2]\delta} \frac{C_0^{3/2}(t)}{i \hat{E}_0^{3/2}(0) \tilde{z}_\zeta^{3/2}(\zeta_s(t), t)} \left(-2 \frac{\partial^2}{\partial \chi^2} (G_\chi^{-1/2}) \right) \\
&\qquad - \mathcal{B}^{1 + \lambda + (1/2)\mu - (\beta + 6/2)\delta} \frac{\hat{\alpha} e^{-i4\theta_0} C_0^{7/2}(t) \hat{E}_0^{1/2}(0)}{2i z_\zeta^{7/2}(\zeta_s(t), t)} \left(\frac{2}{3} \frac{\partial^2}{\partial \chi^2} (G_\chi^{3/2}) \right) \\
&\qquad - \mathcal{B}^{1 + \lambda - (7/2)\mu + (7\beta - 6/2)\delta} \frac{\hat{\alpha} e^{i4\theta_0} \tilde{z}_\zeta^{1/2}(\zeta_s(t), t)}{2i C_0^{1/2}(t) E_0^{7/2}(0)} \left(-\frac{2}{5} \frac{\partial^2}{\partial \chi^2} (G_\chi^{-5/2}) \right).
\end{aligned} \tag{A6}$$

To simplify Eq. (A6), it is convenient to define

$$C_0(t) = \exp\left(\int_0^t dt' q_{1_\zeta}(\zeta_s(t'), t') \right). \tag{A7}$$

It is to be noted that in the event that the leading-order asymptotic solution on the real axis (i.e., the interface dynamics) is still given by the solution of the associated zero-surface-energy problem, it is appropriate to replace q_1, q_{1_ζ}, q_2, and $\tilde{z}_\zeta$ occurring in Eqs. (A5)–(A7) by their corresponding zero-surface-energy solution values. However, by keeping them more general, we account for situations in which the actual solution on the real axis has veered dramatically from the corresponding zero-surface-energy solution by the prior impact of other singularities (including daughter singularities, studied later).

In order to match to the leading-order outer-asymptotic behavior in Eq. (36), $z_\zeta \sim E_0(t)[\zeta - \zeta_s(t)]^{-\beta}$, it is necessary that as $\chi \to \infty$ (for arg χ restricted to an appropriate interval),

$$G_\chi(\chi, \tau) \sim \chi^{-\beta}. \tag{A8}$$

The initial condition is

$$G_\chi(\chi, 0) = \chi^{-\beta}. \tag{A9}$$

Note that in order for Eqs. (A8) and (A9) to be valid, we must require that $\delta > \mu/\beta$ since the outer-asymptotic behavior $z_\zeta \sim E_0(\zeta - \zeta_s)^{-\beta}$ is valid only for $|\zeta - \zeta_s| \ll |E_0|^{1/\beta}$. If δ

$=\mu/\beta$, the matching and initial condition must reflect outer behavior (29). So Eq. (A8) has to be replaced by

$$G_\chi \sim \frac{A_0(t)}{\hat{E}_0(0)C_0(t)} + \chi^{-\beta} \quad \text{for } \chi \to \infty, \tag{A10}$$

while

$$G_\chi(\chi,0) = \frac{A_0(0)}{\hat{E}_0(0)} + \chi^{-\beta}. \tag{A11}$$

It is *a priori* unclear what sectors in the complex χ plane one should invoke the matching conditions (A8) or (A10). In general, as shall be seen later, it is an overspecification to require that the matching condition be applied for all values of arg χ.

In [2], while considering the isotropic Hele-Shaw problem, it was suggested that the matching be guided by two principles.

(a) The sector where Eq. (A8) is demanded in the far-field gives rise to a unique solution to the inner problem.

(b) The range of arg χ where matching is invoked translates in the ζ variable to directions towards the physically relevant region (real axis in our current formulation).

The first principle (a) would be justified if one were to assume that the original initial value problem in the real axis has a unique analytic solution (at least up to some positive time) since its analytic continuation up to an inner neighborhood of $\zeta=\zeta_s$ will also be unique. The second principle (b) was invoked in analogy to the steady-state dendrite or Hele-Shaw problem. For the time-evolving problem, there is no known equivalent to global Stokes lines to check whether invoking principle (b) for each singularity would be tantamount to requiring that the outer zero-surface-energy solution be valid on a part of the complex plane adjacent to the real axis. However, when we applied (b) to the linearized complex dynamics in [1], the results were consistent with what was obtained directly from the real domain equations through Fourier transforms. Also, many of the consequences of the complex dynamics of singularities obtained by applying the principles above have been found to be consistent with direct numerical calculations of the associated isotropic Hele-Shaw flow [12] in the real domain, for a sequence of problems with ever-decreasing surface energy. Thus, there is some indirect evidence that invoking the *ad hoc* principle (ii) is appropriate for the nonlinear dynamical problem as well. We illustrate sectorial matching in Fig. 4.

In order to find a leading-order inner equation, it is necessary to determine which of the terms in Eq. (A6) containing powers of $\mathcal{B}$ are dominant. That determination clearly depends on the values of ordering parameters λ and μ, as well as the choice of ψ. To distinguish the different possible cases, it is convenient to define

$$\lambda_c \equiv \frac{4(\beta-3\mu)}{3(2-\beta)}, \tag{A12}$$

$$\psi_c \equiv \frac{3(2-\beta)}{4\beta}(\lambda-\lambda_c) = \frac{3}{4\beta}[(2-\beta)\lambda - \tfrac{4}{3}(\beta-3\mu)]. \tag{A13}$$

Notice, before proceeding, that large values of λ and μ correspond to *weak* anisotropy and weak singularities, respectively.

1. The case of $\psi_c<0$

For this case, if $\beta<2$, then inspection of the above equations indicates that anisotropy effects are strong; if $\beta>2$, then the anisotropy is weak. It is to be noted that in either case, $\psi_c<0$ necessarily implies that $\mu<\beta/3(1+\lambda)$, i.e., the singularity strength is not ''too weak.'' This condition will be used later.

We note that if we seek consistency in a dominant balance procedure between the first term on the left of Eq. (A6) and the first two terms on the right of Eq. (A6), one is led to the condition $\psi=\psi_c<0$, corresponding to a long time scale, since $\mathcal{B}^\psi \gg 1$. This finding is inconsistent with the observation that condition (iii) in Sec. IV holds for any $t>0$ and therefore the outer perturbation expansion becomes inconsistent for any $t>0$ in a neighborhood of $\zeta=\zeta_s$. Thus, we seek an alternate dominant balance by choosing $\psi=0$, so that the inner time scale $\tau=O(1)$. Then, for $t=O(1)$ we choose

$$\delta = \frac{2(1+\lambda)+\mu}{\beta+6}, \tag{A14}$$

a choice consistent with condition (iii) in Sec. II. Note that $\delta>\mu/\beta$ is required for the validity of Eqs. (A8) and (A9). The resulting leading-order inner equation is simplified if we further choose

$$C_1(t) = \int_0^t dt' \, \frac{\hat{\alpha} e^{-i4\theta_0} C_0^{7/2}(t') \hat{E}_0^{1/2}(0)}{2i\tilde{z}_{0\zeta}^{7/2}(\zeta_s(t'),t')}, \tag{A15}$$

in which case one has the following leading-order parameter-free inner equation:

$$G_\tau = -\frac{2}{3}\frac{\partial^2}{\partial \chi^2}(G_\chi^{e/2}). \tag{A16}$$

The isotropic surface energy term ($G_\chi^{-1/2}$ term) in Eq. (A16) is found to be $O(\mathcal{B}^{-4\beta\psi_0/3})$, and the anisotropic term containing $G_\chi^{-5/2}$ is $O(\mathcal{B}^{(4/3)\beta(1+\lambda)-4\mu})$, both $o(1)$, and hence neglected in the leading-order equation (A16).

The strongly anisotropic equation (A16) has a similarity solution of the form

$$G_\chi = \tau^{-2\beta/\beta+6} e^{-2\pi i(\beta/\beta+6)} F^2(\nu),$$

$$\nu = e^{-2\pi i(1/\beta+6)} \frac{\chi}{\tau^{2/\beta+6}}, \tag{A17}$$

where $F(\nu)$ satisfies

$$F^2F''' + 6FF'F'' + 2F'^3 + \frac{\beta}{\beta+6}F^2 + \frac{2\nu}{6+\beta}FF' = 0, \tag{A18}$$

with asymptotic condition

$$F \sim \nu^{-\beta/2} \tag{A19}$$

as $\nu \to \infty$ in some as-yet undetermined sectors, corresponding to the given initial and far-field matching condition (A8). In applying matching principle (b), discussed above, to the similarity solution, to determine the ranges of $\arg \nu$ over which one should seek the asymptotic behavior (A19), the following problem arises: $\arg \nu$ is related to $\arg \chi$ and $\arg[\zeta - \zeta_s(t)]$ (which defines which directions are towards the real ζ axis) in a complicated manner, through a sequence of transformations [see Eqs. (A3), (A4), and (A17)]. Therefore, matching requires knowledge of the specific outer solution. However, we note that replacing ν by $\nu e^{i\phi_m}$ and F by $Fe^{-i\phi_m \beta/2}$, where $\phi_m = 4\pi m/(\beta+6)$ for any integer m, leaves both Eqs. (A18) and (A19) invariant. The implication is, then, that if one were to find a unique solution $F(\nu)$ to Eq. (A18) satisfying Eq. (A19) for $\arg \nu$ in $[-4\pi/(\beta+6), 4\pi/(\beta+6)]$, as will be shortly determined, there will also be a unique solution to Eq. (A18) satisfying Eq. (A19) for $\arg \nu$ in $[\phi_m - 4\pi/(\beta+6), \phi_m + 4\pi/(\beta+6)]$, which can be generated from the one corresponding to $m=0$. One of these intervals in $\arg \nu$ will be appropriate in invoking principle (b), i.e., would correspond to directions in the ζ plane towards the real axis. Thus, it is enough to discuss the solution for $m=0$.

We now discuss how a unique solution to Eq. (A18) can be expected when Eq. (A18) is certain on only the positive real ν axis. We will demonstrate why Eq. (A19) is in fact satisfied for large $|\nu|$ for $\arg \nu$ in the interval $[-4\pi/(\beta+6), 4\pi/(\beta+6)]$. Using a dominant balance technique, one can extract from Eq. (60) the higher-order asymptotic corrections to Eq. (A19),

$$F \sim \nu^{-\beta/2}[1 + a_1 \nu^{-3-\beta/2} + a_2 \nu^{-6-\beta} + a_3 \nu^{-9-3\beta/2} + \cdots], \tag{A20}$$

where

$$a_1 = -\frac{\beta}{8}(2+3\beta)(4+3\beta), \tag{A21}$$

$$a_2 = \frac{\beta}{128}(2+3\beta)(4+3\beta)(480+774\beta+366\beta^2+55\beta^3), \tag{A22}$$

$$a_3 = -\frac{\beta}{384}(2+\beta)(4+\beta)(2+3\beta)(4+3\beta) \times (20\,160 + 38\,520\beta + 27\,340\beta^2 + 8526\beta^3 + 955\beta^4). \tag{A23}$$

One obtains exponential corrections to the algebraic behavior in Eq. (A20), through either a Borel resummation of the divergent series (A20) involving powers of $\nu^{-3-\beta/2}$, as detailed in [2] for a similar problem, or by linearizing Eq. (A18) about the leading-order asymptotic behavior (A19) and examining WKB solutions of the associated linearized homogeneous equation, as first suggested by Kruskal and Segur [24] for some nonlinear third-order differential equation. The exponential corrections are found to be of the form

$$e^{\pm i[2/(3+\beta/2)^{3/2}]\nu^{3/2+\beta/4}[1+o(1)]}. \tag{A24}$$

By insisting that the leading-order asymptotics for large ν on the positive real ν axis be given by Eq. (A19), we have actually ensured the following three conditions.

(a) The leading-order asymptotic behavior is given by Eq. (A19), rather than a more general $a_0 \nu^{-\beta/2}$ for which $a_0 \neq 1$ [such behavior is still consistent with Eq. (A18)].

(b) No exponential correction of the form

$$e^{-i[2/(3+\beta/2)^{3/2}]\nu^{3/2+\beta/4}[1+o(1)]} \tag{A25}$$

is present in the large $|\nu|$ asymptotics for $\arg \nu = 0$, as otherwise Eq. (A19) could not possibly be valid. Since a Stokes multiplier can only change across an anti-Stokes line where the ratio between two exponential terms is a maximum, it follows that this condition will rule out an exponential of the form (A25) for large $|\nu|$ and $\arg \nu$ in the interval $[0, 2\pi/(\beta+6))$. It also ensures that the formal series (A19) is valid in this range of $\arg \nu$ for large $|\nu|$.

(c) No exponential correction of the form

$$e^{i[2/(3+\beta/2)^{3/2}]\nu^{3/2+\beta/4}[1+o(1)]} \tag{A26}$$

is present for $\arg \nu = 0$. Once again, since the Stokes multiplier can change across an anti-Stokes line only, it follows that this condition will rule out an exponential of the form (A25) for large $|\nu|$ when $\arg \nu$ is in $(-2\pi/(\beta+6), 0]$, which ensures that the formal series (A20) is valid for this range of $\arg \nu$ for large $|\nu|$.

From (b) and (c) above, it follows that the requirement (A19) for large positive ν ensures that this asymptotic series is actually valid for large $|\nu|$ when $\arg \nu$ in $[-2\pi/(\beta+6), 2\pi/(\beta+6)]$. In reality, this is valid for the entire interval $[-4\pi/(\beta+6), 4\pi/(\beta+6)]$, because the exponential term ''born'' at either of the anti-Stokes lines $\arg \nu = 2\pi/(\beta+6), -2\pi/(\beta+6)$ is subdominant compared to terms of the asymptotic series (A19) until one moves outwards to the nearest Stokes lines.

Conditions (a)–(c) select a unique solution to the third-order differential equation (A18), which we implemented numerically by integrating Eq. (A18) along the positive real ν axis towards the origin, starting at $\nu = L$ for some suitably large L and using Eq. (A20) to determine the initial condition $F(L)$, $F'(L)$, and $F''(L)$. Possible spurious solutions are avoided by ensuring that the computed F at some fixed point on the real axis does not change (to within numerical integration accuracy of 10^{-10}) when L is continually increased. An L of 20 seemed to accomplish that. We also found that the asymptotic series (A19) quite accurately describes the computed solution when ν is sufficiently large (more than 10 or so). Indeed, integration from $\nu = L$ to any point closer to the origin, whose argument lies in $[-4\pi/(\beta+6), 4\pi/(\beta+6)]$, suggested that Eq. (A19) remains valid in this extended sector. One must be vigilant in controlling growth of round-off error, generated by exponentials of the form (A24), when integration is done outwards from the origin.

Notice that Eq. (A18) admits one or more isolated singularities ν_{in} for F in the form

$$F \sim A_{\text{in}}(\nu - \nu_{\text{in}})^{1/3}[1 + \tilde{a}_1(\nu - \nu_{\text{in}})^{5/3} + \cdots], \tag{A27}$$

where there is one relation between and $\tilde{a}_1$ and A_{in}, found from substitution of Eq. (A27) into Eq. (A18), and matching

appropriate powers of $\nu-\nu_{\rm in}$. However, $\tilde{a}_1$ and $A_{\rm in}$ cannot be determined fully through a local expansion. What is more, Eq. (A18) *also* allows local solutions for which F has double zeros,

$$F\sim b_0(\nu-\nu_0)^2. \tag{A28}$$

By straightforward adaptation of the numerical procedure detailed in [2] for another differential equation with somewhat different kinds of isolated singularities, we determined from integrating Eq. (A18) that the three pairs of one-third singularities of F whose values of $\nu_{\rm in}$ are closest to the origin are

$$\begin{aligned} &0.001\,073\,7\pm 5.470\,147\,6i,\\ &-0.777\,996\,97\pm 8.184\,871\,44i,\\ &-1.358\,520\,87\pm 10.326\,151\,6i. \end{aligned} \tag{A29}$$

Applying arguments similar to those presented in [2], which have been subsequently confirmed rigorously by other methods [25], for the isotropic Hele-Shaw problem a denumerable infinite set of singularities that asymptotically approaches the anti-Stokes lines (from the outside): $\arg\nu=\pm 4\pi/\beta+6$ can be expected.

In our computation, we encountered no zeros of F [recall Eq. (A28)] within a 16×16 square centered at the origin. This was deduced by noting that when the differential equation (A18), integrated on a once-traversed closed contour C, resulted in F returning to its original value (to within numerical error), $\oint_C d\nu(F'/F)$ was also zero (to within numerical error). We therefore concluded that F did not have any zeros and the only singularity was of the type Eq. (A27).

The existence of singularities (A27) in the similarity variable implies that

$$\begin{aligned} z_\zeta\sim{}&\mathcal{B}^{\mu-(\beta+2/3)\delta}\hat{E}_0(0)A_{\rm in}^2\tau^{-(\beta+2/3)(2/\beta+6)}\\ &\times C_0^{5/3}(t)[\zeta-\zeta_{\rm in}(t)]^{2/3} \end{aligned} \tag{A30}$$

in the neighborhood of the singularity, defined by the restriction

$$|\zeta-\zeta_{\rm in}(t)|\ll\mathcal{B}^{\delta}|C_0^{-1}(t)\nu_{\rm in}\tau^{2/\beta+6}|, \tag{A31}$$

where

$$\zeta_{\rm in}(t)=\zeta_s(t)+\frac{\nu_{\rm in}}{C_0(t)}\,\mathcal{B}^{\delta}\tau^{2/\beta+6}. \tag{A32}$$

Inner-inner region for strong anisotropy

We note that the locally singular behavior (A30) is not consistent with approximating Eq. (A6) by Eq. (A16). In all that follows, the phrase ''inner-inner'' refers to small, finite-surface-energy zones about singular points that arise in regions that are already ''inner'' solutions for the zero-surface-energy outer singularities. The approximation breaks down locally near each $\zeta=\zeta_{\rm in}(t)$, because the first term on the right side of Eq. (A6) is not small. It is appropriate to define inner-inner variables by

$$\zeta-\zeta_{\rm in}(t)=\mathcal{B}^{\hat{\delta}}\,\frac{1}{C_0(t)}\,\hat{\chi}(\zeta,t), \tag{A33}$$

$$C_1(t)=\mathcal{B}^{\hat{\psi}}\hat{\tau}(t), \tag{A34}$$

$$\begin{aligned} z(\zeta,t)\sim{}&\int_0^t dt'\,q_{2_0}(\zeta_s(t'),t')\\ &+\mathcal{B}^{\mu-(\beta+2/3)\delta+(5/3)\hat{\delta}}\hat{E}_0(0)\hat{G}(\hat{\chi}(\zeta,t),\hat{\tau}(t)), \end{aligned} \tag{A35}$$

where

$$\hat{\delta}=\tfrac{3}{4}\{2[(\beta+2/3)\delta-\mu]-\lambda\}>\delta, \tag{A36}$$

$$\hat{\psi}=3\left(\frac{3[(\beta+2/3)\delta-\mu]-3/2}{2}-\lambda\right)>0. \tag{A37}$$

The ''inner-inner'' equation is then

$$\begin{aligned} \dot{C}_1(t)\hat{G}_{\hat{\tau}}=&\frac{C_0^{3/2}(t)}{i\hat{E}_0^{3/2}(0)\tilde{z}_{0\zeta}^{3/2}(\zeta_s(t),t)}\left(-2\,\frac{\partial^2}{\partial\hat{\chi}^2}\,(\hat{G}_{\hat{\chi}}^{-1/2})\right)\\ &-\frac{\hat{\alpha}e^{-i4\theta_0}C_0^{7/2}(t)\hat{E}_0^{1/2}(0)}{2i\tilde{z}_{0\zeta}^{7/2}(\zeta_s(t),t)}\left(\frac{2}{3}\,\frac{\partial^2}{\partial\hat{\chi}^2}\,(\hat{G}_{\hat{\chi}}^{3/2})\right)\\ &-\mathcal{B}^{2\lambda}\,\frac{\hat{\alpha}e^{i4\theta_0}\tilde{z}_{0\zeta}^{1/2}(\zeta_s(t),t)}{2iC_0^{1/2}(t)\hat{E}_0^{7/2}(0)}\left(-\frac{2}{5}\,\frac{\partial^2}{\partial\hat{\chi}^2}\,(\hat{G}_{\hat{\chi}}^{-5/2})\right). \end{aligned} \tag{A38}$$

Note that the last term is retained only for the $O(1)$ anisotropy case, where $\lambda\equiv 0$; otherwise, it is neglected at this order. While we do not know much about the solution to Eq. (A38), we note that, since $\hat{\psi}>0$, one might expect that the solution to Eq. (A38) equilibrates over a short time scale to a state driven by the inner solution, that is, to the solution to the equation for the outer of the two inner regions. The far-field boundary condition on $\hat{G}_{\hat{\chi}}$ must be

$$\hat{G}_{\hat{\chi}}\sim A_{\rm in}^2\tau^{-2(\beta+2/3)/(\beta+6)}\hat{\chi}^{2/3}, \tag{A39}$$

in order to be consistent with Eq. (A30). Since the inner-inner region is centered around inner singularities, that are outside the sector of inner-outer matching, we expect this region to play a passive role.

In Fig. 5, we sketch the various outer, inner, and inner-inner regions in this case.

2. The case of $\psi_c\geq 0$

It is convenient to subdivide this case further into three cases: $\mu\geq\beta/3$ with $0<\beta<2$, $\mu\geq\beta/3$ with $\beta>2$, and $\mu<\beta/3$. The borderline case $\beta=2$ will not be discussed here, since it requires a significantly different analysis.

a. Subcase $\mu\geq\beta/3$, $0<\beta<2$

There is an initial stage, marked by a fast $O(\mathcal{B}^{\psi_c})$ time scale—faster than the time scale over the zero-surface-

energy solution evolves, where there is a dominant balance between the left-hand side of Eq. (A6) and the first two terms on the right of Eq. (A6). In this case, for studying the fast time scale dynamics, it is appropriate to choose the following scales in Eq. (A6):

$$\psi=\psi_c, \quad \delta=\frac{\lambda+2\mu}{2\beta}, \tag{A40}$$

and take $C_1(t)$ in accordance with Eq. (A15). The resulting leading-order inner equation is given by

$$G_\tau=-\tfrac{2}{3}(G_\chi^{3/2})_{\chi\chi}+\frac{2\tilde{z}_{0\zeta}^2(\zeta_s(0),0)e^{i4\theta_0}}{\hat{E}_0^2(0)\hat{\alpha}}(-2G_\chi^{-1/2})_{\chi\chi}$$
$$-\frac{\mathcal{B}^{2\lambda}e^{i8\theta_0}\tilde{z}_{0\zeta}^4}{C_0^4\hat{E}_0^4(0)}(-\tfrac{2}{5}G_\chi^{-5/2})_{\chi\chi}. \tag{A41}$$

The last term in Eq. (A41) is neglected unless $\lambda\equiv 0$. It is to be noted that $\delta\geqslant\mu/\beta$, the equality holding only for $\lambda=0$. Thus, for $\lambda>0$, the inner region is small enough in size even for $\tau=O(1)$ so that the appropriate far-field matching (at least in some complex χ sector) and initial conditions are given by Eqs. (A8) and (A9), respectively. For $\lambda=0$, since $\delta=\mu/\beta$, the matching and initial conditions are instead given by Eqs. (A10) and (A11).

For $\tau\ll 1$, it is clear from the initial condition (A9) that this early time solution must involve a dominant balance between the left-hand side of Eq. (A41) and the first term on the right. The similarity solution (A17), discussed in detail in the context of strong anisotropy, is appropriate in describing the evolution at this time stage since on substituting this into the other terms on the right of Eq. (A16), one obtains small errors for $\tau\ll 1$ (except in a small vicinity of singularities of F). There is once again an inner-inner region around ζ_{in} corresponding to each singularity ν_{in} of F; however, we refrain from any further discussions of this, since we cannot say much about its solution. We will assume, as we have done before, that the inner-inner solution can be matched as appropriate to the inner solution behavior near a singularity. It is to be noted that the similarity solution (A17) for $\tau\ll 1$ also defines a regime $\tau^{2/(\beta+6)}\ll|\chi|\ll 1$, where Eq. (A8) holds in some complex sectors. In this regime, the outer solution, even for $\lambda=0$, behaves like $(\zeta-\zeta_s)^{-\beta}$. Thus, the similarity solution is valid in this regime even for $\lambda=0$.

The similarity solution discussed in the preceding paragraph is invalid when $\tau=O(1)$, since Eq. (A41) is obviously different from Eq. (A16). We are unable to say much about the dynamics at this stage because of the difficulty in solving Eq. (A41). However, for $\lambda=0$, we note that the effective inner region size, deduced from the similarity solution to be $O(\delta\tau^{2/(\beta+6)})$, is now $O(|E_0|^{1/\beta})$ and has now completely engulfed any region over which the outer behavior $(\zeta-\zeta_s)^{-\beta}$ can be observed. Thus, there is no trace of initial singularity left for $\lambda=0$ at this stage and we can say that the initial singularity has dissipated over a fast-time scale, even before t is strictly $O(\mathcal{B}^{\psi_c})$; all we are left with are singularities of the inner regions. The dynamics for $\lambda=0$ for $\tau\gg 1$ will not be discussed any further.

However, for $\lambda>0$ and $\tau\gg 1$ it is natural to assume (based on the assumed continuity of dynamics on the anisotropy parameter α) that the appropriate solution is dictated by a balance between the left of Eq. (A41) and the second term on the right—this is essentially the Harry-Dym equation, which is the inner equation in the absence of anisotropy [2]. To explore this matter further, we introduce new temporal and spatial scales.

Dissipation of weak singularities for $\lambda>0$. We now choose inner time and space scales in Eq. (A6), corresponding to

$$\psi=3\mu/\beta-1, \quad \delta=\mu/\beta \tag{A42}$$

and choose

$$C_1(t)=\int_0^t dt'\,\frac{C_0^{3/2}(t')}{i\hat{E}_0^{3/2}(0)\tilde{z}_{0\zeta}^{3/2}(\zeta_s(t'),t')}. \tag{A43}$$

Since $3\mu/\beta-1<\psi_c$ for $\beta<2$, it is clear that this stage follows that in Sec. V B 1. Also, notice that this time scale coincides with t_i, described in (ib) in Sec. IV. With the substitutions (A49) and (A43) back into Eq. (A6), one obtains, in the limit $\mathcal{B}\to 0$, the Harry-Dym equation,

$$G_\tau=-2\frac{\partial^2}{\partial\chi^2}(G_\chi^{-1/2}). \tag{A44}$$

Clearly, under this limit and on these scales, the behavior is isotropic. When $\tau=O(1)$, the far-field matching condition is given by Eq. (A10), at least in some complex sectors. We are unable to find exact solutions to Eq. (A44) satisfying initial and matching conditions (A10). Nonetheless, Eq. (A44) does have a similarity solution:

$$G_\chi=\tau^{-2\beta/3(2-\beta)}F^{-2}(\nu), \quad \nu=\chi/\tau^{2/3(2-\beta)}, \tag{A45}$$

where $F(\nu)$ satisfies

$$\frac{1}{3(2-\beta)}F^{-3}(\beta F-2\nu F')=F''', \tag{A46}$$

with the asymptotic far-field condition

$$F(\nu)\sim\nu^{\beta/2}, \quad \nu\to\infty. \tag{A47}$$

The solution (A45) remains a valid solution in the present case of interest for the restricted regime $\mathcal{B}^{\psi_c-\psi}\ll\tau\ll 1$, $|\chi|=\tau^{2/[3(2-\beta)]}\ll 1$ since Eq. (A10) reduces to Eq. (A8) for $1\gg|\chi|\gg\tau^{2/[3(2-\beta)]}$.

When $\tau=O(1)$, because the boundary layer width $\mathcal{B}^{\mu/\beta}\tau^{2/[3(2-\beta)]}$ is increased in size to $O(\mathcal{B}^{\mu/\beta})=O(E_0^{1/\beta})$, there is no remnant of the initial singularity behavior left any more. Thus, for $\lambda>0$, the weak singularity has completely dissipated before time t becomes strictly $O(\mathcal{B}^{(3\mu/\beta-1)})$.

Together with the previous conclusion on $\lambda=0$, we conclude that all sufficiently weak initial singularities ($\mu\geqslant\beta/3$) for $0<\beta<2$ get dissipated over a fast time scale and are instead replaced by singularities of the inner equation. Thus, the specific type of singularity we started out with

cannot impact the features observed at the physical interface later in time. We cease to study such singularities any further.

b. Subcase $\mu \geqslant \beta/3$, $\beta > 2$

In this case, since $\psi_c < 3\mu/\beta - 1$, the time stage given by Eq. (A42) is the first relevant time scale in the dynamics. The same scales (A42) and (A43) and the resulting equation (A44) are still valid. However, since the initial and matching conditions are given by Eqs. (A11) and (A10), the solution in general for $\tau = O(1)$ remains unclear. However, for $|\chi| \ll 1$, it is consistent to assume that the solution is given by

$$G_\chi \sim \tau^{2\beta/[3(\beta-2)]} F^{-2}(\chi \tau^{2/[3(\beta-2)]}), \tag{A48}$$

where $F(\nu)$ satisfies Eq. (A46) as before, except that the matching condition (A47) is invoked now for $\nu \to 0$ rather than ∞. It is clear that as $\tau \to \infty$, the region in which G_χ has the singular behavior $G_\chi \to \chi^{-\beta}$ shrinks. Thus, over the fast time scale $O(\mathcal{B}^\psi)$, as identified in Eq. (A42), any trace of the initial singularity is wiped out by surface energy effects. We cease to discuss this case any further.

c. Subcase $\mu < \beta/3$

From the expressions for ψ_c, it follows that in this case $\beta < 2$ necessarily. Thus, in this subcase, $\lambda \geqslant \lambda_c > 0$, $0 < \beta < 2$, which means that the anisotropy is weak but the singularity strength is not too weak.

As before for $\psi_c > 0$, there is an initial stage of evolution where the inner equation is given by Eq. (A6) with the choice of time and space scale corresponding to Eq. (A40), leading to Eq. (A41), except that the $O(\mathcal{B}^{2\lambda})$ term is now necessarily negligible. For $\tau \ll 1$, once again there is a similarity solution as described in the preceding subsection, with inner-inner regions around each singularity. Once again for τ strictly $O(1)$, not much can be said because of the difficulty of solving Eq. (A41).

While the time evolution of Eq. (A41) for $\tau = O(1)$ remains an open problem at this stage, we note that for $\tau \gg 1$, a consistent solution can be found by neglecting anisotropic terms in Eq. (A41) for which the similarity solution (A46) to the Harry-Dym equation is obtained. However, since this solution continues to be valid until time t is strictly $O(1)$, it is sensible to study this in the context of the equations valid for $t = O(1)$ by looking at the special case $t \ll 1$, as we shall do now.

The stage $t = O(1)$. In this case, it is necessary to go back to Eq. (A6) and choose

$$\psi = 0, \quad \delta = \frac{2 - 3\mu}{3(2-\beta)}. \tag{A49}$$

It is to be noted that since $\mu < \beta/3$, $\delta > \mu/\beta \geqslant 0$, a condition consistent with the initial and matching conditions (A9) and (A8). With these specifications for Eq. (A49), and C_1 chosen in accordance with Eq. (A43), the resulting leading-order equation, derived from Eq. (A6), is again the Harry-Dym equation (A44). The neglected anisotropic terms are $O(\mathcal{B}^{(\lambda-\lambda_c)})$ and $O(\mathcal{B}^{(\lambda+\lambda_c)})$, each of which is small in this subcase (recall also that now we are left with $\psi_c > 0$).

The solution to Eq. (A44) that satisfies the asymptotic matching condition is given by Eq. (A45), where F satisfies Eqs. (A46) and (A47). We know that the similarity equation above admits inner singularities of the form

$$F(\nu) \sim A_{\rm in}(\nu - \nu_{\rm in})^{2/3}, \tag{A50}$$

$$A_{\rm in} = \left(\frac{3\nu_{\rm in}}{2(\beta-2)} \right)^{1/3}, \tag{A51}$$

for various values of $\nu_{\rm in}$, which have been determined numerically [2]. In outer variables, the solution in the vicinity of one of these inner singularities becomes

$$z_\zeta \sim \mathcal{B}^{\mu-(\beta-4/3)\delta} \frac{\hat{E}_0(0)}{A_{\rm in}^2} \tau^{-(\beta-4/3)(2/3(2-\beta))} \times C_0^{-1/3}(t)[\zeta - \zeta_{\rm in}(t)]^{-4/3}. \tag{A52}$$

(Notice that if $\beta \equiv \frac{4}{3}$, the inner singular solution with surface energy effects is the same as the outer, zero-surface-energy solution.) The particular inner singularity at $\nu_{\rm in}$ is then located at

$$\zeta_{\rm in}(t) = \zeta_s(t) + \frac{\nu_{\rm in}}{C_0(t)} \mathcal{B}^\delta \tau^{2/3(2-\beta)}. \tag{A53}$$

The vicinity of $\zeta = \zeta_{\rm in}$ (corresponding to $|\nu - \nu_{\rm in}| \ll 1$), where Eq. (A52) is valid, is given by the restriction

$$|\zeta - \zeta_{\rm in}(t)| \ll \mathcal{B}^\delta |C_0^{-1}(t)\nu_{\rm in}\tau^{2/3(2-\beta)}|. \tag{A54}$$

Inner-inner equation for $t = O(1)$.

It is clear from substituting Eq. (A52) into the original equation (A6) that the approximation leading to Eq. (A44) is invalid in an immediate neighborhood of each singularity $\zeta = \zeta_{\rm in}$.

We introduce inner-inner variables in the form

$$\zeta - \zeta_{\rm in}(t) = \mathcal{B}^{\hat{\delta}} \frac{1}{C_0(t)} \hat{\chi}(\zeta, t), \tag{A55}$$

$$C_1(t) = \mathcal{B}^{\hat{\psi}} \hat{\tau}(t), \tag{A56}$$

$$z(\zeta, t) \sim \int_0^t dt' q_{2_0}(\zeta_s(t'), t') + \mathcal{B}^{\mu-(\beta-4/3)\delta-(1/3)\hat{\delta}} \hat{E}_0(0) \hat{G}(\hat{\chi}(\zeta, t), \hat{\tau}(t)). \tag{A57}$$

The choice of inner-inner scales

$$\hat{\delta} = \tfrac{3}{8}\{\lambda + 2[\mu - (\beta - 4/3)\delta]\} > \delta, \tag{A58}$$

$$\hat{\psi} = \tfrac{3}{8}(\lambda - 2\{4/3 - 3[\mu - (\beta - 4/3)\delta]\}) = \tfrac{3}{8}(\lambda - \lambda_c) > 0, \tag{A59}$$

produces the same form of an inner-inner equation as Eq. (A38). However, the far-field matching condition in this case must correspond to

$$\hat{G}_{\hat{\chi}} \sim A_{\rm in}^{-2} \tau^{-2(\beta-4/3)/[3(2-\beta)]} \hat{\chi}^{-4/3} \tag{A60}$$

to reflect the inner-equation singular behavior (A52), at least in some sector of the complex $\hat{\chi}$ plane. As mentioned earlier in the context of strong anisotropy, we are unable at this point to shed much light on the dynamics of the inner-inner region, though we believe appropriate solutions exist that match the inner equation. The structure of the various outer, inner, and inner-inner scales and solutions for the weakly anisotropic singularity investigated above is the same as in Fig. 5, but with the following scales: (a) outer singularity $z_\zeta \sim E_0(t)[\zeta-\zeta_s(t)]^{-\beta}$, (b) size of inner region $O(\mathcal{B}^{2-3\mu/3(2-\beta)})$, (c) inner singularity (there are actually a countably infinite number of inner singularities) $z_\zeta \sim C(t)[\zeta-\zeta_{\rm in}(t)]^{-4/3}$, (d) size of inner-inner region $O(\mathcal{B}^{3/8\{\lambda+2[\mu-(\beta-4/3)\delta]\}})$.

In summary, if initial singularities are sufficiently far from the real axis and are also sufficiently weak ($\mu \geqslant \beta/3$), then all traces of those singularities disappear on a fast time scale, and therefore one need not consider the effect of such singularities approaching the real axis later in time. For singularities that are stronger, the zero-surface-energy singularity is preserved as an ''outer singularity,'' in the sense that there is a subregion for $\mathcal{B}^\gamma \ll |\zeta-\zeta_s(t)| \ll 1$ for some positive γ, where the zero-surface-energy singular behavior at $\zeta=\zeta_s(t)$ remains valid. This ''outer singularity'' is in fact the center of an inner region where surface energy effects are significant. The precise nature of the inner equations, however, depends on the relative orderings of anisotropy, singularity strength, and surface energy parameter $\mathcal{B}$. Indeed, it appears there are multiple inner regions in general. However, when the ''outer singularity'' comes very close to the real axis, as it must eventually, the inner limits discussed in this section are invalid, and we must investigate again the inner space and time scales, as we will in the following section. Note that this paragraph answers those questions raised as issue (i) in Sec. I.

APPENDIX B: INNER EQUATIONS AROUND ZERO AND DAUGHTER SINGULARITIES FAR FROM REAL AXIS

As with singularities in Appendix A, we have noted that the regular perturbation (22) becomes disordered in the immediate vicinity of a zero of $z_{0\zeta}$. In the analysis of this section, we require that the zero be further from the real axis than $O(\mathcal{B}^\delta)$, where $\delta=\frac{2}{7}$ for $\lambda \geqslant \frac{4}{7}$ and equal to $\frac{2}{11}(1+\lambda)$ for $\lambda<\frac{4}{7}$. This restriction allows, as in the singularity analysis in Sec. IV, asymptotic approximations to $q_1, \tilde{z}_\zeta$ using the leading terms of its Taylor expansion at $\zeta=\zeta_0(t)$. In the neighborhood of a zero, we define the inner variables as

$$\zeta-\zeta_0(t)=\mathcal{B}^\delta \frac{1}{C_0(t)}\chi(\zeta,t), \tag{B1}$$

$$\tau(t)=\mathcal{B}^{-\delta_1}C_1(t), \tag{B2}$$

$$z(\zeta,t)\sim \mathcal{B}^{2\delta}C_2(t)G(\chi(\zeta,t),\tau(t)) + \int_0^t dt' q_{2_0}(\zeta_0(t'),t')+z(\zeta_0(0),0), \tag{B3}$$

where $C_0(t)$, $C_1(t)$, and $C_2(t)$ will be determined to simplify the resulting inner equation.

With the $\mathcal{B}^{2\delta}$ scaling factor in front of G in Eq. (B3), it is seen that a requirement $G_\chi \sim \text{const}\ \chi$ for an appropriate constant allows matching to the leading-order outer solution that locally behaves as Eq. (125), and determines the scale factor $\mathcal{B}^{2\delta}$ in Eq. (B3).

Substituting Eqs. (B1)–(B3) into the full equation (21) and collecting the dominant terms in $\mathcal{B}$, we find an inner equation of the form

$$\dot{C}_1(t)\mathcal{B}^{\delta-\delta_1}G_\tau = -\frac{q_{2_\zeta}(\zeta_0(t),t)}{z_{0\zeta\zeta}(\zeta_0(t),t)}C_0G_\chi + \frac{q_{2_{0\zeta}}(\zeta_0(t),t)}{C_0(t)C_2(t)}\chi + \frac{\mathcal{B}^{1-(7/2)\delta}C_0^{3/2}(t)}{i\tilde{z}_{0\zeta}^{3/2}(\zeta_0(t),t)C_2^{3/2}(t)}\left(-2\frac{\partial^2}{\partial\chi^2}(G_\chi^{-1/2})\right) - \mathcal{B}^{1+\lambda-(11/2)\delta}\frac{\hat{\alpha}e^{i4\theta_0}\tilde{z}_{0\zeta}^{1/2}(\zeta_0(t),t)}{2iC_0^{1/2}(t)C_2^{7/2}(t)}\left(-\frac{2}{5}\frac{\partial^2}{\partial\chi^2}(G_\chi^{-5/2})\right) - \mathcal{B}^{1+\lambda-(3/2)\delta}\frac{\hat{\alpha}e^{-i4\theta_0}C_2^{1/2}C_0^{7/2}}{2i\tilde{z}_{0\zeta}^{7/2}(\zeta_0(t),t)}\left(\frac{2}{3}\frac{\partial^2}{\partial\chi^2}(G_\chi^{3/2})\right). \tag{B4}$$

The choice of δ and δ_1 depends on the relative size of anisotropy and the stage of evolution. There are two cases depending on whether $\lambda \geqslant \frac{4}{7}$ (weak anisotropy) or $0 \leqslant \lambda < \frac{4}{7}$ (strong anisotropy).

1. Weakly anisotropic case: $\lambda \geqslant \frac{4}{7}$

There appear to be many differing stages of evolution of the zero/daughter singularity pair, so for purposes of clarity it is worthwhile separating these stages into the differing subsections below.

a. Short-time development

At the earliest stage, an appropriate choice of time and space scale is

$$\delta_1=\frac{(9\lambda-4)}{4}, \quad \delta=\frac{\lambda}{2}. \tag{B5}$$

Note that if $\lambda=\frac{4}{7}$, the choice of δ and δ_1 is the same as given in the next subsection. Thus, the discussions in the next subsection would suffice to describe the earliest stage when $\lambda=\frac{4}{7}$. In the rest of this subsection, we limit ourselves to $\lambda>\frac{4}{7}$.

With the choice of δ_1 and δ, as above, Eq. (B4), to the leading order, reduces to

$$k_1 G_\tau = k_2(-2G_\chi^{-1/2})_{\chi\chi} + k_3(-\tfrac{2}{5}G_\chi^{-5/2})_{\chi\chi}, \tag{B6}$$

where

$$k_1 = \dot{C}_1(0), \tag{B7}$$

$$k_2 = \frac{C_0^{3/2}(0)}{i\tilde{z}_{0\zeta}^{3/2}(\zeta_0(0),0)C_3^{3/2}(0)}, \tag{B8}$$

$$k_3 = \frac{\hat{\alpha}e^{i4\theta_0}\tilde{z}_{0\zeta}^{1/2}(\zeta_0(0),0)}{4iC_0^{1/2}(0)C_2^{7/2}(0)}. \tag{B9}$$

With appropriate choices of $C_0(0)$, $\dot{C}_1(0)$, and $C_2(0)$, there is no loss of generality in setting k_1, k_2, and k_3 in Eq. (B6) to 1 and at the same time demand

$$G_\chi \sim \chi \tag{B10}$$

for large $|\chi|$ in some sector of the complex plane, to match to the outer solution. Further, the appropriate initial condition is

$$G_\chi(\chi,0) = \chi. \tag{B11}$$

It is clear that for $\tau \ll 1$, the second term on the right of Eq. (B6) is more important than the first. With this balance, it is found to be consistent to assume that for $\tau \ll 1$,

$$G_\chi \sim \tau^{2/13}F^{-2}(\nu), \quad \nu \equiv \chi/\tau^{2/13}, \tag{B12}$$

where F satisfies the ordinary differential equation:

$$-\frac{1}{13F^3}(F + 2\nu F') = (F^5)''' \tag{B13}$$

with the asymptotic matching condition

$$F \sim \nu^{-1/2} \quad \text{as} \quad |\nu| \to \infty \tag{B14}$$

along a ray in a sector arg ν in $(-\frac{4}{13}\pi, \frac{4}{13}\pi)$. Such solutions have been numerically computed, using a procedure similar to that described in Appendix A.

For $\tau = O(1)$, the asymptotic solution (B12) becomes invalid and there are no similarity solutions to Eq. (B6) that satisfy the asymptotic matching condition at ∞. It is unclear what happens at this stage. However, for $\tau \gg 1$, it is consistent to assume that

$$G_\chi \sim \tau^{2/9}\tilde{F}^{-2}(\tilde{\nu}), \quad \tilde{\nu} \equiv \chi/\tau^{2/9}, \tag{B15}$$

where $\tilde{F}$ satisfies

$$-\tfrac{1}{9}\tilde{F}^{-3}(\tilde{F} + 2\tilde{\nu}\tilde{F}') = \tilde{F}''', \tag{B16}$$

which is a similarity solution of $G_\tau = (-2G_\chi^{-1/2})_{\chi\chi}$. The condition matching the solution to the far-field, zero-surface-energy solution imposes

$$\tilde{F}(\tilde{\nu}) \sim \tilde{\nu}^{-1/2} \quad \text{as} \quad \tilde{\nu} \to \infty \tag{B17}$$

for arg ν in $(-4\pi/9, 4\pi/9)$. Such solutions have been calculated for the isotropic Hele-Shaw problem [2], and are known to contain a string of $\frac{2}{3}$-power singularities of F that asymptotically approach the Stokes line arg $\nu = \pm 4\pi/9$, from the outside of the sector $(-4\pi/9, 4\pi/9)$. Around each such singularity, since G_χ is singular with $a\ -\frac{4}{3}$ power, there is necessarily an inner-inner region, where there is a balance between $(G_\chi^{-1/2})_{\chi\chi}$ and $(G_\chi^{-3/2})_{\chi\chi}$, occurring in Eq. (B4). However, this inner-inner region appears to be dynamically uninteresting with no apparent effect on the outer-inner region or later on the real axis dynamics and therefore will not be discussed any further.

b. Intermediate time development

Beyond this initial stage described above, there comes a next stage that corresponds to a choice

$$\delta_1 = \delta = \tfrac{2}{7} \tag{B18}$$

in Eq. (B4). In this case, to put the equations in the simplest form, it is prudent to choose

$$C_1(t) = \int_0^t dt' \, \frac{q_{2_{0\zeta}}(\zeta_0(t'),t')}{z_{0\zeta\zeta}(\zeta_0(t'),t')} C_0(t'), \tag{B19}$$

$$C_2(t) = \frac{z_{0\zeta\zeta}(\zeta_0(t),t)}{C_0^2(t)}, \tag{B20}$$

$$C_0(t) = [i\tilde{z}_{0\zeta}^{3/2}(\zeta_0(t),t)]^{2/7} z_{0\zeta\zeta}^{1/7}(\zeta_0(t),t) q_{2_{0\zeta}}^{2/7}(\zeta_0(t),t). \tag{B21}$$

The leading-order inner equations for $t = O(B^{2/7})$, i.e., $\tau = O(1)$, becomes

$$G_\tau = -G_\chi + \chi - 2(G_\chi^{-1/2})_{\chi\chi} + \mathcal{B}^{\lambda - 4/7}k_4(-\tfrac{2}{5}G_\chi^{-5/2})_{\chi\chi}, \tag{B22}$$

where

$$k_4 = \frac{\hat{\alpha}e^{i4\theta_0}\hat{z}_{0\zeta}^{1/2}(\zeta_0(0),0)C_0^{3/2}}{2iz_{0\zeta\zeta}^{5/2}(\zeta_0(0),0)q_{2_{0\zeta}}(\zeta_0(0),0)}. \tag{B23}$$

It is to be noted that the last term on the right of Eq. (B22) is only to be included when $\lambda = \frac{4}{7}$.

For $\lambda = \frac{4}{7}$, this is the earliest stage of evolution. In that case, for $\tau \ll 1$, the appropriate asymptotic solution is again given by the similarity solution (B12), though with somewhat differing definitions of χ and τ.

For $\lambda > \frac{4}{7}$, we drop the k_4 term in Eq. (B22). The resulting equation has been previously given by Tanveer [2] for zero evolution for isotropic Hele-Shaw flow. For $\tau \ll 1$, an asymptotic similarity solution to Eq. (B22) (without the k_4 term) is again given by Eq. (B15), though with differing definitions of χ and τ. Thus, this solution matches to the earlier-time structure.

This similarity solution is the same for the singularities (A18), provided we use $\beta = -1$. We know this equation admits singularities that in the variable z_ζ corresponds to

$$\zeta_\zeta \sim \mathcal{B}^{2/3} \frac{\tau^{14/27}}{A_{\rm in}^2} C_2(t) C_0^{-1/3}(t) [\zeta - \zeta_{\rm in}(t)]^{-4/3}, \quad \text{(B24)}$$

provided ζ is sufficiently close to $\zeta_{\rm in}(t)$. The location of an inner $-\frac{4}{3}$ singularity is given by

$$\zeta_{\rm in}(t) = \zeta_0(t) + \frac{\nu_{\rm in}}{C_0(t)} \mathcal{B}^{2/7} \tau^{2/9}, \quad \text{(B25)}$$

for various values of $\nu_{\rm in}$ which were determined numerically [2]. The condition

$$|\zeta - \zeta_{\rm in}(t)| \ll \mathcal{B}^{2/7} |C_0^{-1}(t) \nu_{\rm in} \tau^{2/9}| \quad \text{(B26)}$$

defines the immediate neighborhood of $\zeta_{\rm in}$ where the local behavior (B24) is valid. $\zeta_{\rm in}(t)$ also defines the center of an inner-inner region where the anisotropic term $(G_\chi^{3/2})_{\chi\chi}$ in Eq. (B4), neglected in Eq. (B22), becomes as important as the $(G_\chi^{-1/2})_{\chi\chi}$ term. The time evolution in this inner-inner scale is faster than here and it may be expected that there a steady state is reached for $\tau = O(1)$. Since the inner-inner equations appear to be dynamically unimportant, we do not discuss this any further.

For both cases, $\lambda > \frac{4}{7}$ and $\lambda = \frac{4}{7}$, the dynamics for $\tau = O(1)$ remains uncertain. The solution to this problem would require one to solve Eq. (B22) in the complex plane with the given matching conditions at ∞. How this can be done, even numerically, remains an open problem.

However, for $\lambda \geqslant \frac{4}{7}$ and $\tau \gg 1$, it is consistent to assume that if $\chi = O(1)$, then the solution to Eq. (B22) equilibrates to a steady solution of

$$0 = -G_\chi + \chi - 2(G_\chi^{-1/2})_{\chi\chi} + \mathcal{B}^{\lambda - 4/7} k_4 (-\tfrac{2}{5} G_\chi^{-5/2})_{\chi\chi} \quad \text{(B27)}$$

with matching conditions $G_\chi \to \chi$ at ∞ along certain sectors.

Interestingly, notice that there is a differing long-time structure, following a moving disturbance, hence $\chi - \tau = O(1)$. In this case, the time dependence persists, because the solution cannot be time independent since the appropriate far-field matching condition for $\tau \gg |\chi - \tau| \gg 1$ must be $G_\chi \to \tau$. In such a case, it is consistent to assume that

$$G_\chi \sim \tau F^{-2}(\nu), \quad \text{where} \quad \nu = (\chi - \tau)\tau^{1/6}, \quad \text{(B28)}$$

where $F(\nu)$ now satisfies

$$F^{-3}(F - \tfrac{1}{3}\nu F') = 1 - 2F''', \quad \text{(B29)}$$

with

$$F(\nu) \to 1 \quad \text{as} \quad \nu \to \infty \quad \text{(B30)}$$

when $\arg \nu$ is in $(-\pi, \pi/3)$. There is a one-parameter family of such solutions that were found by Tanveer [2]. It was surmised that the dynamics for $\tau = O(1)$ selected a unique solution out of this similarity solutions. It is to be noted that the size of the effective inner region, in terms of the ζ variable, implied by Eq. (B18) and the similarity variable (B29), is $\mathcal{B}^{2/7}\ \tau^{-1/6}$, which becomes $O(\mathcal{B}^{1/3})$ when $\tau = O(\mathcal{B}^{-2/7})$, i.e., when $t = O(1)$. This result is consistent with the scaling results in the following section for $t = O(1)$. Whether Eq. (B28) is indeed the asymptotic similarity solution for large τ remains uncertain and needs to be investigated. However, we proceed further with the hypothesis that such is the case, for its consequences appear to be consistent with direct numerical solutions of the Hele-Shaw interface [11], though other large time dynamics of Eq. (B18) can presumably lead to the same scales observed in the numerics. It is to be noted that the similarity solution (B29) has $\frac{2}{3}$-power singularities, implying that G_χ has a $-\frac{4}{3}$ singularity. Thus, there must be an inner-inner region where the anisotropic term $(G_\chi^{3/2})_{\chi\chi}$ in Eq. (B4), neglected in Eq. (B22), enters into the equation.

c. Daughter singularity inner equations at longer times

On examining the relation between G and z_ζ and χ and τ to ζ and t, it is seen that the consequence of the similarity solution (B28) with a singularity at $\nu = \nu_{\rm in}$ is that z_ζ is at least $O(1)$ different from the zero-surface-energy solution in the neighborhood of $\zeta = \zeta_d(t)$ [note that $\zeta = \zeta_{\rm in}$ that corresponds to $\nu = \nu_{\rm in}$ is within a $\mathcal{B}^{1/3}\ t^{-1/6}$ neighborhood of $\zeta_d(t)$] at least when $1 \gg t \gg \mathcal{B}^{2/7}$.

The differing limits of $\tau \to \infty$, depending on whether $\chi = O(1)$ or $\chi - \tau = O(1)$ signify the separation of the inner regions around a zero $\zeta_0(t)$ and the corresponding daughter $\zeta_d(t)$ when $t \gg O(\mathcal{B}^{2/7})$. We now discuss the inner region around the daughter singularity $\zeta_d(t)$ for $t = O(1)$, when it has completely separated from the inner region around $\zeta_0(t)$. However, we still examine time scales for which restrictions $\mathrm{Im}\ \zeta_d < 0$ and $|\mathrm{Im}\ \zeta_d| \gg \mathcal{B}^{1/3}$ are not violated.

In that case, we introduce inner variables

$$\zeta - \zeta_d(t) = \mathcal{B}^{1/3} \frac{\chi}{C_0(t)}, \quad \text{(B31)}$$

$$\tau = -\int_0^t \frac{q_{2\zeta}(\zeta_d(t'), t')}{C_2(t') C_0(t')}\, dt', \quad \text{(B32)}$$

$$z(\zeta, t) = z_0(\zeta_d(t), t) + C_2 \mathcal{B}^{1/3} G(\chi, \tau), \quad \text{(B33)}$$

where

$$C_0(t) = \exp\left[\int_0^t dt' q_{1\zeta}(\zeta_d(t'), t') \right] \quad \text{(B34)}$$

and

$$C_2(t) = -\frac{C_0^5(t)}{4 \tilde{z}_{0\zeta}^3(\zeta_d(t), t) q_{2\zeta}^2(\zeta_d(t), t)}. \quad \text{(B35)}$$

Then the leading-order inner equation is given by

$$G_\tau - D(\tau)\chi = -(2G_\chi^{-1/2})_{\chi\chi}, \quad \text{(B36)}$$

where

$$D(\tau) = \frac{z_{0\zeta}(\zeta_d(t), t)}{C_0(t)}. \quad \text{(B37)}$$

The anisotropic terms neglected in Eq. (B36) are $O(\alpha) \ll 1$. The matching condition to the outer-zero-surface-energy solution requires

$$G_\chi \sim \frac{z_{0\zeta}(\zeta_d(t),t)}{C_2 C_0} \tag{B38}$$

as $\chi \to \infty$ in a certain sector in the complex χ plane. Note that the most singular terms of the higher-order perturbation term z_{1_ζ} appearing in Eq. (135) are not relevant to the leading-order matching since they are $O(\mathcal{B}^{\lambda-1/2}, \mathcal{B}^{1/6}) \ll 1$ when $|\zeta - \zeta_d| \gg \mathcal{B}^{1/3}$.

Equation (B36) is equivalent to that derived for daughter singularities in the isotropic Hele-Shaw problem [Eq. (7.4) in [2]]. We know little about its solution. We assume that a solution exists and satisfies the given matching condition. The scaling information is essential in determining what happens when the daughter singularity impacts the real axis, as shall be seen later. In Fig. 9, we display the various outer, inner, and inner-inner scales and solutions for the weakly anisotropic zero investigated above.

We end this section with a note that Eqs. (B31)–(B37) hold even for $\frac{1}{2} < \lambda < \frac{4}{7}$, though the earlier stages are complicated by apparently many different time scales that we have been unable to fully resolve. The end scaling result of an $O(\mathcal{B}^{1/3})$ inner region around $\zeta_d(t)$, where z_ζ differs from the outer solution by $O(1)$ and contains many actual singularities of z_ζ (hence called a daughter singularity cluster), holds for any $\lambda > \frac{1}{2}$.

2. Strongly anisotropic case: $\lambda < \frac{1}{2}$

As before, there are different time scales in the dynamics, separately analyzed below.

a. Short-time dynamics

The first stage here corresponds to a choice in Eqs. (B1)–(B4) of

$$\delta = \delta_1 = 2(1+\lambda)/11, \tag{B39}$$

where $C_0(t)$ is chosen in this case to be

$$C_0(t) = \left(\frac{\hat{\alpha} e^{i4\theta_0}}{2i} \tilde{z}_{0\zeta}^{1/2}(\zeta_0(t),t) \right)^{-2/11} \times z_{0\zeta\zeta}^{5/11}(\zeta_0(t),t) q_{2_{0\zeta}}^{2/11}(\zeta_0(t),t). \tag{B40}$$

The inner equation is the following parameter-free partial differential equation:

$$G_\tau + G_\chi = \chi + \frac{2}{5} \frac{\partial^2}{\partial \chi^2} (G_\chi^{-5/2}). \tag{B41}$$

The surface energy terms in Eq. (B4), neglected in Eq. (B41), are $O(\mathcal{B}^{(4-7\lambda)/11})$ and $O(\mathcal{B}^{8(1+\lambda)/11})$. Equation (B41) has a similarity solution, asymptotically valid for $t \ll \mathcal{B}^{2(1+\lambda)/11}$,

$$G_\chi = \tau^{2/13} F^{-2}(\nu), \quad \nu = (\chi - \tau)/\tau^{2/13}, \tag{B42}$$

where $F(\nu)$ satisfies Eq. (B13), with matching condition (B14) for large $|\nu|$ for $\arg\nu$ in $(-4\pi/13, 4\pi/13)$. For $t = O(B^{2/11(1+\lambda)})$, this similarity solution becomes invalid since all the terms in Eq. (B41) become equally important. The dynamics at these early stages is complicated, and we do not further address this matter here.

b. Daughter singularity inner equations for intermediate time scales: $t = O(1)$

We now seek a consistent inner-equation structure around $\zeta = \zeta_d(t)$ for $t = O(1)$. We find that multiple inner regions are necessary for consistency with the outer matching condition and the singularity structure the solutions inherit from earlier stages.

There is an important restriction on the time stage when the results in this section are valid, namely, $\mathrm{Im}\zeta_d < 0$ and that $|\mathrm{Im}\zeta_d| \gg \mathcal{B}^{2(1+\lambda)/9}$. We introduce

$$\zeta - \zeta_d(t) = \mathcal{B}^\delta \frac{\chi}{C_0(t)}, \tag{B43}$$

$$z(\zeta,t) = z_0(\zeta_d(t),t) + \mathcal{B}^{\delta_2} G(\chi,\tau), \tag{B44}$$

where

$$C_0(t) = \exp\left[\int_0^t dt' q_{10_\zeta}(\zeta_d(t'),t') \right]. \tag{B45}$$

On substituting Eqs. (B43)–(B45) into Eq. (21) and collecting all possible dominant contributions, we get

$$\begin{aligned} &\mathcal{B}^{\delta_2} \frac{d\tau}{dt} G_\tau - q_{2_{0\zeta}}(\zeta_d(t),t) \mathcal{B}^\delta \frac{\chi}{C_0} \\ &= \frac{\mathcal{B}^{1-(1/2)\delta_2-(3/2)\delta} C_0^{3/2}}{i\tilde{z}_{0\zeta}^{3/2}(\zeta_d(t),t)} (-2G_\chi^{-1/2})_{\chi\chi} \\ &\quad - \frac{\hat{\alpha} e^{-i4\theta_0} C_0^{7/2} \mathcal{B}^{1+\lambda+(3/2)\delta_2-(7/2)\delta}}{2i\tilde{z}_{0\zeta}^{7/2}(\zeta_d(t),t)} (\tfrac{2}{3} G_\chi^{3/2})_{\chi\chi} \\ &\quad - \frac{\hat{\alpha} e^{i4\theta_0} \tilde{z}_{0\zeta}^{1/2}(\zeta_d(t),t) \mathcal{B}^{1+\lambda-(5/2)\delta_2+(1/2)\delta}}{2iC_0^{1/2}} (-\tfrac{2}{5} G_\chi^{-5/2})_{\chi\chi}. \end{aligned} \tag{B46}$$

The outermost inner scale must involve matching to the zero-surface-energy solution, i.e.,

$$G(\chi,\tau) \sim \mathcal{B}^{\delta-\delta_2} z_{0_\zeta}(\zeta_d(t),t) \frac{\chi}{C_0(t)}. \tag{B47}$$

In order for the matching condition on the leading-order inner solution $G(\chi,\tau)$ to be free of $\mathcal{B}$, it is necessary to choose

$$\delta = \delta_2. \tag{B48}$$

Recall that the outer asymptotic expansion in a neighborhood of $\zeta = \zeta_d(t)$ behaves as

$$\begin{aligned} z \sim\ & z_0(\zeta_d(t),t) + z_{0\zeta}(\zeta_d(t),t)[\zeta - \zeta_d(t)] \\ & - \tfrac{2}{3} \mathcal{B} A_1 [\zeta - \zeta_d(t)]^{-3/2} - \tfrac{2}{7} \hat{\alpha} F_1(t) \mathcal{B}^{1+\lambda} (\zeta - \zeta_d)^{-7/2}. \end{aligned} \tag{B49}$$

The outermost inner region

We notice from Eq. (B49) that the largest spatial scale at which this perturbation expansion becomes invalid is when $\zeta-\zeta_d=O(\mathcal{B}^{2(1+\lambda)/9})$ suggesting that the largest of the inner scale (in case there are nested inner scales) corresponds to

$$\delta_2=\delta=\tfrac{2}{9}(1+\lambda). \tag{B50}$$

With this choice of δ and hence δ_2, one obtains from Eq. (B46) the following leading-order equation:

$$G_t=q_{2_{0\zeta}}(\zeta_d(t),t)\,\frac{\chi}{C_0}. \tag{B51}$$

Surface energy terms do not enter this equation at the leading order. The isotropic surface energy term in Eq. (B46) is $O(\mathcal{B}^{1-3\delta})\ll 1$, while both the anisotropic surface energy terms in Eq. (B46) are $O(\mathcal{B}^{1+\lambda-3\delta})\ll 1$. We notice that at the next order, isotropic surface energy terms are more important than the anisotropic ones. The solution (B51) that matches with Eq. (B49) is given by

$$G=z_{0\zeta}(\zeta_d(t),t)\,\frac{\chi}{C_0}-\frac{2\hat{\alpha}}{7}\,F_1(0)\chi^{-7/2}. \tag{B52}$$

This is clearly not valid as $\chi\to 0$ since the neglected term $G_\chi^{3/2}$ must eventually become important with shrinking $|\chi|$ and this is discussed next.

The innermost region, with evolution on an $O(1)$ time scale

We notice that in the outermost spatial scale, neglected surface energy terms play a role only on a long time scale $t=O(\mathcal{B}^{3\delta-1})\gg 1$. We now seek an inner scale where the surface energy effects occur in the leading-order equation over an $O(1)$ time scale. The choice is

$$\delta_1=\tfrac{2}{7}(1+\lambda);\quad \delta_2=0 \tag{B53}$$

and

$$\tau=\int_0^t \frac{\hat{\alpha}e^{-i4\theta_0}C_0^{7/2}(t)}{2i\tilde{z}_{0\zeta}^{7/2}(\zeta_d(t),t)}. \tag{B54}$$

Then, Eq. (B46) leads to

$$G_\tau=-\tfrac{2}{3}(G_\chi^{3/2})_{\chi\chi}. \tag{B55}$$

The neglected isotropic surface energy term is $O(\mathcal{B}^{(4-3\lambda)/7})$, while the other anisotropic term in Eq. (B46) is $O(\mathcal{B}^{8(1+\lambda)/7})$. The appropriate far-field matching condition for solution G above, corresponding to matching of the outer-inner solution, is

$$G_\chi\sim\hat{\alpha}F_1(0)\chi^{-9/2}. \tag{B56}$$

There exists a similarity solution satisfying this matching condition in the form (A16), with $\beta=9/2$. At singularities $\zeta_{\rm in}$ of this solution, where G_χ is locally proportional to $(\zeta-\zeta_{\rm in})^{2/3}$, one must require an inner-inner region where the neglected isotropic surface energy term in Eq. (B46) is the same order as the $G_\chi^{3/2}$ term.

Bridging the gap between the $\zeta-\zeta_d=O(\mathcal{B}^{2/7(1+\lambda)})$ and $O(\mathcal{B}^{2/9(1+\lambda)})$ spatial scales is an intermediate spatial scale where there is a balance between the $(G_\chi^{3/2})_{\chi\chi}$ anisotropy term and the $(G_\chi^{-1/2})_{\chi\chi}$ isotropic surface energy term. This intermediate spatial scale corresponds to $|\zeta-\zeta_d|=O(\mathcal{B}^{10(1+\lambda)/(39)})$ if $\lambda<\frac{4}{9}$ and $O(\mathcal{B}^{(2+3\lambda)/9})$ for $\lambda\geq\frac{4}{9}$. The time variation in this case occurs over a long time scale, and therefore for initial zeros an $O(1)$ distance from the real axis, such effects will not be seen by the time the daughter singularity cluster hits the real axis.

The structure of the various inner scales around an initial zero and a subsequent daughter singularity in the case of strong anisotropy is the same as in Fig. 9, but with the following scales: (a) outer daughter singularity $z_\zeta\sim z_{0\zeta}+\alpha\mathcal{B}F_1(t)[\zeta-\zeta_d(t)]^{-9/2}$, (b) size of the daughter singularity's inner region $O(\mathcal{B}^{2/9(1+\lambda)})$, (c) inner singularity (countably infinite in number) $z_\zeta\sim C(t)[\zeta-\zeta_{\rm in}(t)]^{2/3}$, (d) outer zero $z_\zeta\sim z_{0\zeta\zeta}[\zeta-\zeta_0(t)]$, (e) size of the zero singularity's inner region $O(\mathcal{B}^{2/11(1+\lambda)})$.

Lower bound on singularity strength for distinct inner regions

Recall that we had earlier found that the initial strength of a singularity $|E_0(0)|$, not too close to the real axis, had to be larger than $\mathcal{B}^{\beta/3}$, otherwise any trace of this initial singularity is wiped out by surface energy effects on a fast time scale. It turns out that the same limitation occurs when we require that the inner regions around a singularity and a zero induced by a singularity be distinct. Otherwise, traces of initial singularity or a zero cannot persist for long.

To understand these limitations, recall that for $|E_0(0)|\ll\mathcal{B}^{\beta/3}$, the analysis of Sec. A 2 suggests that the inner scale around such an initial singularity quickly expands to a size $O(|E_0(0)|^{1/\beta})$. With local singular behavior $z_\zeta\sim A_0(0)+E_0(0)[\zeta-\zeta_s(0)]^{-\beta}$, with $|E_0(0)|\ll 1$ and $A_0(0)$ of order $O(1)$, it is clear there can be a zero $\zeta_0(0)$ nearby so that $|\zeta_0(0)-\zeta_s(0)|=O(|E_0(0)|^{1/\beta})$. Thus, the inner region around a singularity will have engulfed such a zero very quickly, before the corresponding zero-surface-energy singularity $\zeta_s(t)$ or zero $\zeta_0(t)$ has a chance to move far. From the viewpoint of an initial zero, induced by the weak singularity, the inner spatial scale for weak anisotropy implied by Eqs. (B1), (B18), and (B21) suggests an inner region around $\zeta_0(0)$ that scales as $\mathcal{B}^{2/7}z_{\zeta\zeta}^{-1/7}(\zeta_0(0),0)$. Since $z_{\zeta\zeta}(\zeta_0(t),t)=O(|E_0(0)|^{-1/\beta})$, it follows that this inner spatial region with $O(\mathcal{B}^{2/7}|E_0(0)|^{1/(7\beta)})$ dimension includes $\zeta_s(0)$, when $|E_0(0)|\ll\mathcal{B}^{\beta/3}$. In the case of strong anisotropy, from Eqs. (B1), (B39), and (B40), it follows that the inner region scales as $O(\mathcal{B}^{2(1+\lambda)/11}|E_0(0)|^{5/(11\beta)})$, which may not include $\zeta_s(0)$. However, it is clear that in all cases, the initial traces of a weak distinct singularity and its corresponding zero are wiped out completely by surface energy effects acting on a fast time scale.

On the other hand, if $|E_0(0)|\gg\mathcal{B}^{\beta/3}$, following the scaling results of Sec. A 2 and above, the inner regions are found to be distinct.

Thus, we conclude that the cutoff singularity strength is defined by

$$|E_0(0)|_{\rm cutoff}=O(\mathcal{B}^{\beta/3}). \tag{B57}$$

For a pole, this is $O(\mathcal{B}^{1/3})$.

APPENDIX C: MOTION OF DAUGHTER SINGULARITIES VERSUS ZERO SINGULARITIES IN SMALL-RESIDUE EXACT SOLUTIONS

We noted before in Appendix B that corresponding to each initial zero of z_ζ, there exists a daughter singularity, $\zeta_d(t)$, where an assumed asymptotic expansion for z in powers of $\mathcal{B}$ becomes disordered, even though $\zeta_d(t)$, in general, is a regular point of the associated zero-surface-energy solution. $\zeta_d(t)$, while not an actual singularity of z_ζ, defines the center of a cluster of actual singularities (referred to as a daughter singularity cluster) of z_ζ, until the time that $\zeta_d(t)$ impacts the real axis. Beyond this time, the concept of a daughter singularity cluster does not exist since the cluster appears to break up and disperse. Nonetheless, it is known that the impact of a daughter singularity cluster on the real axis can singularly perturb an interface and cause it to veer from the corresponding zero-surface-energy solution even when such solutions are smooth.

In [1], we noted that, in the context of exact pole solutions of the zero-surface-energy problem, zeros of z_ζ can impact the real axis, even when they are initially at $O(1)$ distance from the real axis. Such impact causes formation of an interfacial cusp, and, beyond that time, the solution is unphysical. Thus, we naturally ask how it is that arbitrarily small surface energy modifies this cusp-formation conclusion of the corresponding zero-surface-energy solution. One possible scenario is that the interface comes close to forming a cusp before surface energy effects become important and modify the structure. A second option is that the interface veers sharply away from the zero-surface-energy solution, due to the impact of daughter singularities, long before any zero comes close to the real axis. For specific solutions, prior analytical and numerical calculations for the isotropic Hele-Shaw problem suggest the latter explanation is the right one for an exterior problem where a sink is located at ∞. The question remains: Is the latter scenario correct in general? Does a daughter singularity necessarily impact the real axis before the corresponding zero, thus preventing an interface from developing a cusp? In general, we do not know the answer to that question. However, we consider in this section a wide class of exact solutions containing large numbers of poles with small residues (strengths), and find our intuition verified. Further, numerical solutions for special cases, as described in Sec. C 3, support the same conclusion, even when the residues are *not* small.

We found in Sec. IV, that, as for the isotropic Hele-Shaw problem [2], the daughter singularity trajectory is governed by the same equations as any other zero-surface-energy singularity, provided the daughter singularity has not hit the real axis. (As mentioned above, the daughter singularity concept does not make sense beyond the impact time.) In [1], we examined the zero-surface-energy problem in great detail for the class of initial conditions for which all singularities of z_ζ are poles. In this section, we will now add the daughter trajectories to these pole solutions.

1. Daughter singularity equations

When all the singularities of the $\mathcal{B}=0$ solution are poles of z_ζ, the integral of the governing equation for the daughter singularity dynamics, Eq. (131), can be evaluated with the residue theorem, using a contour in $\mathrm{Im}(\zeta)>0$, just as in the first paper for the pole solutions. The resulting system of equations for the daughter trajectories becomes

$$\dot{\zeta}_{dj}(t) = -2i \sum_{n=1}^{N+1} \frac{1}{\tilde{z}_{\zeta\zeta}(\zeta_{0n}^*(t),t) z_\zeta(\zeta_{0n}^*(t),t)[\zeta_{0n}^*(t) - \zeta_{dj}(t)]}, \tag{C1}$$

$$\zeta_{dj}(0) = \zeta_{0j}(0), \quad j = 1, \ldots, N+1. \tag{C2}$$

Recall from the first paper that there are N poles and $N+1$ zeros, and so there are $N+1$ daughters, one for each zero. In the numerical solution of the pole equations, we could easily append Eq. (C1) to the system of equations in the first paper and numerically obtain the daughter trajectories while we obtain the pole trajectories.

For the special case of an Ivantsov initial condition with $E_j=0$ in Eq. (27), the only zero remaining is the Ivantsov zero ζ_{0N+1}. Therefore, only the Ivantsov daughter singularity at $\zeta=\zeta_{dN+1}$ remains in Eq. (C1), and its governing equation reduces to

$$\zeta_{0N+1}(t) = -i, \tag{C3}$$

$$\dot{\zeta}_{dN+1}(t) = -\frac{1}{i - \zeta_{dN+1}}, \tag{C4}$$

$$\zeta_{dN+1}(0) = -i. \tag{C5}$$

This equation has the solution

$$\zeta_{dN+1}(t) = i(1 - \sqrt{4-2t}), \tag{C6}$$

indicating that the Ivantsov zero moves along the imaginary axis from $\zeta=-i$ to the origin, hitting at $t=\frac{3}{2}$. This simple case demonstrates again that the singular nature of the $\mathcal{B}\to 0$ limit is not limited only to the vicinity of the zeros and singularities of the $\mathcal{B}=0$ solution. For $\mathcal{B}\equiv 0$, an initial Ivantsov parabola remains unchanged for all time. However, for any small nonzero surface energy, a daughter singularity impacts the origin in the ζ plane (crystal tip in the z plane) at $t=\frac{3}{2}$, signaling the time when arbitrarily small surface energy will generally cause the actual solution to veer away from the Ivantsov parabola.

2. Small-residue theory

We now incorporate the daughter singularities into the extensively developed small-residue theory of [1], in which all the $E_j=\epsilon\hat{E}_j$, $\epsilon \ll 1$. As we shall see, this approach meets with moderate success only. There are therefore $N+1$ zeros. The first N of the related daughters are associated with the N poles; the $(N+1)$st daughter is associated with the Ivantsov zero. As in the first paper, we divide theoretical considerations into several cases, according to the size of η_s, η_0, and now η_d, but in this paper we consider only the initial segments of the trajectories for which η_s, η_d, $\eta_0 \gg O(\epsilon)$ only.

As in [1], we begin by defining a regular asymptotic expansion for the daughter singularities. If all the poles are so far from the real axis that $|\eta_{sj}| \gg \epsilon$, the motion of the daugh-

ter singularities is governed by

$$\zeta_{dj}(t) \sim \zeta_{d_{0j}}(t) + \epsilon \zeta_{d_{1j}}(t) + O(\epsilon^2), \tag{C7}$$

$$q_1(\zeta,t;\mathcal{B}=0) \sim q_{1_0}(\zeta,t) + \epsilon q_{1_1}(\zeta,t) + O(\epsilon^2), \tag{C8}$$

$$\dot{\zeta}_{d_{0j}}(t) = -q_{1_0}(\zeta_{d_{0j}}(t),t), \tag{C9}$$

$$\dot{\zeta}_{d_{1j}}(t) = -q_{1_0}(\zeta_{d_{0j}}(t),t)\zeta_{d_{1j}}(t) + q_{1_1}(\zeta_{d_{0j}}(t),t), \tag{C10}$$

$$\zeta_{d_{0j}}(0) = \zeta_{0_{0j}}(0), \tag{C11}$$

$$\zeta_{d_{1j}}(0) = \zeta_{0_{1j}}(0). \tag{C12}$$

Note that all the 0 and 1 perturbation subscripts refer to powers of ϵ, *not* powers of $\mathcal{B}$, since all of the analysis in this section is for zero surface energy. Recall from [1] that $\zeta_{0_{0j}} = \zeta_{s_{0j}}$ for $j = 1,...,N$. Therefore, the equations for the first N daughter singularities (the ''companion'' daughter singularities) are identical to those for the pole singularities, with the differing initial conditions for $\zeta_{d_{1j}}$. We can thus find the location of the first N daughter singularities in terms of the pole locations,

$$\zeta_{dj}(t) \sim \zeta_{sj}(t) - \epsilon \frac{i\hat{E}_j}{i-\zeta_{sj}(t)} \left(\frac{i-\zeta_{sj}(0)}{i+\zeta_{sj}(0)} \right) + O(\epsilon^2),$$
$$j = 1, \ldots, N. \tag{C13}$$

Note the resemblance to the equation for the companion zeros from the first paper. Also, since the outer solution for the pole breaks down as $\eta_s \to 0$, this outer solution for the daughters will also break down as $\eta_d \to 0$. We see that the first N daughter singularities remain in $O(\epsilon)$ neighborhoods of their companion pole and zero singularities. Therefore, the supposition from Sec. IV that daughter singularities move away from the zero singularities is true in terms of the $\mathcal{B}$ scales, but not in terms of ϵ scales. Recall from the first paper that the zero singularities depend only on the instantaneous location of the poles, but, from Eq. (C13), the daughter singularities also depend on where the pole started. Since the pole also depends on its initial condition, developing a criterion for the daughter singularity collision with the real axis, analogous to that for the zeros found in the first paper, is quite a task.

The $(N+1)$st daughter singularity (the Ivantsov daughter), however, is special in that there is no companion pole and the Ivantsov zero remains in the neighborhood of $\zeta = -i$. Therefore, the Ivantsov daughter will proceed to the neighborhood of the origin alone according to

$$\zeta_{dN+1}(t) \sim i(1 - \sqrt{4-2t}) + O(\epsilon), \tag{C14}$$

which, to the leading order, is the same as the one for an Ivantsov initial condition (C6). Unlike the first N daughter singularities, though, this expansion is regular as $\eta_d \to 0$. Once again, we see very nicely that the Ivantsov daughter singularity reaches the neighborhood of the origin at $t = \frac{3}{2} + O(\epsilon)$. In fact, the daughter singularity will hit the axis in finite time, unless by chance it is shielded by another singularity, say a pole.

Although Eq. (C14) makes it clear that the Ivantsov daughter singularity hits the real axis in finite time, we are also interested in finding the conditions that determine whether or not the companion daughter singularities reach the vicinity of the real axis before poles or zeros. The equations for the imaginary coordinates of the zero and daughter singularities are simplest if they are written relative to the pole (for $-\eta_s \gg \epsilon$),

$$\begin{aligned}
&\mathrm{Im}\left(\frac{\zeta_{dj} - \zeta_{sj}}{\epsilon} \right)(t) \\
&\quad = \mathrm{Im}\left(\frac{\zeta_{0j} - \zeta_{sj}}{\epsilon} \right)(0) \\
&\qquad \times \frac{\xi_{sj}(0)\xi_{sj}(t) + [1-\eta_{sj}(0)][1-\eta_{sj}(t)]}{\xi_{sj}^2(t) + [1-\eta_{sj}(t)]^2} \\
&\qquad + \mathrm{Re}\left(\frac{\zeta_{0j} - \zeta_{sj}}{\epsilon} \right)(0) \\
&\qquad \times \frac{\xi_{sj}(0)[1-\eta_{sj}(t)] - \xi_{sj}(t)[1-\eta_{sj}(0)]}{\xi_{sj}^2(t) + [1-\eta_{sj}(t)]^2},
\end{aligned} \tag{C15}$$

$$\mathrm{Im}\left(\frac{\zeta_{0j} - \zeta_{sj}}{\epsilon} \right)(t) = -\frac{\mathrm{Re}(\hat{E}_j)\xi_{sj}(t) + \mathrm{Im}(\hat{E}_j)[1+\eta_{sj}(t)]}{\xi_{sj}^2(t) + [1+\eta_{sj}(t)]^2}, \tag{C16}$$

$$\mathrm{Re}\left(\frac{\zeta_{0j} - \zeta_{sj}}{\epsilon} \right)(t) = -\frac{\mathrm{Re}(\hat{E}_j)[1+\eta_{sj}(t)] - \mathrm{Im}(\hat{E}_j)\xi_{sj}(t)}{\xi_{sj}^2(t) + [1+\eta_{sj}(t)]^2}. \tag{C17}$$

It is generally difficult to determine the sign of $\mathrm{Im}[(\zeta_{dj} - \zeta_{sj})/\epsilon](t)$. The equations simplify dramatically, however, if we start the pole on the imaginary axis between the Ivantsov zero and the real axis, so that $0 < -\eta_{sj}(t) \leqslant -\eta_{sj}(0) < 1$. In this case, the imaginary parts become

$$\mathrm{Im}\left(\frac{\zeta_{dj} - \zeta_{sj}}{\epsilon} \right)(t) = -\frac{\mathrm{Im}(\hat{E}_j)}{1-\eta_{sj}(t)} \frac{1-\eta_{sj}(0)}{1+\eta_{sj}(0)}, \tag{C18}$$

$$\mathrm{Im}\left(\frac{\zeta_{0j} - \zeta_{sj}}{\epsilon} \right)(t) = -\frac{\mathrm{Im}(\hat{E}_j)}{1+\eta_{sj}(t)}, \tag{C19}$$

which can be combined to give us

$$\begin{aligned}
\mathrm{Im}\left(\frac{\zeta_{dj} - \zeta_{0j}}{\epsilon} \right)(t) &= \mathrm{Im}\left(\frac{\zeta_{0j} - \zeta_{sj}}{\epsilon} \right)(t) \\
&\quad \times \frac{2[\eta_{sj}(t) - \eta_{sj}(0)]}{[1-\eta_{sj}(t)][1+\eta_{sj}(0)]}.
\end{aligned} \tag{C20}$$

The factor on the right is positive, therefore, if the zero is closer to the real axis than the pole, which means $\mathrm{Im}[(\zeta_{0j} - \zeta_{sj})/\epsilon] > 0$, then the daughter singularity is closer still, $\mathrm{Im}[(\zeta_{dj} - \zeta_{0j})/\epsilon] > 0$. On the other hand, if the pole is closer to

the real axis, the daughter singularity and the zero are both shielded by the pole. The Ivantsov daughter singularity ζ_{dN+1} will be initially shielded for both of these cases, too. If $\mathrm{Re}(E_j)=0$, then the pole will continue heading for the origin for all time, otherwise the pole will head for $\xi=\pm\infty$ once it is close enough, as in the first paper. If the pole should leave the imaginary axis, then the Ivantsov daughter singularity will no longer be shielded and will continue heading for the origin. If the pole starts on the imaginary axis below $\zeta=-i$, then the Ivantsov daughter singularity gets to the real axis before the pole-zero-daughter group. Observe that in all cases discussed so far, the zero cannot be closest to the real axis; it is always shielded by the pole or daughter singularity. Furthermore, the only way to prevent the Ivantsov daughter from reaching the origin is to have $\mathrm{Re}(E_j)=0$, which corresponds to an indentation running along the longitudinal axis of the crystal, a tip-splitting situation. For initial conditions that do not lead to tip splitting, the Ivantsov daughter will reach the crystal tip by $t=\frac{3}{2}+O(\epsilon)$ and the zero-surface-energy solution will no longer completely describe the leading-order crystal evolution.

Equation (C15) also simplifies if we start the pole on $\eta_s(0)=-1$, with $|\xi_{sj}(0)|\gg O(\epsilon)$ to maintain consistency with the assumptions of the first paper. For $1\gg-\eta_s(t)\gg\epsilon$, the imaginary parts become

$$\mathrm{Im}\left(\frac{\zeta_{dj}-\zeta_{0j}}{\epsilon}\right)(t)=\frac{2}{\xi_{sj}^2(t)+1}\left(-\mathrm{Re}(\hat{E}_j)\,\frac{1}{\xi_{sj}(0)}+\mathrm{Im}(\hat{E}_j)\,\frac{\xi_{sj}(0)-\xi_{sj}(t)}{\xi_{sj}(0)}\right), \quad \text{(C21)}$$

$$\mathrm{Im}\left(\frac{\zeta_{0j}-\zeta_{sj}}{\epsilon}\right)(t)=-\frac{\mathrm{Re}(\hat{E}_j)\xi_{sj}(t)+\mathrm{Im}(\hat{E}_j)}{\xi_{sj}^2(t)+1}. \quad \text{(C22)}$$

In order for the zero to approach the real axis first, we need $\mathrm{Im}[(\zeta_{dj}-\zeta_{0j})/\epsilon]<0$ and $\mathrm{Im}[(\zeta_{0j}-\zeta_{sj})/\epsilon]>0$. This is possible if

$$\frac{\mathrm{Re}(\hat{E}_j)}{\xi_{sj}(0)-\xi_{sj}(t)}<\mathrm{Im}(\hat{E}_j)<-\mathrm{Re}(\hat{E}_j)\xi_{sj}(t), \quad \text{(C23)}$$

so that there is a range of parameters and initial conditions that allows the zero singularity to get ahead of the pole and daughter singularities. This may be a temporary condition, however, since the daughter singularity's expansion breaks down as $\eta_d\to 0$ and inner equations adjacent to the real axis may allow the daughter singularity to catch up to the zero singularity. These inner equations proved to be analytically intractable, so we turn now to the numerical solutions of the governing equations (C1) and (C2).

3. Numerical solutions

We turn now to the task of obtaining the daughter trajectories numerically, by modifying the computer program used in [1] to include Eq. (C1), for the case when the initial distribution of singularities includes poles only. We find that

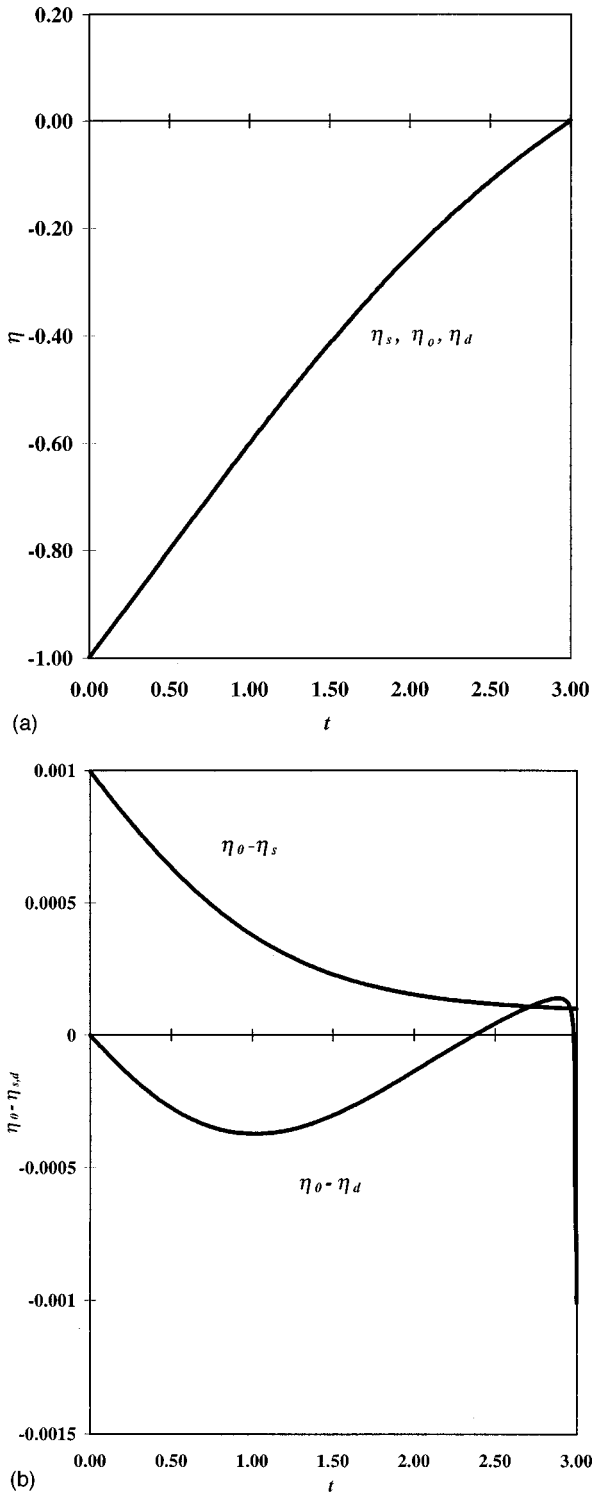

FIG. 10. Simulation showing (a) the trajectory of a pole, zero, and daughter group, (b) the zero singularity's temporary lead over the daughter and pole singularities, followed by the daughter singularity's acceleration and impact with the real axis ahead of the zero singularity, preventing cusp formation.

when the daughter singularity approaches the real axis first, then the zero and pole are always behind the daughter and the daughter hits the real axis in finite time. Next, if the pole approaches first, then the zero and daughter are always shielded by the pole. On the other hand, if the zero approaches first, then once it is close enough to the real axis, it

generates a speed-up in the daughter singularity, which has just enough time to get ahead of the zero and reach the real axis first (Fig. 10).

Therefore, we tentatively conclude that the zero singularities never hit the real axis first; they are always shielded by the pole singularities or outrun by the daughter singularities, even if the zero is temporarily ahead of both. Therefore, one role of surface energy is to prevent an initially smooth interface from ever getting close to formation of a cusp—in spite of the fact that the corresponding zero-surface-energy solution predicts a cusp. The daughter singularity impact causes the solution to veer dramatically from the $\mathcal{B}\equiv 0$ solution. Surprisingly, such a dramatic departure from the $\mathcal{B}\equiv 0$ solution occurs in spite of the fact that the curvature term in the full equations, evaluated for the zero-surface-energy solution, is not large.

[1] M. D. Kunka, M. R. Foster, and S. Tanveer, Phys. Rev. E **56**, 3068 (1997).
[2] S. Tanveer, Philos. Trans. R. Soc. London, Ser. A **343**, 155 (1993).
[3] J. S. Langer, in *Chance and Matter*, edited by J. Souletie (North Holland, Amsterdam, 1987).
[4] D. A. Kessler, J. Koplik, and H. Levine, Adv. Phys. **37**, 255 (1988).
[5] P. Pelce, *Dynamics of Curved Fronts* (Academic, Boston, 1988).
[6] M. E. Glicksman and S. P. Marsh, *The Dendrite*, in *Handbook of Crystal Growth*, edited by D. T. J. Hurle (Elsevier, New York, 1993), Vol. 1.
[7] M. Barber, A. Barbieri, and J. S. Langer, Phys. Rev. A **36**, 3340 (1987).
[8] S. Richardson, J. Fluid Mech. **56**, 609 (1972).
[9] A. A. Lacey, J. Aust. Math. Soc. B, Appl. Math. **24**, 171 (1982).
[10] G. R. Baker, M. Siegel, and S. Tanveer, J. Comput. Phys. **120**, 348 (1995).
[11] M. Siegel, S. Tanveer, and W. Dai, J. Fluid Mech. (to be published).
[12] S. Tanveer, Phys. Rev. A **40**, 4756 (1989).
[13] L. A. Galin, Dokl. Akad. Nauk SSSR **47**, 246 (1945).
[14] P. Ya Polubarinova-Kochina, Dokl. Akad. Nauk SSSR **47**, 254 (1945).
[15] P. G. Saffman, Q. J. Appl. Math. **12**, 146 (1959).
[16] S. Howison, J. Fluid Mech. **167**, 439 (1986).
[17] B. I. Shraiman and D. Bensimon, Phys. Rev. A **30**, 2840 (1985).
[18] P. Constantin and M. Pugh, Nonlinearity **6**, 393 (1993).
[19] R. Almgren, Phys. Fluids **8**, 344 (1996).
[20] S. C. Huang and M. E. Glicksman, Acta Metall. **29**, 701 (1981).
[21] B. Caroli, C. Caroli, and B. Roulet, J. Phys. (Paris) **48**, 1423 (1987).
[22] P. Voorhees and M. Glicksman, Metall. Trans. A **15A**, 995 (1984).
[23] O. Costin and S. Tanveer (unpublished).
[24] M. Kruskal and H. Segur, Aeronautical Research Associates of Princeton Tech. Memo 85-25 (unpublished).
[25] A. S. Fokas and S. Tanveer, Math. Proc. Camb. Philos. Soc. **124**, 169 (1998).
[26] E. D. Kelly and E. J. Hinch, Eur. J. Appl. Math **8**, 533 (1997).